The University Of Sheffield.

SITraN
Sheffield Institute for Translational Neuroscience

The pre-clinical development and characterisation of two novel antioxidant and anti-excitotoxic therapies for multiple sclerosis

By

David John Burrows

Submitted for the degree of Doctor of Philosophy (PhD)

Sheffield Institute for Translational Neuroscience

October 2020

Acknowledgements

First and foremost I would like to thank my supervisor, Professor Arshad Majid for your patience, guidance and invaluable insights throughout this journey. I have learnt a lot from you that I will take forward with me. Thank you also to my secondary supervisor Professor Basil Sharrack for generously contributing your expertise throughout the duration of my PhD.

A special thanks to my lab group, in particular Dr Saurabh Jain and Dr Milena de Felice for always going above and beyond to help me in my times of need, which were admittedly far too frequent. Thank you also to the SITraN community of researchers, technicians, staff and students for your practical suggestions, helpful advice and for making SITraN a great place to work. I would also like to extend my thanks to all of the staff at the Biological Services Unit for your training and expert guidance throughout.

Last, but not least, thank you to my family. Thank you for your support and encouragement, the many laughs and for giving me the motivation to keep going.

Statement of Originality

The experimental data contained within this thesis are the product of my own work, unless otherwise stated in the Methods section.

Abstract

Background: Multiple sclerosis (MS) is a chronic autoimmune disease of the central nervous system (CNS). Numerous pathological pathways culminate in axonal demyelination and eventual neurodegeneration. These include reactive oxygen species (ROS) release from immune and glial cells in the CNS and glutamate excitotoxicity, mediated predominantly by N-methyl-D-aspartate receptors (NMDARs). Previous work in our research group has demonstrated the neuroprotective properties of antioxidant L-carnosine (β-alanine-L-histidine) in pre-clinical ischaemic stroke. Further work has identified that immunisation against a short peptide sequence (peptide 8) located on NMDAR1 is also neuroprotective in pre-clinical ischaemic stroke. This thesis aims to build on this work by investigating the therapeutic potential of carnosine and peptide 8 immunisation in the context of MS.

Methods: The Biozzi ABH and C57BL/6 MOG_{35-55} experimental autoimmune encephalomyelitis (EAE) models of MS were used for *in vivo* efficacy studies. These were conducted alongside primary mouse cortical neuron and astrocyte culture models as well as tissue protein and gene expression analysis to investigate mechanisms of action.

Results: Carnosine significantly reduced NMDA-induced excitotoxicity and ROS accumulation in primary neurons and astrocytes. Subsequent *in vivo* studies found carnosine (550-2000 mg/kg) did not significantly improve neurological outcomes in the C57BL/6 MOG_{35-55} EAE model. Peptide 8 immunisation significantly reduced neurological deficits in the MOG_{35-55} EAE model without influencing locomotor or habitual behaviours. Overnight incubation with peptide 8 immunogenic serum

significantly increased primary neuronal firing and NMDAR1 expression. Differential gene expression analysis of EAE spinal cord further identified novel target pathways involved in calcium signalling, immune regulation and cell death. These need to be explored further.

Conclusions: Following promising *in vitro* data, carnosine did not significantly reduce neurological outcomes at the dose ranges tested. *In vivo* efficacy and behavioural outcome data indicates that peptide 8 immunisation is a viable therapeutic option to explore further for MS.

Table of contents

List of figures

List of tables

Abbreviations

AD	Alzheimer's disease
ALS	Amyotrophic lateral sclerosis
AMPA	α-Amino-3-hydroxy-5-methyl-4-isoxazolepropionic acid
APC	Antigen presenting cell
ATD	Amino terminal domain
AUC	Area under the curve
Bag-4	Bcl-2-associated athanogene 4
BBB	Blood-brain barrier
CAMK	Calmodulin dependent protein kinase
CD244	Cluster of differentiation 244
CFA	Complete Freund's adjuvant
CNS	Central nervous system
CTF	Carboxyl terminal domain
DIV	Days *in vitro*
DNA	Deoxyribonucleic acid
DOCK1	Dedicator of cytokinesis 1
dpd	Days post-demyelination
dpi	Days post-induction
EAE	Experimental autoimmune encephalomyelitis
EBV	Epstein-Barr Virus
ELISA	Enzyme-linked immunosorbent assay
FACS	Fluorescent-activated cell sorting
GFAP	Glial fibrillary acidic protein
GluR	Glutamate receptor
GMCSF	Granulocyte-macrophage colony-stimulating factor
HLA	Human leukocyte antigen
IFN	Interferon
IL	Interleukin
Itgax	Integrin Subunit Alpha X
LBD	Ligan binding domain
LDH	Lactate dehydrogenase
LTP/LTD	Long-term potentiation/depression
mAb	Monoclonal Antibody
MAPK	Mitogen-activated protein kinase
MBP	Myelin basic protein
MHC	Major histocompatibility complex
MOBP	Myelin oligodendrocyte basic protein
MOG	Myelin oligodendrocyte protein
MS	Multiple Sclerosis
NFH	Neurofilament heavy chain

NK	Natural killer cell
NMDA	N-methyl d-aspartic acid
NO	Nitric oxide
Nrf2	Nuclear factor erythroid 2-related factor 2
NV	Non-vaccinated
OPC	Oligodendrocyte progenitor cell
OSC	Organotypic slice culture
P8	Peptide 8
pERK1/2	Phosphorylated extracellular-regulated kinase 1/2
PPMS	Primary-progressive multiple sclerosis
RIN	RNA Integrity Number
RNA	Ribonucleic acid
ROS	Reactive oxygen species
RRMS	Relapsing-remitting multiple sclerosis
SIGLEC-F	Sialic acid binding Ig-like lectin F
SMPH	Succinimidyl-6-[beta-maleimidopropionamido] hexanoate
SPMS	Secondary-progressive multiple sclerosis
Th	T helper cell
tMCAO	Transient middle cerebral artery occlusion
TMD	Transmembrane domain
TNF	Tissue necrosis factor
Treg	T regulatory cell
VEGF	Vascular endothelial growth factor
VLP	Virus-like protein

1 Introduction

1.1 Multiple sclerosis – background and epidemiology

Multiple sclerosis (MS) is an autoimmune disease of the central nervous system (CNS) that is characterised by targeted myelin attack, demyelination and subsequent neuronal loss. This process results in the formation of plaques/lesions that are expressed clinically through impairments in motor, visual, sensory and autonomic systems[1]. These may manifest as sensory disturbances, fatigue, visual impairments, mobility problems, bladder and bowel dysfunction and pain depending on the specific brain region affected[2]. MS places a profound burden on both patients and society and significant therapeutic advances are essential to improve patient quality of life and reduce this burden[3].

MS affects more than 2 million people worldwide[4] and is the most common cause of disability in young adults[5]. The estimated prevalence of MS is 190 cases per 100,000 in England, which equates to around 106,000 people at any one time[6]. Disease incidence is more prevalent in females[7], with a prevalence of 272 female versus 106 male per 100,000[6]. This figure has been steadily rising in the last few decades, which is attributed to more effective treatments and therefore MS patients living longer[8]. In the UK, MS places a great financial burden on the National Health Service (NHS) and wider community, with MS-related costs amounting to around £1.4 billion per year in the UK[9]. Bladder issues, respiratory infections and disease relapse were the most common cause of admission[10]. This rise in MS patient number is predicted to further increase and with it the demand for more effective treatments.

1.2 Clinical course of MS

MS patients typically present with a clinically isolated syndrome (CIS), defined as a single episode of neurological symptoms[11]. CIS patients present with inflammatory demyelination, however without fully established disease and further diagnostic tests are required. This said, the recent 2010 revision of the McDonald diagnostic criteria classifies CIS patients into distinct MS phenotypes, based on specific scan criterion[12]. This has resulted in a reduction in total CIS diagnosis number and therefore this should be considered when reviewing more recent prevalence data. Around 80% of CIS patients convert to MS within 20 years of diagnosis[13]. Out of these patients, relapsing-remitting MS (RRMS) presents in approximately 85% of patients and is characterised by acute exacerbations of disease, followed by periods of remission[14]. These periods of remission correlate with innate repair mechanisms in the CNS, however these are not sustainable and recovery becomes less complete with time[15]. This marks the transition into secondary progressive MS (SPMS), where the disease predominantly becomes neurodegenerative in nature[15]. There are currently no immunological pathological or clinical criteria that can specifically mark this transition. Approximately 90% of patients with RRMS eventually progress to SPMS[16]. This neurodegenerative, progressive disease course can also occur from onset, without any prior relapses, and PPMS occurs in approximately 10-15% of patients[17] (Figure 1.1).

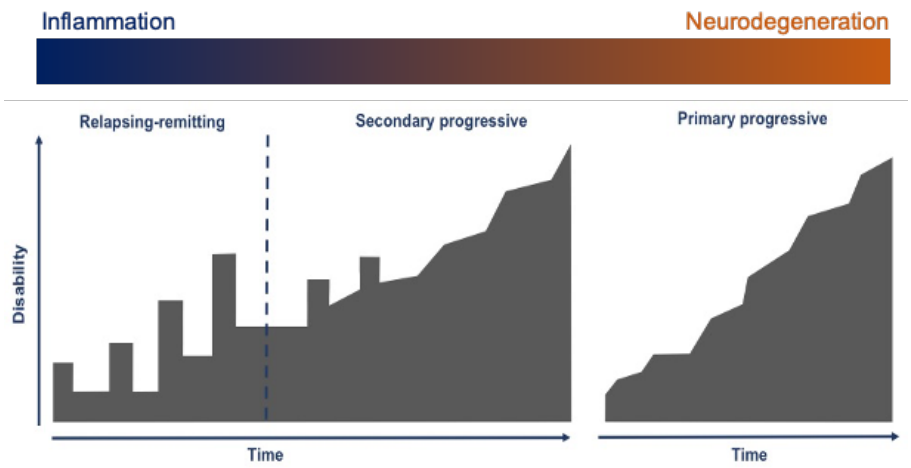

Figure 1.1 Multiple sclerosis clinical disease course.
Graph depicting clinical disease disability progression through time. Relapsing-remitting MS (RRMS) is characterised by acute periods of disease, which are followed by periods of remission and clinical improvement. Relapse recovery becomes less complete with time and disease becomes progressively worse and relapses become less distinct. This marks the transition into secondary-progressive MS (SPMS). This neurodegenerative, progressive course can also occur from onset, without any prior relapses. This is clinically defined as primary-progressive MS (PPMS). Figure adapted from reference [18].

1.3 Causes - genetic and environmental risk factors

The genetic and environmental risk factors associated with MS are complex and not yet fully understood[19]. A number of environmental factors have been identified that increase MS risk. These include Epstein-Barr virus (EBV) infection[20], exposure to tobacco smoke[21], childhood obesity[22], low sunlight exposure and/or low vitamin D levels[23]. Latitude has also been associated with increased MS risk and distance from the equator positively correlates with MS prevalence[24]. Gut microbiota imbalances have also been associated with MS risk. The microbiome is very closely linked to the immune system and resident immune cells monitor and eliminate pathogens in the intestinal lumen. An imbalance in this environment can shift the resident immune cells into a pro-inflammatory state. This increases intestinal permeability, allowing bacterial antigens to enter the bloodstream, which compromises blood-brain barrier (BBB) integrity and allows immune cell infiltration into the CNS[25].

Genetic risk factors have been associated with the human leukocyte antigen (HLA) complex. The HLA complex contains approximately 200 genes, which mostly have functions in the immune system. These genes can be broadly categorised into Class I and Class II genes. Class I genes encode from proteins involved in antigen presentation T cells, whereas Class II gene protein products present antigens to CD4

T cells. The Class II gene *HLA-DRB1*15:01* haplotype is most significantly associated with MS risk. *HLA-DRB1*15:01* has an odds ratio (OR) of around 3[26], indicating a significant association between this gene and MS prevalence. The reason for this association is not fully clear, however this may be due to increased binding capacity of CNS autoantigens and therefore increased antigen presentation[26].

These genetic and environmental risk factors lead to the precipitation of autoimmunity. One proposed mechanisms that leads to this autoimmunity is through molecular mimicry, where invading pathogens express structurally similar proteins to self-antigens, leading to T cell recognition of both the pathogen and self-antigen and the onset of autoimmunity[27]. This is supported by studies showing that CD4 T cells isolated from MS patients recognise a number of CNS proteins, including myelin basic protein (MBP), myelin oligodendrocyte glycoprotein (MOG), proteolipid protein (PLP) and myelin associated oligodendrocyte basic protein (MOBP)[28,29].

1.5 Current approved therapies for multiple sclerosis

Research into MS disease-modifying therapies (DMTs) have mainly focussed on the immune mechanisms of disease pathology. As a result, a number of effective treatments for RRMS are currently approved for use in the UK (Summarised in Table 1). This high rate of clinical translation can be largely attributed to the autoimmune nature of the disease, as the peripheral immune system is much easier to study and target than the CNS. This is highlighted by a recent meta-analysis comparing CNS and non-CNS investigative compounds which found that CNS-targeting drugs had an approval rate of less than half over the period of 1995 to 2007. Furthermore, approval of CNS drugs is much slower, taking on average 5 months longer between the periods of 1999-2013[30]. The reason for this stark difference may be due to lack of candidate drugs being able to cross the BBB, unfavourable pharmacokinetic profiles, lack of efficacy, failure of safety and/or toxicology profiling, lack of disease-relevant animal models or the absence of clinically relevant biomarkers[31]. Despite the significant therapeutic advances made so far in RRMS, very few of these treatments have any influence the chronic, progressive or neurodegenerative aspects of MS pathology. Switching research focus towards neuroprotection, as opposed to immunomodulation may provide a long-term treatment option for progressive MS patients.

Table 1.1 Current approved therapies for multiple sclerosis

Compound (*Brand name*)	Mechanism of action	Clinical indication	Reference
Interferon β	• Suppression of pro-inflammatory chemokine production through down regulation of MHC-II proteins • Promotes production of anti-inflammatory IL-10, shifting T cell population towards a Th2 phenotype • T-cell migration inhibition due to blockade of metalloproteases and adhesion molecules	RRMS	[32]
Mitoxantrone (*Novantrone*)	• Synthetic anthracenedione that intercalates into DNA that reduces T cell, B cell and macrophage proliferation by interfering with DNA repair • Reduces antigen presentation, inhibits monocyte and lymphocyte migration • Induces apoptosis in B cells and other APCs	RRMS SPMS	[33]
Glatiramer acetate (*Copaxone*)	• Precise mechanism not fully understood • May compete with MBP for binding MHC proteins on APCs inhibiting MBP-specific T cell responses • Shifts T cell populations from Th1 to Th2 phenotype • Regulatory effects on T cells, B cells and DCs	RRMS	[34]
Dimethyl fumarate (*Tecfidera*)	• Targets Nrf2-ERK1/2 MAPK pathway activating anti-inflammatory pathways, protecting against oxidative cellular injury • Shifts T cell populations from Th1 to Th2 phenotype • Suppression of IL-12, IL-1β, TNF-α, and IL-6 release • Stimulation of Treg cells • Reduction in CD8 T cell population	RRMS	[35]
Fingolimod (*Gilenya*)	• Sphingosine 1-phosphate (S1P) receptor partial agonist • Suppresses egress of lymphocytes from secondary lymphoid tissue	RRMS	[36]
Teriflunomide (*Aubagio*)	• Blocks *de novo* pyrimidine synthesis in proliferating lymphocytes by inhibiting mitochondrial enzyme dihydroorotate dehydrogenase • Reduces B and T cell proliferation • Inhibits IL-2 and TNF and reduces NO production	RRMS	[37]
Natalizumab (*Tysabri*)	• Humanised monoclonal antibody against CD49, the α4 subunit of VLA4 • Blocks T cell infiltration into the CNS by interfering with endothelial and immune cell interaction • Reduces stimulatory ability of DCs towards antigen-specific T-cell responses	RRMS	[38]
Alemtuzumab (*Lemtrada*)	• Humanised monoclonal antibody against CD52 • Depletion of CD52 expressing cells - T and B cells, NKCs, DCs and macrophages	RRMS	[39]
Ocrelizumab (*Ocrevus*)	• Humanised monoclonal antibody against CD20 • Depletion of circulating immature and mature B cells	RRMS	[40]
Cladribine (*Mavenclad*)	• Synthetic chlorinated deoxyadenosine analogue • Reduction of circulating T and B lymphocytes	RRMS	[41]

1.6 Multiple sclerosis disease mechanisms

MS disease pathology is multifactorial and involves many immune cell types that drive the aberrant response of the adaptive and innate immune system as well as CNS-resident cells. Furthermore, release of chemokine, cytokine and reactive oxygen species (ROS) exacerbate tissue injury and further recruit immune cells into the CNS. It is vital to understand these pathological mechanisms to realise how these may therapeutically targeted. Therefore, the role of each of these cell types and factors in MS pathology will be discussed.

1.6.1 The adaptive immune response

1.6.1.1 The Th1/Th17 paradigm

Under physiological conditions, the adaptive immune system relies on a complex network of specialised immune cells, chemokines and cytokines to neutralise invading pathogens. However, dysfunctions in this adaptive response can lead to a number of diseases, including autoimmunity[42].

It was historically thought that CD4 T helper cells (Th) could only differentiate into one of two distinct lineages, defined by the type of immune response they produce – type 1 (Th1) and type 2 (Th2). Th1 cells are induced by interleukin-12 (IL-12) and subsequently release interferon gamma (IFNγ) to produce a pro-inflammatory response. Th2 cells are induced by interleukin-2 (IL-2) and IL-4 and are considered to have anti-inflammatory effects[43]. However, more recently it was discovered that Th cells could also differentiate into another distinct Th17 cell lineage, whose signature cytokine is the IL-17 family. Th17 cells have been implicated in a number of autoimmune disorders, including MS. Neuroinflammation drives T cell differentiation

towards a Th17 phenotype, which drives MS disease pathology. **Error! Reference source not found.** summarises the factors that drive naïve CD4 T cell differentiation.

Naïve CD4 T cells are initiated towards the Th17 lineage in the peripheral lymphoid tissue by tumour necrosis factor-β (TNF-β) as well as IL-6 or IL-21. Terminal differentiation into mature effector Th17 cells requires IL-23. This IL-23-induced Th17 cell differentiation is inhibited by IL-4[44]. Evidence for the role of Th17 cells in MS initially came from animal studies, which identified IL-23 as a critical cytokine for experimental autoimmune encephalomyelitis (EAE) development[45]. This was further supported through analysis of MS patient samples. RRMS patient blood and CSF samples have significantly higher IL-17 mRNA levels compared to healthy controls and this correlates with periods of disease relapse[46]. Furthermore, increased IL-17 levels and Th17 cells are found in the brains of MS patients[47].

Th17 cells also facilitate immune cell infiltration by mediating BBB disruption through the release of IL-22 and IL-17A. This increases tight junction permeability and allows immune cell migration into the subarachnoid space[48]. IL-17A further impairs BBB integrity by promoting ROS generation within the epithelium of the choroid plexus[49]. Furthermore, Th17 upregulation of chemokines IL-1 and IL-2[50] and epithelial cell upregulation of CCR6[51] allows immune cell migration into the CNS.

Granulocyte macrophage colony stimulating factor (GM-CSF) is another pro-inflammatory cytokine that is important for disease initiation. GM-CSF is produced by Th1 and Th17 cells[52] and induces the proliferation and activation of resident microglia. Activated microglia release ROS, tissue necrosis factor-α (TNF-α) and IL-1β, which exacerbates the pro-inflammatory environment and further promotes BBB

permeability[53,54]. Pre-clinical animal studies have identified GM-CSF as the main cytokine that contributes towards encephalitogenicity[55]. Additionally, GM-CSF has a positive feedback loop with IL-23, which drives the expansion of pathogenic Th17 cells and a pro-inflammatory phenotype[55]. To date, numerous trials have attempted to target GM-CSF in autoimmune and inflammatory diseases[56,57]. Treatment of MS patients with a humanised monoclonal antibody against GM-CSF (Otilimab) shows modest efficacy and is well tolerated and may provide a new therapeutic avenue for MS[58].

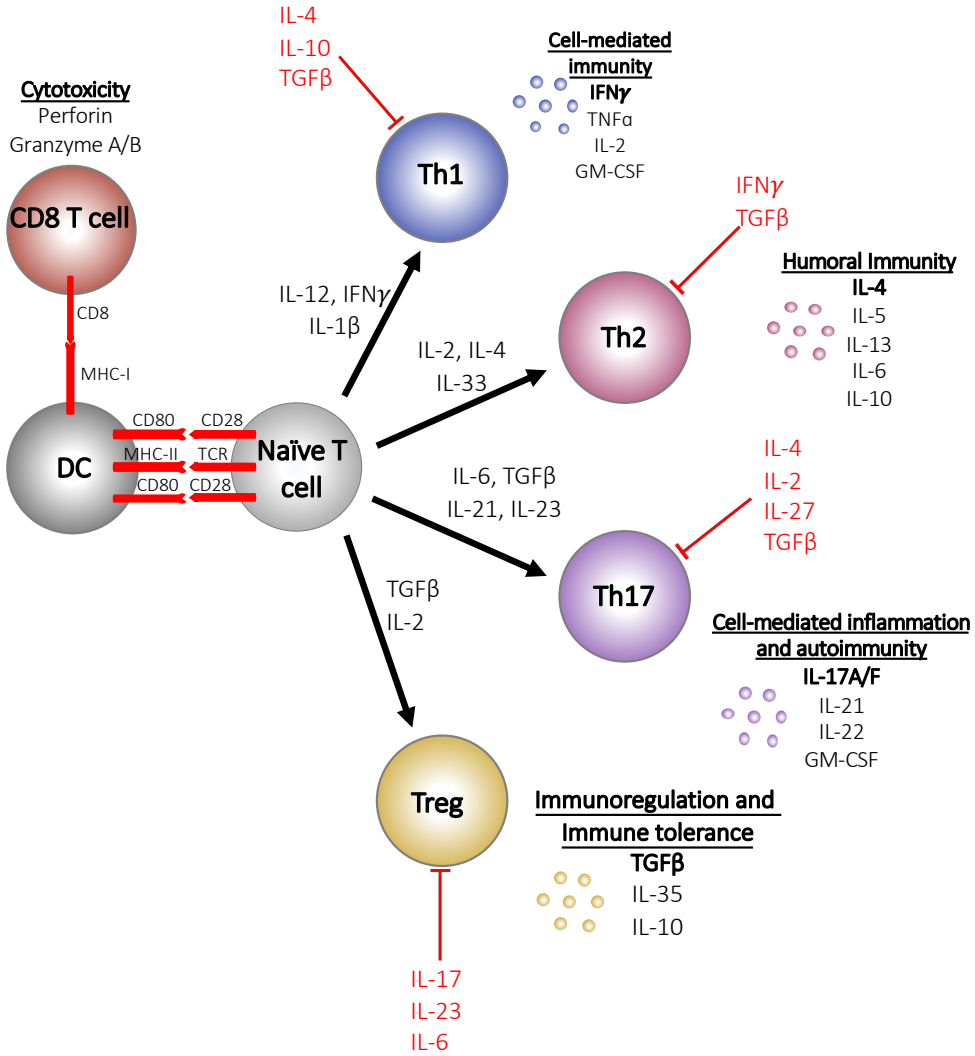

Figure 1.2 T cell differentiation
In the peripheral lymph nodes, dendritic cells (DCs) present naïve CD4 T cells with foreign antigens. Naïve CD4 T cell populations differentiate into distinct T cell lineages which is dependent on the cytokine and chemokine environment. These differentiated T cell populations orchestrate the adaptive immune response in health and disease.

1.6.1.2 Effector CD8 T cells

Although a lot of research has been focussed on CD4 T cells, effector CD8 T cells also play a major role in disease pathology. CD8 T cells recognise MHC-I molecules and through the actions of granzyme-A and granzyme-B kill cells through cell-mediated contact[59]. MHC-I molecules are ubiquitously expressed on all cells, however expression of both MHC-I and MHC-II are increased on neurons, astrocytes and oligodendrocytes in MS which indicates direct engagement of CD8 T cells[60].

CD8 T cells are found on the edge of chronic active lesions, and clonally expanded CD8 T cells are found in higher frequency than CD4 T cells[61,62]. This number correlates with axonal damage[63] and granzyme-B$^+$ CD8 T cells are found adjacent to demyelinated axons and in close proximity to oligodendrocytes[64]. *In vitro* studies show that CD8 T cells isolated from MS patients are capable of killing neurons and oligodendrocytes, which is mainly mediated through TNFα and IFNγ release[65,66]. Furthermore, isolated CD8 T cells react to peptides derived from human myelin proteins, including MBP and PLP[67]. Infiltrated CD8 T cells produce IL-17, which further contributes towards disease pathology[68]. IL-17 producing CD8 T cells are found in MS patient CSF[69] and in higher frequency ins patient blood when compared to healthy controls[70]. Interestingly, immunomodulatory drug dimethyl fumarate (DMF, Tecfidera®) supresses IL-17+ CD8 T cell populations. The mechanism of DMF remains yet to be fully elucidated[35,71], this suppression likely contributes towards its success as a disease-modifying drug for RRMS.

1.6.1.3 T regulatory cells (T_{regs})

T regulatory cells (T_{regs}) help control the development of autoimmunity by having major inhibitory effect on the immune system[72] and have major inhibitory effects on Th17 cells through IL-6 release[73]. They are immunologically characterised by expression of the transcription factor forkhead box protein 3 (FoxP3), which is essential for their inhibitory activity[74]. *In vitro* experiments show that T_{regs} are able to supress T cell populations via a cell-cell interaction[75]. T_{regs} isolated from MS patients have a decreased suppressive ability when in co-culture with T effector cells[76]. This is also due to T effector cells being more resistant to the IL-6 mediated suppressive activities of T_{regs}[77].

1.6.1.4 B cells

B cells perform several immunological functions, including antibody production, antigen presentation and cytokine production[78] and can produce both pro-inflammatory (TNFα, IL-6 and GM-CSF) and anti-inflammatory (IL-10 and IL-33) cytokines[79]. Th17 cells enhance B cell proliferation and survival through the release of IL-21[80] and mature B cell number and activity in MS patient CSF correlates with disease severity[81]. Oligoclonal bands (OCBs) are also detected in MS patient blood and CSF as a result of clonally expanded Ig-secreting cells[82]. OCBs are present in over 95% of MS patient samples[83] and is such a hallmark of MS that is now used as a diagnostic tool in MS[84].

Clonally expanded B cells are found throughout the brain, meninges and in the CSF[85] and exacerbate disease progression through the production of autoantibodies, chemokines, cytokines and by acting as antigen presenting cells (APCs) to T cells[78].

B cells isolated from MS patients show increased pro-inflammatory GM-CSF and IL-6 expression and decreased anti-inflammatory IL-10 expression[86]. This pro-inflammatory B cell phenotype is predictive of disease activity during the early phases of disease[86].

A number of established therapies have been shown to exert their beneficial effects though modulating B cell function. These include glatiramer acetate and fingolimod, which shift the B cell phenotype towards a more anti-inflammatory phenotype[87]. This observation provided evidence that B cells are a viable therapeutic target for MS. CD20 is expressed on maturing B cells before their differentiation into plasma cells. Targeting this antigen with anti-CD20 monoclonal antibody Rituximab (MabThera) significantly reduces the number of disease relapses and decreases levels of T cells in MS patient blood and CSF by depleting B cell populations[88,89].

1.6.2 The innate immune response

RRMS is mainly mediated through the adaptive immune response, however it is the innate immune system, including CNS-resident microglia and astrocytes that exacerbate disease progression and neurodegeneration.

1.6.2.1 Regulatory natural killer cells

Natural killer (NK) cells are the largest lymphocyte subset of the innate immune system and are involved in early host defence against infection and malignancies. NK cells recognise MHC-I molecules and deliver inhibitory signals to a number of cells, including autoreactive T cells[90]. Previous studies have shown that NK cells can both suppress and promote autoimmune disease progression through the release of both

anti-inflammatory (IL-4, IL-10) and pro-inflammatory (IFNγ, TNFα) cytokines as well as through direct cytotoxicity[91]. NK cells are immunologically identified by being $CD56^+$ and $CD3^-$ and can be categorised into two subpopulations based on the surface density of the CD56 antigen[92]. Low density expression ($CD56^{dim}$) represent around 90% of the NK cell population and produces low levels of cytokines but are highly cytotoxic. By contrast, high CD56 expressing NK cells ($CD56^{bright}$) are more immunomodulatory, produce high levels of cytokines and acquire cytotoxicity through time[93]. The role of NK cells in MS was identified through treatment with daclizumab, an anti-IL-2 monoclonal antibody. Daclizumab shows beneficial effects in relapsing-remitting MS, likely through its effects on NK cells[94]. $CD56^{bright}$ NK cells from MS patients show reduced inhibitory capacity toward autoreactive T cells, which may be due to NK cell dysfunction or loss of T cell sensitivity[95].

1.6.2.2 Mechanisms of immune cell infiltration

The CNS has historically been thought of as an immune-privileged organ, however this has later been refined to an immune-specialised organ. This is controlled by the BBB, which tightly regulates cell and macromolecule migration. Immune cells infiltrate the CNS by proceeding through a number of steps that allows them to slow down, roll along the epithelial layer and eventually migrate into the CNS parenchyma. In order to do this, leukocytes upregulate PSGL-1 and VLA-4, which can bind to P-selectin and VCAM-1 expressed on endothelial cells, respectively. This slows them down and allows them to roll along the epithelial layer. They are then activated by a number of chemokines and eventually arrested through the binding of VCAM-1 to VLA-4 and ICAM-1 to LFA-1. They then crawl to the preferred site of migration and cross the epithelial layer into CNS parenchyma[96]. Central inflammation is first detected in the

subarachnoid space. Previously peripherally activated CD4+ T cells are then reactivated by APCs through the presentation of major histocompatibility complex (MHC) class II-associated peptides. This results in T cell proliferation and aggregation[97] that subsequently triggers the production of soluble markers which promotes the recruitment of other inflammatory cells[98]. This inflammatory activation leads to eventual demyelination, axonal damage and present clinically as neurological deficits.

1.6.3 The role of CNS-resident cells

1.6.3.1 Microglia

Microglia are resident immune cells of the CNS that are vital for brain development and the formation of neuronal networks. Microglia play an important role in CNS injury through phagocytosis and removal of microbes, dead cells and protein aggregates. They also secrete many factors, including chemokines, cytokines and neurotrophins[99]. Microglia become activated in MS and lose their normal phenotype and release pro-inflammatory cytokines, proteinases and complement proteins. Activated microglia internalise myelin during periods of oligodendrocyte death and are involved in antigen presentation to T cells. Activated microglial chemokine release further attracts immune cells into the CNS and drives an inflammatory astrocyte phenotype[100].

Microglia are also one of the main sources of ROS in neuroinflammation. Microglia have high expression of antioxidant proteins so are largely protected against fluctuations in redox conditions[101]. Myeloperoxidase, a lysosomal peroxidase enzyme, is released by activated microglia, which oxidises Cl^- and converts hydrogen peroxide (H_2O_2) into the highly cytotoxic hypochlorous acid (HOCl). Age-dependent iron

accumulation in microglia is also exacerbated in MS lesions and a high number of these senescent microglia are found in MS lesions[102]. MS patient CSF samples show increased microglial markers and this correlates with disease severity[103]. Some MS therapies have been shown to influence microglial biology. IFNβ and glatiramer acetate decrease microglial activation[104]. Fingolimod reduces microglial TNFα, IL-1β and IL-6 expression by binding to the sphingosine-1-phosphate (S1P) receptor[105]. This likely contributes towards the therapeutic effect of fingolimod in MS as well as other disorders related to microglia activation[105,106].

1.6.3.2 Astrocytes

Astrocytes were classically thought of as the 'glue' of the CNS, simply holding neurons in place. However, astrocytes encompass a heterogeneous cell population with complex and diverse functions in both health and disease[107].

Physiologically, astrocytes not only provide structural support to CNS neurons, they provide energy to neurons through the astrocyte-neuron lactate shuttle. Their unique morphology and cell-cell contact through astrocytic end-feet allow astrocytes to detect and respond to changes in energy demand based on neuronal activity[108]. Astrocytes provide the most significant source of glycogen stores in the CNS that is able to sustain neuronal activity during periods of high neuronal activity[109]. Astrocytes are also able to influence synaptic plasticity by expressing a number of ion permeable channels and transporters. An increase in astrocytic intracellular calcium induces the release of 'gliotransmitters' that influence neuronal excitability and neurotransmitter release[110]. Cerebral blood flow is also tightly regulated by astrocytic end-feet that extend to make contact with the vasculature. This is modulated by neurotransmitter release, blood

glucose and oxygen concentration and gliotransmitter release, including nitric oxide (NO), prostaglandins and arachidonic acid[111]. Astrocytes also control water homeostasis through the expression of aquaporin-1 (AQP1) and AQP4 on astrocytic end-feet that contact epithelia via connexins and maintain fluid homeostasis[112].

The diverse physiological function of astrocytes means that their role is complex in response to injury and astrocytes significantly influence the innate immune response in MS. Following CNS injury, the glial response is shaped by the production of chemokines, cytokines, growth factors and ROS and this response can play both damaging and reparative roles.

Astrocytes can be broadly categorised into two main subtypes – fibrous and protoplasmic. Fibrous astrocytes have small cell bodies with an elongated morphology and are predominantly found in brain white matter. Protoplasmic astrocytes have increased primary processes with more branches and are primarily located in the grey matter[113]. Glial fibrillary acidic protein (GFAP) is a characteristic marker to immunologically identify astrocytes and expression patterns differ during injury. GFAP expression is positively correlated with astrocyte reactivity. Reactive GFAP+ astrocytes are found throughout the CNS in MS patients, particularly in active lesions. Chronic lesions still show GFAP+ astrocytes, mainly concentrated at the lesion edge, however GFAP expression is not as strong[114].

With disease progression, reactive astrocytes form a glial scar around the core of the demyelinated plaque[115]. These astrocytes upregulate tight junctions claudin 1 and claudin 4 on their processes and act as a physical barrier to limit damage to the

surrounding brain parenchyma[116,117]. This said, this is a non-supportive environment for tissue repair and OPCs are unable to migrate to these demyelinated sites[118]. However, more recent animal studies have shown that remyelination is still evident, even with the presence of a glial scar[119].

Astrocytic chemokine release attracts peripheral immune cells into the CNS through the secretion of IL-2, IL-10 and IL-8[120]. Cytokines secreted by astrocytes can also promote T cell differentiation into either a Th1 or Th17 cells. *In vitro* studies have shown that astrocytes can up-regulate IFNγ and IL-17 to induce the production of Th1 and Th17 cells, respectively[121]. Astrocytes also express B cell activating factor (BAFF), which plays an important role in B cell development, survival and immunoglobulin production[122].

Astrocytes are closely associated to the CNS vasculature and swollen astrocytic cell bodies and end-feet compromise BBB integrity. Furthermore, increased expression of vascular endothelial growth factor A (VEGF-A) in astrocytes induces downregulation of claudin-5 and occludin, further compromising BBB integrity[123]. Astrocytes further facilitate immune cell infiltration through regulating the expression of ICAM-1 on endothelial cells, which is a key adhesion molecule involved in immune cell transmigration[96,124,125].

Lastly, astrocytes can also exacerbate the immune response by exhibiting APC functions. Astrocyte cultures express MHC-II molecules following IFNγ stimulation[126]. However, their expression of co-stimulatory molecules is less clear though. Astrocytes have been shown to express co-stimulatory molecules CD80 and CD86 following IFNγ

treatment *in vitro*[127] as well as in chronic active lesions[128]. However, IFNγ stimulated human astrocytes are unable to induce the proliferation of T cells[129], so their role as APCs in MS lesions may not be as important as others.

1.6.4 Mechanisms of axonal loss and neurodegeneration

1.6.4.1 Neuropathological mechanisms leading to axonal and neuronal loss – demyelination, failure of remyelination and degeneration

Axonal and subsequent neuronal loss contributes towards neurological disability in MS. The mechanisms that lead to this degeneration are complex, however experimental interrogation using *in vivo* MS models, as well as analysis of MS patient post-mortem tissue has shed light on some of the key mechanisms that contribute towards this neuropathology. Transected axons are detected in MS brains and are identified by the presence of terminal axonal ovoids. Axonal transection disrupts transport along the axon and is positively correlated with immune cell number during periods of inflammatory disease[130]. Furthermore, axonal neurofilament phosphorylation contributes towards ovoid formation. Phosphorylation increases interfilament spacing and axonal diameter, leading to subsequent ovoid formation and eventual axonal loss[130]. Other neuropathological mechanisms include mitochondrial dysfunction leading to 'virtual hypoxia', due to an imbalance in neuronal energy supply and demand[140,141]. Following demyelination, axonal sodium channel redistribution significantly increases the energy demand for nerve conduction and compromises the capacity of mitochondrial ATP production. Additionally, energy supply is further compromised by the presence of oedema within the MS lesion, which blocks action potential generation and conduction. This depletion of energy supply further increases

neuronal susceptibility to extracellular stressors and contributes towards neuronal death and disease progression[142].

Although there is significant axonal loss during periods of disease, innate repair mechanisms can effectively remyelinate demyelinated axons during periods of disease remission to restore neuronal function. Oligodendrocyte progenitor cells (OPCs) that are abundantly present in the brain become activated, proportionally to the inflammatory reaction, and are able to migrate to the site of damage which is regulated by chemo-attractant factors[131]. The migrated OPCs subsequently differentiate into myelinating oligodendrocytes and remyelinate axons and form shadow plaques[132]. This remyelination process is extensive. A study analysing cerebral tissue of two post-mortem RRMS-SPMS patients found that approximately 73% of the 168 lesions analysed showed at least partial remyelination[133]. However, this remyelination process becomes less efficient with age and disease progression and the accumulation of axonal demyelination drives a neurodegenerative phenotype and the transition into progressive MS[15]. The mechanisms that drive this change in capacity to remyelinate are not fully clear and this remyelination failure may be due to OPC depletion and/or impairment of OPC migration or differentiation[134].

OPCs are still present in active MS lesions therefore the absence of factors necessary for remyelination or the presence of inhibitory factors may influence this change in remyelinating capacity[135,136]. The myelin sheath provides significant trophic and structural support, therefore demyelination leaves the axons susceptible to chronic injury[137,138]. Evidence for this comes from knock out mouse studies. Removal of oligodendrocyte proteins MAG or PLP results in late-onset axonal degeneration,

however does not affect the immediate process of myelination[139]. This research highlights that oligodendrocyte trophic support is needed for long-term axonal survival and the removal of this support leads to neuronal degeneration and the accumulation of neurological deficits.

1.6.4.2 Reactive oxygen species in multiple sclerosis

Reduction and oxidation (redox) reactions must be balanced in order to maintain intracellular equilibrium. Aberrant 'pro-oxidant- and 'anti-oxidant' reactions lead to oxidative stress and an increase in intracellular ROS. ROS are highly reactive radicals that, if not properly monitored, lead to cellular stress and eventual death. Examples of ROS include hydroxyl radicals, peroxides and superoxides.

Cells are equipped with their own defence mechanisms to protect against the deleterious effects of oxidative stress. One of the main ways is through the transcription factor nuclear factor erythroid 2–related factor 2 (Nrf2). During period of oxidative stress, Nrf2 targets genes that encode for antioxidant proteins and detoxifying enzymes including the activation of the glutathione and thioredoxin antioxidant system[143].

ROS contributes significantly towards MS lesion formation, tissue damage and disease progression. The aberrant adaptive immune response is strongly linked with ROS-mediated tissue injury. This is mediated by CNS-resident astrocytes and microglia, as well as infiltrating macrophages and immune cells. This is evidenced by the presence of oxidised lipids, proteins and DNA, such as malondialdehyde and oxidised phospholipids in active lesions, particularly on oligodendrocytes[144]. Neurons

have a particularly high energy demand, which is needed for action potential generation and propagation. Axonal demyelination, which is exacerbated by ROS, further increases this energy demand[145]. Mitochondria are particularly sensitive to these changes and an increase in oxidative stress changes neuronal metabolism, reducing ATP production and depleting neuronal energy supplies[146]. This imbalance in energy homeostasis, coupled with mitochondrial dysfunction observed in MS patients[147], drives neuronal death and neurodegeneration.

Tissue damage is further exacerbated during active demyelination through ROS release from infiltrating peripheral immune cells. The cytotoxic effects of NK cells and CD8 T cells are partly brought about through ROS production. Extracellular ROS release also plays an important role in MS pathology by increasing protein phosphorylation and activating transcription factors[148]. ROS are also critical for effector T cell function. An increase in intracellular ROS levels triggers the oxidative signal. Subsequent calcium influx drives a change in T cell gene expression, with increased expression of genes involved in the pro-inflammatory nuclear factor NF-κB pathway. However, this is a fine balance and a sustained increase leads to impaired activation and T cell apoptosis[144].

1.6.4.3 Excitotoxicity in multiple sclerosis

Glutamate is a non-essential amino acid that is the main excitatory neurotransmitter in the CNS. Glutamate receptors (GluRs) can be categorised into two main classes – ionotropic (iGluRs) and metabotropic (mGluRs)[149]. iGluRs can be classified into α-Amino-3-hydroxy-5-methyl-4-isoxazolepropionic acid (AMPA), kainate, and N-methyl-D-aspartate (NMDA) receptors[149].

NMDARs are ionic heteromeric transmembrane channels that are mainly expressed in the CNS, however expression is also observed in the heart[150], pancreatic-islet cells[151], immune cells[152] and bone cells[153]. Seven NMDAR subunits have been identified – NR1, NR2A-D and NR3A-B[154]. The NR1 subunit is critical for NMDAR function[154,155]. NR1 is encoded by a single gene, *grin1*, however splice variants generate at least 8 variants that influence the receptor function. All NMDARs contain two mandatory NR1 subunits and two of NR2A-D or NR3A-B subunits. NR2 and NR3 subunits add to the heterogeneity of NMDARs and influence ionic permeability[149,156,157]. NMDARs consists of external amino terminal domain (ATD), ligand binding domain (LBD), transmembrane domain (TMD) and intracellular carboxyl terminal domain (CTD)[158] (Figure 1.3).

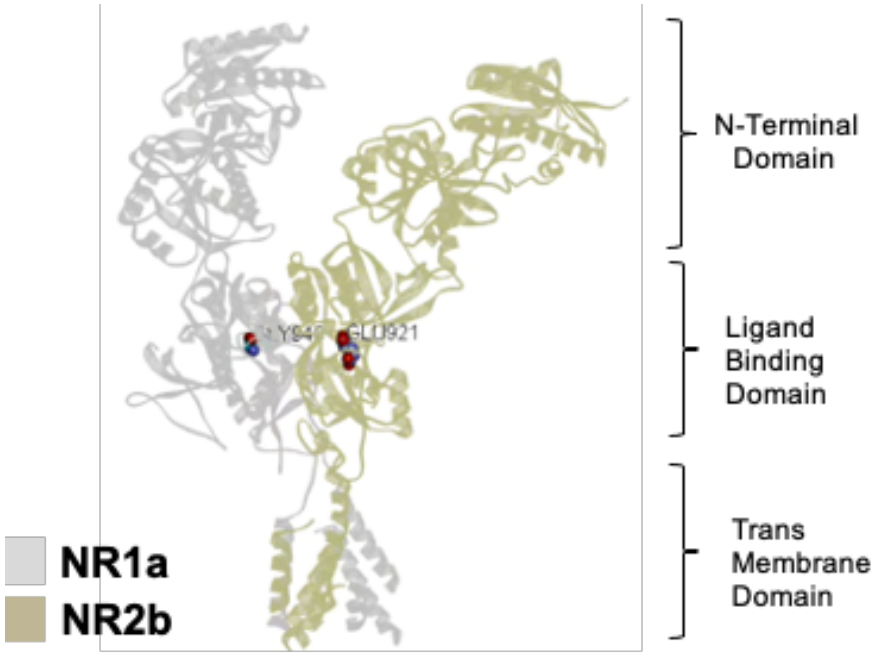

Figure 1.3 Structure of heterotetrameric NMDAR1.
Crystal structure of NR1a (grey) and NR2b (gold) subunits shows a heterotetrameric channel consisting of two NR1a subunits and two NR2b subunits. These come together and form modular domains that control channel function. PDB: 4PE5, Organism: *Rattus norvegicus*.

Binding of both glycine and glutamate to the NR1/NR3 and NR2 subunits, respectively, are required for channel activation[159]. At a resting membrane potential, a magnesium ion (Mg^{2+}) blocks the NMDAR channel pore. Membrane depolarisation of sufficient amplitude repels the Mg^{2+} ion from the pore, facilitating the flow of ions through the channel. Ion flux through NMDARs trigger specific intracellular signalling cascades, including activation of the mitogen-activated protein kinase (MAPK) Erk1/2, protein kinase C members and the phosphatidylinositol 3-kinase (PI3-K)–Akt pathways. This results in the activation of transcription factors and changes in gene expression involved in neuronal survival, plasticity and death[160]. In particular, increased intracellular calcium through NMDARs is required for long-term potentiation (LTP) and long-term depression (LTD)[161] and synaptic plasticity[162,163].

NMDARs are sensitive to small synaptic changes in glutamate as well as membrane depolarisation, therefore, it is paramount to tightly control intracellular and extracellular levels. Excess glutamate release can result in excitotoxic neuronal death, which is mainly mediated through excessive calcium entry through NMDARs[164,165]. Increased calcium influx activates a number of calcium-dependent enzymes, including calpains[166], calmodulin-dependent protein kinases (CaMKs) and calcineurins, which are all involved in calcium homeostasis maintenance[167]. Furthermore, calpain cleaves and activates Bid, a member of the pro-apoptotic BCl-2 family, ultimately facilitating excitotoxic-mediated cell death[168].

NMDA-induced excitotoxicity is widely used as a tool to study excitotoxic mechanisms through NMDARs[169–172]. NMDA-induced excitotoxicity causes significant loss of dendritic spines[173,174]. Interestingly, cortical neurons cultured from $NR1^{-/-}$ knockout

mice are resistant to NMDA-induced excitotoxicity[175]. Furthermore, suppression of NR1 expression with anti-sense oligonucleotide reduces excitotoxicity[176]. This data indicates a key role of the NR1 subunit in excitotoxicity. Excitotoxicity is linked to a number of neurological diseases, including Alzheimer's disease (AD)[177], ischaemic stroke[178], Huntington's[179], Parkinson's disease[180], neuropsychiatric disorders[181] and MS[174,182]. Evidence of glutamate dysregulation and excitotoxicity in MS comes from increased glutamate levels in the brain[183] and CSF[184] of patients. NMDAR expression is also increased in MS lesions[185]. This leaves NMDARs a valuable drug target for these neurological diseases[186].

1.7 Pre-clinical in vivo and in vitro models of multiple sclerosis

The utilisation of animal models of MS has been fundamental to further our understanding of the underlying mechanisms of MS pathogenesis and progression.

1.7.1 Experimental autoimmune encephalomyelitis (EAE)

The complex nature of MS means that it is difficult to fully replicate the human disorder using *in vivo* models, therefore a number of different models have been developed to mimic certain stages of the disease course. Myelin mutants and chemically-induced lesion models can be used to identify the processes involved in remyelination following oligodendrocyte insult. Viral and transgenic models are also used to investigate disease aetiology and genetic mechanisms[187]. Autoimmune models, including EAE, are used to study the neuroinflammatory and neurodegenerative mechanisms of MS[188].

EAE is the most commonly used animal model in MS drug research. A meta-analysis by Vesterinen and colleagues showed that out of 1152 publications that tested a drug intervention in an *in vivo* animal model of MS, 1117 used an EAE model and the majority of these were in mice (494/1152) or rats (481/1152). In turn, the EAE model has contributed towards the development of a number of first-line treatments[188].

EAE is an induced inflammatory disease of the CNS following the induction of an immune response against CNS specific antigens. The EAE disease course is influenced by a number of factors, including species, strain, sex and age. In general, the course of EAE can take either an acute, chronic progressive or relapsing-remitting pathology[189]. Each of these EAE models have their own advantages and limitations (summarised in Table 1.2). Therefore, these factors must be carefully considered throughout experimental design and the choice of EAE model is dependent on the experimental question at hand.

EAE can be induced in susceptible strains by using encephalitogenic peptides, such as MOG, PLP and MBP. These are usually emulsified in complete Freund's adjuvant (CFA) as well as Pertussis toxin which helps yield a high incidence of disease[190].

Table 1.2 Summary of the different models of experimental autoimmune encephalomyelitis.

Species/Strain	Encephalito-genic peptide	Disease Course	Pathological markers	Time Course – Days post immunisation (p.i.)	Advantages	Limitations	Reference
C57BL/6 Mouse	MOG_{35-55}	Acute, monophasic with a severe chronic phenotype	Lesions limited to spinal cord Marked axonal loss 7 p.i. Minimal demyelination CD4+ T cell driven, CD8+ and B cells play less of a role	9-14 p.i. - Clinical signs appear Partial recovery of symptoms over the next 10-20 days	Transgenic mice bred on C57BL/6 background Availability of research tools Widely used allowing greater comparison between studies Good for basic neuro-immunological questions	Use of adjuvant and pertussis toxin influences the immunological reaction Cannot be used to address neurodegenerative research questions	191,192
Biozzi ABH Mouse	SCH	Initial relapsing-remitting disease course Slowly develop secondary progressive disease	Marked demyelination, glial cell activation, gliosis and neuronal loss	16 p.i. – Disease onset Subsequent paralytic disease lasts approximately 6-9 days typically followed by 15-18 days of remission. 65-80 days p.i. – mice enter chronic phase of disease from which they do not recover	Slowly accumulate neurological deficit, useful to evaluate symptom development Ability to assess therapeutic agents in both the immune-mediated and progressive forms of disease	Chronic disease is not progressive but a stable level of moderate-high neurological disability is observed, not the progressive phenotype shown in human MS	193–197
SJL Mouse	$PLP_{139-151}$	Relapsing remitting disease course Chronic, with limited recovery	T lymphocyte infiltration into the brain and spinal cord Spinal cord demyelination and axonal damage	11-12 p.i. – Disease onset 20 p.i. – Peak of acute disease	Relapsing disease course allows for testing immunomodulatory strategies	Aggressive disease course, rapidly reaches experimental endpoint Variability in frequency of relapses	198–202
Lewis Rat	MBP_{68-86}	Acute onset followed by spontaneous recovery, resembling a relapse that is seen in clinical MS Following recovery, animals are resistant to re-induction of EAE	Lesions in the spinal cord and brain stem Lesions typically show oedema, mononuclear cell infiltration and gliosis, however demyelination is rarely seen	Encephalitogenic T cells are present 5 p.i. Spontaneous recovery within 5-7 days	Robust response to disease induction and lack of reliance on pertussis toxin to achieve disease	Demyelination and axonal loss does not occur	203–207
Dark Agouti Rat	SCH	Relapsing disease with spontaneous recovery	Mononuclear infiltration of the spinal cord at day 18 p.i.	9-15 p.i. – disease onset	Does not require adjuvant , decreasing variability Disease can be re-induced, although at a lower severity	No progressive phenotype	208
Non-human primate: Common Marmoset, Rhesus Macaque	MOG_{34-56}	Chronic disease course	Spinal cord demyelination Lesions infiltrated with T cells and macrophages that contain phagocytosed myelin debris	Paresis and paralysis eventually develops, although timing is highly variable	Genetic background more closely reflects humans Outbred nature also better reflects the heterogeneity seen in the MS population can be used to assess preclinical efficacy and safety	Ethical and legal implications Expensive Outbred	209,210

1.7.1.1 EAE – Pathological mechanisms

Years of accumulated research have identified the pathological mechanisms of EAE and how these may translate to MS. EAE was initially thought to be driven by Th1 cells. Early studies demonstrated that IFNγ significantly reduced neurological deficits and played a protective role in EAE[211]. This subsequently led to the clinical trial of IFNγ treatment in MS patients. However, it was found that IFNγ administration exacerbated the disease, so the trial was ended[212]. More recently researchers identified that IL-23, and not IL-12, was largely responsible for regulating EAE disease pathogenesis[213,214]. IL-23 drives naïve CD4 Th cell differentiation into Th17 cells, therefore research efforts switched focus to Th17 cells. Genetic deletion of IL-17A and IL-17F does not totally remove disease incidence[215], which suggests that although Th17 cells play a major role, other pathogenic mechanisms are involved.

Immunisation against a myelin peptide results in the activation of myelin antigen-specific T cells and their subsequent proliferation and differentiation into effector T cells. The expression of integrins on these effector T cells enables them to cross the blood-brain barrier BBB[216]. Once in the CNS they are re-activated by resident myelin APCs[217] which results in pro-inflammatory cytokine expression by effector T cells, namely IFNγ, IL-17, TNFα and GM-CSF. Furthermore, pathogenic chemokine production recruits T cells, macrophages, monocytes and neutrophils into the CNS[213,218] and these processes are largely responsible for the destruction of the myelin sheath and onset of neurological symptoms (Figure 1.4). The presenting neurological symptoms typically appear as ascending paralysis, starting at the tail, followed by the hind limbs and progressing onto the upper limbs[219].

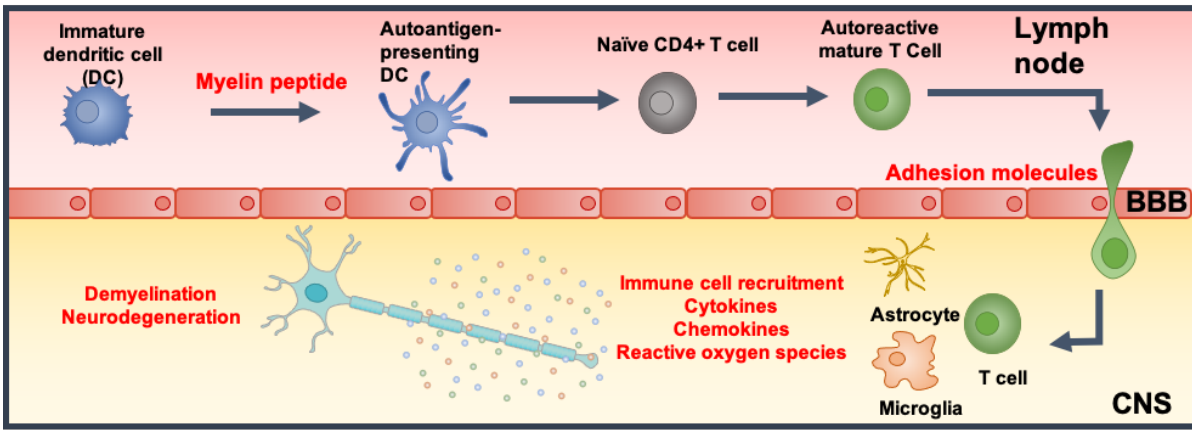

Figure 1.4 Immunopathology of EAE.
Immature dendritic cells become autoreactive through immunisation against a myelin peptide, which in turn activate self-reactive CD4+ T-cells in peripheral lymph nodes, resulting in their migration into the CNS. This is promoted by the expression of adhesion molecules on the epithelial cells of the BBB. Infiltrated T cells are then re-stimulated by resident APCs, including astrocytes or microglia. This is followed by microglia activation and the production of cytokines and chemokine, including TNF-α, IL-1β and IL-6, that cause damage to the myelin sheath. Chemoattractants and further BBB breakdown facilitates the recruitment of other immune cells, including B cells and CD8 T cells, into the CNS and further contributes to neuronal damage and the manifestation of neurological symptoms. Demyelination significantly increases the energy demand of neurons and failure to effectively remyelinate these axons results in neuronal death and neurodegeneration.

1.7.2 *In vitro* models of multiple sclerosis

In vitro and *ex vivo* models are also useful tools in pre-clinical research to interrogate specific pathways or mechanisms that play a role in disease pathology. Primary cell cultures are widely used throughout MS research and these include neuronal, astrocyte, microglia and oligodendrocyte cultures. These are cultured either individually or in a co-culture system to evaluate both cell-specific and cell-cell interactions[220]. The main advantage of utilising *in vitro* cultures is the high inter- and intra-experimental reproducibility and ability to produce robust assays. This said, protocol and user variability must be taken into account whilst comparing and analysing data sets.

Organotypic brain slice cultures (OSCs) are seen as a bridge between *in vitro* and *in vivo* models and offer a number of practical and ethical advantages over animal models. OSCs preserve the structural integrity of multiple cell types, thus maintaining synaptic connections and biological pathways. OSCs can be obtained from a number of brain regions, including spinal cord, cerebellum, hippocampus and forebrain[221]. Cerebellar slices are frequently used as an *ex vivo* model in MS research. The homogeneity of neuronal cell types and extensive myelination means that these are a useful tool to study demyelination and remyelination meachanisms[222].

1.8 Aims and hypotheses of the project

The mechanisms that lead to MS pathogenesis and progression are complex and not yet fully elucidated. As highlighted in Table 1.1., research has been focussed on developing therapies that target the immune system to limit immune cell migration and downstream tissue damage. Targeting other pathological mechanisms, including oxidative stress and excitotoxicity, is a promising therapeutic avenue to explore.

1.8.1 Aim 1 – Evaluate the therapeutic potential of carnosine in MS

L-carnosine (β-alanine-L-histidine) is an endogenous dipeptide found in a number of tissues throughout the body, including human cardiac and skeletal muscle and nervous tissue[223]. Two isomers exist of carnosine, the natural isomer L-carnosine and the non-natural isomer D-carnosine[224,225]. From herein, carnosine will refer to the natural isomer L-carnosine unless otherwise stated. Carnosine exhibits a number of biological properties, including radical species scavenging, heavy metal ion chelation, cytosolic buffering and anti-excitotoxic activity[226]. Initial experiments identified that carnosine is abundant in skeletal muscle, as well as other tissues, including the CNS.

These experiments found that skeletal muscle carnosine levels were significantly elevated in power athletes when compared to both endurance athletes and untrained controls and it was proposed that carnosine may act by delaying fatigue during high-intensity exercise[227]. More recent studies have demonstrated that free beta-alanine supplementation increases skeletal muscle carnosine levels and further improves exercise performance and capacity[228] likely through reduced lactate accumulation[229]. Endogenous CNS carnosine is found in less abundance than in skeletal tissue. The majority of CNS carnosine is synthesised in neuronal and glial cells, predominantly in olfactory receptor neurons, astrocytes and oligodendrocytes[230,231].

Reviews have highlighted the therapeutic potential of carnosine in neurodegenerative diseases[232]. Carnosine has diverse biological functions that make it a viable therapeutic candidate, including free radical scavenging, anti-excitotoxic and metal ion chelating activity[233–235], anti-aggregating effects[236], nitric oxide (NO) metabolism regulation[237], neurotransmission[238] and haematopoietic stem cell biology modulation[239]. These diverse functions shows that carnosine could play an important role in combatting pathological mechanisms involved in neurological diseases, including cerebral ischemia[240], Parkinson's disease[241] and Alzheimer's disease[242]. Carnosine is hydrophilic, well tolerated in mice and humans[234,243], easily absorbed in the digestive tract[244] and penetrates the BBB, thought to be through influencing matrix metalloproteinase activity[245]. Furthermore, carnosine is not toxic in the therapeutic ranges previously tested[243] and does not accumulate within the body's tissues due to its rapid hydrolysis by circulating carnosinases into beta-alanine and L-histidine[224].

Previous experiments and recently published data in our research group have demonstrated that carnosine is a powerful neuroprotective agent in the transient middle cerebral artery occlusion (tMCAO) mouse model of ischaemic stroke[240]. Other researchers hypothesise carnosine as a promising therapeutic option for obesity, type 2 diabetes and cardiovascular disease[246–248]. Evidence for the role of carnosine in MS is limited. Serum carnosinase activity[249] and muscle carnosine levels are decreased in MS patients compared to healthy controls[250]. Decreased muscle carnosine concentrations are also decreased in EAE, which is not restored through exercise[250]. Therapeutic dosing of carnosine in MS and EAE has not yet been explored.

Hypothesis 1: This thesis explores the hypothesis that carnosine administration will limit the disease-associated neurological deficits and disease-associated weight loss in the EAE animal model by reducing oxidative stress and excitotoxicity within the CNS.

The proceeding work will be broken down into the following specific aims for this chapter:

1) Characterise the antioxidant and anti-excitotoxic properties of carnosine in CNS-relevant cultures.
2) Evaluate carnosine efficacy using two animal models of MS:
    i. Biozzi ABH EAE model.
    ii. C57BL/6 MOG_{35-55} EAE model.

1.8.2 Aim 2 – Evaluate the efficacy of therapeutic vaccination against NMDAR1

Excitotoxicity is mediated by calcium permeable ionotropic glutamate receptors, mainly through NMDARs. Excessive calcium influx, specifically through NMDAR1, activates downstream calcium-dependent pathways that ultimately result in neuronal death. As discussed in Chapter 1.6.4.3, excitotoxicity exacerbates tissue damage in MS and EAE[182]. Targeting NMDAR1 through therapeutic vaccination may provide a viable option for reducing this cellular and tissue damage.

The therapeutic vaccine approach remains a largely unexplored avenue in CNS disorders. The term vaccination dates back to the 18th century when Edward Jenner used cowpox as a treatment for smallpox[251]. In the context of therapeutic vaccination and of this thesis, vaccination can be defined as 'the generation or induction of an immune response that is beneficial to the host in halting a pathological process'[252]. Therapeutic vaccines have been used in other CNS disorders, including Alzheimer's disease (AD) and MS. Active immunisation against amyloid-beta peptide[253] as well as passive infusion of antibodies targeting amyloid beta[254] cleared amyloid deposits in a mouse model of AD. Vaccination has also been used in rodent EAE models. Glatiramer acetate (GA) is a copolymer of four amino acids, initially designed to mimic MBP. GA administration reduces EAE severity, principally by eliciting a T_{reg} response[34]. Other clinical studies have aimed to 'vaccinate' against MBP by subcutaneously administering an MBP altered peptide ligand to mitigate the MBP specific T cell response. However, these studies were halted as this exacerbated disease symptoms[255]. Therapeutic vaccination against other pathological pathways may provide a prophylactic option for managing disease severity and progression.

Previous work in our lab aimed to design a therapeutic vaccine that would specifically target NMDAR1 as a neuroprotective strategy for ischaemic stroke. There is significant overlap between stroke and MS pathological mechanisms. These include BBB dysfunction, inflammation, cytokine and chemokine release, glial activation, excitotoxicity, oxidative stress, demyelination and neurodegeneration[256]. During the peptide design process, 18 peptide sequences were designed using an *in silico* screening assay to target different sections of the LBD of the NR1a subunit of NMDAR1 (Figure 1.5A). These peptide sequences were also virtually screened using an online B cell epitope prediction tool such that a significant antibody challenge is mounted. Peptide sequences were synthesised and conjugated to a Qb virus-like particles (Qb-VLP) so that an immune response could be induced against the peptide. VLPs are non-genetic multi-protein structures that can be utilised for vaccine development as they carry many viral characteristics and lack a viral genome, rendering them unable to replicate[257]. Qb-VLP comprises 180 subunits of the Qb capsid protein, forming an icosahedral shape and allowing presentation of multiple copies of the conjugated antigen[258]. VLPs can be produced in a number of expression hosts, including yeast and mammalian cells. However, the majority of VLPs are produced in bacterial systems, which generally give the highest yield. VLPs are small in size and are typically around 20 – 200 nm in size, allowing efficient migration and egress from the lymphoid tissues[259]. VLP conjugation has been proven to be a safe and effective method in humans to initiate an immune response against the presented antigen[260].

Subsequent serum immunogenicity towards each of the peptide sequences was determined via enzyme-linked immunosorbent assay (ELISA). Those serum samples that induced a significant immune response were screened in an *in* vitro cortical neuron excitotoxicity assay to quantify protection against NMDA-induced excitotoxicity. Serum samples that significantly reduced NMDA-induced excitotoxicity proceeded onto *in vivo* studies. Mice were immunised against each of the peptide sequences and neuroprotection assessed using the tMCAO mouse model of ischaemic stroke. From this efficacy screen, peptide 8 (Val 40, Lys 41, Lys 42, Val 43, Ise 44, Cys 45, Thr 46, Gly 47) significantly reduced infarct volume and improved functional outcomes, without showing any adverse effects. Interestingly, this effect was only seen using the peptide 8 epitope in comparison to sham mice and other sequences tested. Furthermore, epitope mapping performed on the peptide 8 sequence confirmed high sequence specificity of generated antibodies. This project aims to build on this work and will focus on determining the efficacy of peptide 8 immunisation in the EAE model and identifying the underlying mechanism(s) of any hypothesised efficacy.

Hypothesis 2 - Peptide 8 immunisation will limit the disease-associated neurological deficits and disease-associated weight loss in the EAE animal model by reducing calcium influx through NMDAR1 and thus reduce downstream excitotoxic pathways and therefore reduce overall neuronal damage.

To determine this, the proceeding work will be broken down into the following specific aims:

1) Characterise any behavioural changes in mice as a result of peptide 8 immunisation.
2) Determine if peptide 8 immunisation improves neurological outcomes in the C57BL/6 MOG_{35-55} EAE model.
3) Investigate the mechanism of action:
    iii. Use electrophysiology to study neuronal excitability following peptide 8 serum incubation.
    iv. Use immunocytochemistry to quantify neuronal NMDAR1 expression following peptide 8 serum incubation.
    v. Spinal cord analysis using western blot to investigate glial reactivity and NMDAR1 downstream pathways.
4) Determine gene expression signature changes following EAE induction and peptide 8 immunisation.

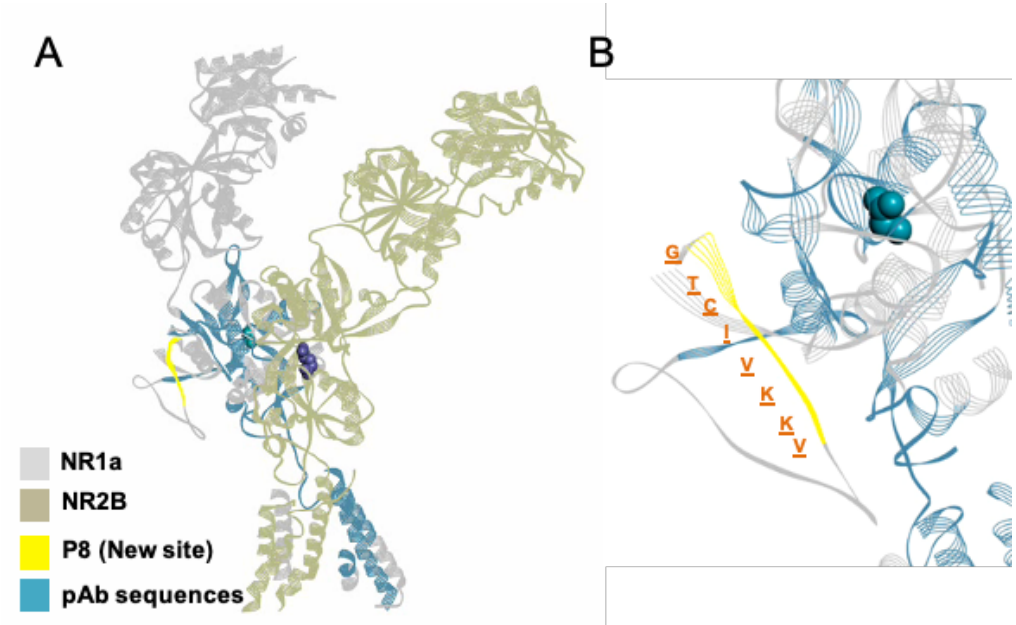

Figure 1.5 Peptide design and peptide 8 location on NMDAR1.
A) Crystal structure of NMDAR1 highlights short peptide sequences of the ligand binding domain that antibodies were designed to target. 18 peptide sequences were identified and synthesised to take forward for experimentation. Glycine (blue), glutamate (purple). B) Peptide 8 (labelled, yellow) immunisation elicited significant neuroprotection in comparison to sham and other sequences tested. The crystal structure highlights that the peptide 8 sequence is located near to the glycine binding site. PDB: 4PE5, Organism: *Rattus norvegicus*. Glycine (blue).

2 Materials and methods

2.1 Materials

All general materials were purchased from Thermo Fisher Scientific® Incorporated, unless otherwise stated. Materials and reagents can be found in Table 2.1. Solutions and dissection tools were autoclaved in the MP25 autoclave (Rodwell) at 121°C, 15 psi for 15 mins when required.

Table 2.1 Materials and reagents list.

Reagent category	Reagent	Supplier	Catalogue Number	Comments
In vitro	Oxoid™ Phosphate Buffered Saline Tablets	ThermoFisher Scientific	10209252	1X - 1 tablet in 100 ml dH2O
	HBSS-/-	Sigma Aldrich	55021C	
	Trypsin (2.5%), no phenol red	ThermoFisher Scientific	15090046	
	Deoxyribonuclease I	Sigma Aldrich	D5025	
	HBSS+/+	Sigma Aldrich	24020117	
	AlbuMax™	ThermoFisher Scientific	11020021	
	Trypsin inhibitor from Glycine max (soybean)	Sigma Aldrich	T9003	
	Poly-D-lysine	Sigma Aldrich	P7405	
	Neurobasal™ Medium	ThermoFisher Scientific	21103049	
	50X B27-supplement	ThermoFisher Scientific	17504044	
	Glutamax	ThermoFisher Scientific	35050061	
	Penicillin-Streptomycin	Lonza	17-602E	
	DMEM, high glucose, no glutamine	ThermoFisher Scientific	11960044	
	Tetracycline-free foetal bovine serum (FBS), South American origin, sterile filtered	Biosera	FB-1001T	
	L-carnosine	Sigma Aldrich	C9625	
	Pierce LDH Cytotoxicity Assay Kit	Sigma Aldrich	88953	
	N-Methyl-D-aspartic acid (NMDA) ≥98%	Sigma Aldrich	M3262	
	6-carboxy-2',7'-dichlorodihydrofluorescein diacetate (DCFDA)	ThermoFisher Scientific	C400	
	Paraformaldehyde	Sigma Aldrich	158127	4% in 1X PBS
	Bovine Serum Albumin	Sigma Aldrich	A7906	
	Triton™-X 100	Sigma Aldrich	X100	
	Millicell Cell Culture Insert	Merck	PICMORG50	
	Opti-MEM™	ThermoFisher Scientific	31985070	
	Horse Serum, heat inactivated, New Zealand origin	ThermoFisher Scientific	26050070	
	L-α-Lysophosphatidylcholine from egg yolk	Sigma Aldrich	L4129	
	Fluoromount™ Aqueous Mounting Medium	Sigma Aldrich	F4680	
Primary and secondary antibodies	Hoechst 33342	ThermoFisher Scientific	H3570	1 in 10,000
	Neurofilament H (NFH) antibody, Chicken	Merck	AB5539	1 in 1000
	Glial fibrillary acidic protein (GFAP) antibody, Rabbit	Agilent Technologies	Z0334	1 in 1000
	Myelin basic protein (MBP) antibody, Rat	Abcam	ab40390	1 in 500
	p44/42 MAPK (Erk1/2) antibody, Rabbit	Cell Signalling Technology	9102S	1 in 1000
	a-Tubulin, Mouse	Sigma Aldrich	T9026	1 in 10,000
	Goat Anti-Mouse IgG H&L (HRP)	Abcam	ab205719	1 in 2000
	Goat Anti-Rat IgG H&L (HRP)	Abcam	ab97057	1 in 2000
	Goat Anti-Rabbit IgG H&L (HRP)	Abcam	ab6721	1 in 2000
	Goat anti-Chicken IgY (H+L), Alexa Fluor 488	ThermoFisher Scientific	A11039	1 in 1000
	Goat anti-Rabbit IgG (H+L), Alexa Fluor 546	ThermoFisher Scientific	A11010	1 in 1000
In vivo	Sawdust - Eco-Pure Chips 6 Premium	Datesand Group	ECO6	
	Paper Wool	Datesand Group	CS1C00	
	Food pellets - Teklad global 18% protein	Envigo	2018S	
	HydroGel™	ClearH2O	70-01-5022	
	Incomplete Freund's adjuvant (IFA)	Sigma Aldrich	F5506	
	Mycobacterium tuberculosis H37 Ra	BD Difco	231141	
	Mycobacterium butyricum	BD Difco	264010	
	Myelin Oligodendrocyte Glycoprotein	RayBiotech	228-11133-2	
	Pertussis toxin (*Bordetella pertussis*)	Enzo Life Sciences	BML-G100	
	Fingolimod	Tocris	6176	
Molecular biology	Peptide 8	Mimotopes	N/A	Custom made
	Qb-VLP		N/A	Collaborator
	Dimethyl Sulfoxide (DMSO)	Sigma Aldrich	276855	
	SIGMAFAST™ OPD	Sigma Aldrich	P9187	
	Uric Acid	Sigma Aldrich	U2625	
	RIPA Lysis Buffer, 10X	Merck	20188	
	cOmplete™ Protease Inhibitor Cocktail	Merck	11697498001	
	PhosSTOP™	Sigma Aldrich	4906845001	
	Zirconium Oxide Beads 1.0 mm	Thistle Scientific	ZROB10	
	Pierce™ BCA Protein Assay Kit	ThermoFisher Scientific	23225	
	Prestained Protein Ladder (10 – 180 kDa)	Abcam	ab234617	
	PVDF Transfer Membrane	Merck	IPVH00010	
	Clarity™ ECL Western Blotting Substrates	Bio-Rad	1705060	
	TRIzol® reagent	ThermoFisher Scientific	15596026	
	Chloroform	Sigma Aldrich	C0549	
	Isopropanol	Sigma Aldrich	I9516	
	Ethanol	Sigma Aldrich	652261	
	nCounter® Mouse Neuroinflammation Panel	Nanostring Technologies	XT-CSO-MNROI1-12	

2.2 Methods

2.2.1 Cell culture methods

2.2.1.1 Primary mouse cortical neuron culture

C57BL/6 mice were bred at the Biological Services Unit. Pregnant female mice were culled by cervical dislocation in accordance with Schedule 1 procedure authorised by the UK Home Office. Cerebral cortices were isolated from embryonic day 14 (E14) embryos whilst submersed in cold $HBSS^{-/-}$. Meninges were removed manually using dissecting forceps and tissue was washed once in 10 ml $HBSS^{-/-}$ prior to resuspension in 5 ml $HBSS^{-/-}$. Trypsin was added to a final concentration of 0.025% and incubated for 13 minutes at 37°C to allow tissue dissociation. 5 ml DNAse solution (10 µg/ml DNAse in $HBSS^{+/+}$) was added for 2 minutes and supernatant aspirated. Tissue was resuspended in 1 ml triturating solution (1% albumax, 10 mg/ml trypsin inhibitor, 10 µg/ml DNAse) and triturated through flame-polished glass Pasteur pipettes with progressively smaller openings to obtain a single cell suspension. Cells were counted and plated on poly-D-lysine coated 96- and 24-well plates at a density of 4.5 million/plate in supplemented neurobasal media (1X B27-supplement, 1X GlutaMax, 50 U/mL penicillin-streptomycin) and maintained at 37°C and 5% CO_2. A half media change was conducted every 3-4 days until the day of experiment. Biological replicates from separate culture preparations were used to determine biological variability. Technical replicates were used to determine assay variability.

2.2.1.2 Primary mouse cortical astrocyte culture

C57BL/6 mice were bred at the Biological Services Unit. Postnatal day 2 pup mice were culled by intraperitoneal injection of pentobarbitone in accordance with Schedule 1 procedure authorised by the UK Home Office. Cerebral cortices were isolated from

postnatal day 2 (P2) pups whilst submersed in cold $HBSS^{-/-}$. Meninges were removed manually using dissecting forceps and transferred into 5 mL HBSS-/-. Trypsin was added to a final concentration of 0.025% and incubated for 13 minutes at 37°C to allow tissue dissociation. 5 ml DNAse solution (10 µg/ml DNAse in $HBSS^{+/+}$) was added for 2 minutes and supernatant aspirated. Tissue was resuspended in 1 ml triturating solution (1% albumax, 25 mg trypsin inhibitor, 10 µg/ml DNAse) and triturated using a 1ml pipette to obtain a single-cell suspension. Cells were washed and resuspended in supplemented DMEM (10% v/v FBS, 50 U/mL penicillin/streptomycin) and seeded in poly-D-lysine coated T-75 flask, 4 cortices per flask. Mixed glia were cultured for 10-14 days until confluence was reached. Oligodendrocyte progenitor cells (OPCs) and microglia were separated from confluent astrocytes by mechanical dissociation using an orbital shaker (200 rpm, 37°C, overnight). Confluent astrocytes were subsequently detached using trypsin-EDTA and either passaged or plated for further experiments. All astrocytes plated for experiment were used at 3 days post-passage.

2.2.2 *In vitro* assays

2.2.2.1 Carnosine cytotoxicity assay

Primary mouse cortical neurons were seeded in 24-well plates at a density of 4.5 million per plate. At 10-14 DIV, neurons were exposed to carnosine (0-30 mM) for 24 h and lactate dehydrogenase (LDH) release was measured using the Pierce LDH Cytotoxicity Assay Kit as per manufacturers' instructions. Absorbance was measured at 490 nm and 680 nm using a PHERAstar FS microplate reader (BMG Labtech Ltd.).

2.2.2.2 Excitotoxicity assay

Primary mouse cortical neurons were seeded in 24-well plates. At 10-14 DIV, cortical neurons were cultured in the presence of carnosine for 24 h. Neurons were subsequently exposed to 30 μM NMDA for 30 minutes. Wells were carefully washed in plain neurobasal media and supplemented neurobasal medium was replaced with ± L-carnosine (0-300 μM). LDH release was measured at 24 h with the Pierce LDH Cytotoxicity Assay Kit as per manufacturers' instructions. Absorbance was measured at 490 nm and 680 nm using a PHERAstar FS microplate reader (BMG Labtech Ltd.).

2.2.2.3 Reactive oxygen species (ROS) accumulation assay

ROS accumulation in primary cells was measured using the cell permeant dye 6-carboxy-2',7'-dichlorodihydrofluorescein diacetate (DCFDA). DCFDA (20 μM) was loaded in primary neurons or astrocytes for 45 minutes prior to induction of oxidative stress. Non-fluorescent DCFDA enters the cell and intracellular esterases remove the acetate group, leaving it negatively charged and unable to leave the cell. The molecule is converted to a green fluorescent form by oxidation within the cell, therefore intracellular ROS accumulation can be measured. Primary mouse neurons were seeded in 96-well plates and oxidative stress induced at 10-14 DIV by 24-hours B27-supplement withdrawal ± carnosine (0 – 300 μM). Oxidative stress was induced in primary mouse astrocytes, seeded in 96-well plates, by 24-hours serum withdrawal ± carnosine (0 – 1000 μM). The fluorescence of oxidised DCF was read at Ex/Em: ~492–495/517–527 nm using the PHERAstar FS microplate reader.

2.2.3 Immunocytochemical staining of primary cultures

Cells were fixed in 4% paraformaldehyde for 15 minutes and blocked for 1 h (3% BSA, 0.1% Triton-X) at room temperature. Primary antibodies (1:1000) were added in blocking solution and incubated at 4^{o}C overnight. Wells were washed in PBS and secondary antibodies (1:1000) and Hoechst (1:5000) added in blocking solution for 1 h at room temperature. 20x photomicrographs were taken using the InCell Analyzer 2000 and images were processed using ImageJ.

2.2.4 Organotypic cerebellar slice cultures

Cerebellar slices (300 µm) from P8-10 male and female C57BL/6 pups were prepared using the McIlwain Tissue Chopper. Slices were cultured on cell culture inserts (PICMORG50) with OSC medium (50% Opti-mem, 25% HBSS, 25% heat-inactivated horse serum, 2 mM Glutamax, 28 mM D-glucose, 50 U/mL penicillin/streptomycin, 25 mM HEPES). Cerebellar slices were demyelinated after 10 days in culture with lysophosphatidylcholine (LPC, 0.5 mg/ml) for 16 hr. Slices were washed and allowed to remyelinate for 3 days.

2.2.4.1 Immunocytochemical staining of brain slices

Slices were fixed in 4% paraformaldehyde for 45 minutes at RT. Slices were then blocked for 1 h (3% heat-inactivated horse serum, 2% bovine serum albumin and 0.5% Triton X-100 in PBS) at RT, prior to incubation overnight at 4^{o}C in primary antibodies myelin basic protein (MBP, 1:400) and neurofilament-H (NFH, 1:1000). Slices were washed and incubated overnight at 4^{o}C in the relevant secondary antibody (1:1000), mounted using fluoromount and imaged with a Leica TCS SP5 confocal microscope. Images were taken at 1 µm intervals over 10 µm, with up to 3 fields of view per slice.

2.2.4.2 ImageJ Co-localisation analysis of OSCs

Analysis methods were taken from Dombrowski et al[261]. First of all, each channel (MBP – red, NFH – green) was pre-processed by smoothing with a 3D isotropic Gaussian filter (sigma = 0.5 μm). Next, the background estimate was subtracted by applying a 3D morphological opening (filter radius = 1 μm). A threshold was then applied, which was automatically determined using the 'triangle' method in ImageJ (Min = 28, Max = 255). Co-localisation between the red and green channels was determined using the 'Just Another Colocalisation Plugin' (JACoP) plugin. Values were represented using the Manders' coefficient[262].

2.2.5 Experimental autoimmune encephalomyelitis

2.2.5.1 Ethics statement

All animal experiments were conducted under the terms of the UK Animals (Scientific Procedures) Act 1986 and under a UK Home Office project license. Mice were housed and cared for in accordance with the Home Office Code of Practice for Housing and Care of Animals used in Scientific Procedures. All procedures were conducted by personal license holders. We employed a double-blind randomisation process, where experimental groups were blind to the experimenter weighing, scoring the neurological behaviour and analysing the data. During experiments, mice were tail-marked or ear-clipped for identification.

2.2.5.2 Housing

Mice were housed in the conventional holding rooms, up to five per cage. The facility uses a 12 h light/dark cycle (on ay 7am/off at 7pm) and a room temperature of 21^{o}C.

A layer of fine sawdust and a small red plastic house was placed in each cage. Cages were environmentally enriched with tunnels and shredded paper. Mice were provided rodent diet and water *ad libitum*. During periods of disease, sawdust was replaced with a layer of paper towel to facilitate mice movement and access to water and food. Hydrogel and mashed food were provided on the cage floor *ad libitum*.

2.2.5.3 Biozzi ABH EAE model

Stock male and female Biozzi ABH mice were kindly provided by Professor David Baker, Queen Mary University London. Mice were housed at the Biological Services Unit and maintained by non-brother sister mating to mitigate genetic drift.

2.2.5.3.1 Preparation of spinal cord homogenate (SCH)

Adult male and female mice were sacrificed through an overdose of isoflurane and exsanguination. Spinal cords were immediately removed from the spinal column by hydraulic extrusion and homogenized using a 15 mL glass mortar and borosilicate glass pestle (GPE Scientific Ltd.). The mortar was sealed using parafilm and holes made in the top. The homogenate was then freeze-dried for 48 h using a 1.5 L microdulyo freeze drier until there was no visible sign of moisture. The freeze-dried spinal cord was transferred onto tin foil and made into a fine dust using a double-edge razor. This was then aliquoted and stored at -80^{o}C until preparation of the adjuvant.

2.2.5.3.2 Preparation of adjuvant containing SCH for subcutaneous injection

4 mL of incomplete Freund's adjuvant (IFA) was mixed with 16 mg *mycobacterium tuberculosis* and 2 mg *mycobacterium butyricum* – this was termed Stock A. To make the working solution, 1 mL of Stock A (vortexed before use) was added to 11.5 mL of IFA. This is termed completed Freund's adjuvant (CFA). To prepare the SCH emulsion, 5 mL of autoclaved PBS and 33 mg of SCH was added to a 20 mL syringe, covered in parafilm and vortexed gently. 5 mL of the CFA was added to the 20 mL syringe, covered in parafilm, vortexed gently and then sonicated for 10 minutes. To obtain a thick adjuvant, a 1 mL syringe was inserted into the 20 mL syringe and the adjuvant was pumped on ice for 20-25 minutes. The adjuvant was deemed thick enough when a drop did not disperse when added to water. 1 mL syringes were filled with the adjuvant and a 16 mm, 25G needle attached ready for injection.

2.2.5.3.3 Disease induction

6-8 week old male and female Biozzi ABH mice were used for experiment. 150 µL of the adjuvant was subcutaneously injected into left and right flank of each mouse. This was repeated on day 7, however in a more posterior position to the original injection site performed on day 0. Thus, each animal received a total of 1 mg spinal cord emulsified in Freund's adjuvant containing a total of 60 µG mycobacterium.

2.2.5.4 C57BL/6 EAE model

Female C57BL/6 mice (8-12 weeks old, 18-20g), were purchased from Charles River UK Ltd. and maintained at the Biological Services Unit.

2.2.5.4.1 Preparation of the MOG_{35-55} emulsion

Lyophilised MOG_{35-55} peptide (MEVGWYRSPFSRVVHLYRNGK) was diluted in ddH_2O to a final concentration of 2 mg/mL. 100 mg of desiccated mycobacterium tuberculosis was ground in a mortar and pestle to produce a thin powder. This was added to 10 mL of incomplete Freund's adjuvant (IFA), resulting in a 10 mg/mL complete Freund's adjuvant (CFA) stock solution. On the day of induction, stock CFA was further diluted in IFA to obtain a 2 mg/mL CFA solution. Next, 1 mL of the 2 mg/mL CFA and 1 mL of the 2 mg/mL MOG_{35-55} solution was taken up into two separate 2 mL syringes and connected to a three-way-valve. The emulsion was sent from one syringe to the other to mix thoroughly. Emulsification was performed for 15-20 minutes to obtain a thick adjuvant, such that a drop did not disperse in water and there was no separation of phases. 1 mL syringes were then filled to ensure accurate injection of the adjuvant and a 16 mm, 25G needle attached.

2.2.5.4.2 Preparation of Pertussis Toxin

50 µg of lyophilised pertussis toxin was reconstituted in 500 µL ddH_2O to obtain a 100 µG/mL stock solution. On the day of induction, the stock solution was diluted 1:50 in autoclaved PBS to obtain a 2 µG/mL solution. 1 mL syringes were filled and a 16 mm, 25G needle attached.

2.2.5.4.3 Disease induction

On day 0, mice were immunized through the subcutaneous injection of 100 µL of the MOG35-55/CFA emulsion into each hind flank and intraperitoneal injection of 200 µL of pertussis toxin. A second dose of pertussis toxin was administered on day 2. Thus, each mouse received 200 µG of the MOG_{35-55} peptide and a total of 800 ng pertussis

toxin. For the sham-immunised control group, the MOG_{35-55} peptide was removed from the adjuvant preparation. These mice still received the pertussis toxin injection.

The weight and neurological score of immunised animals were both assessed daily for signs of disease onset and progression (Table 2.2, Figure 2.1). Disease severity was scored using the following neurological scale:

Table 2.2 EAE neurological scoring criteria.

Score	Meaning	Description
0	**Normal**	
1	**Fully flaccid tail**	At this score, the tail is completely paralysed. If the tail does not lift, but has some tone, such that the tail can bend round finger, this is scored as 0.5. This is typical of animals in remission 1. This can be confirmed when the animal is scruffed by the neck and lifted, if the tail rotates, it is scored 0.5.
2	**Impaired righting reflex**	When the animal is turned on its back, it will not right itself. If it rights itself slowly, it will receive a score of 1.5.
3	**Hindlimb paresis**	Indicates significant loss of motor function of the hindlimbs. If the animals only have a hindlimb gait disturbance, they will receive a score of 2.5.
4	**Complete hindlimb paralysis**	Both hindlimbs are completely paralysed and are dragged behind the animal. If the limbs are virtually paralysed but have some minor movement, they will receive a score of 3.5.
5	**Moribund/death**	If the animals' forelimbs become paralysed in addition to the hindlimbs then the animal reaches an endpoint.

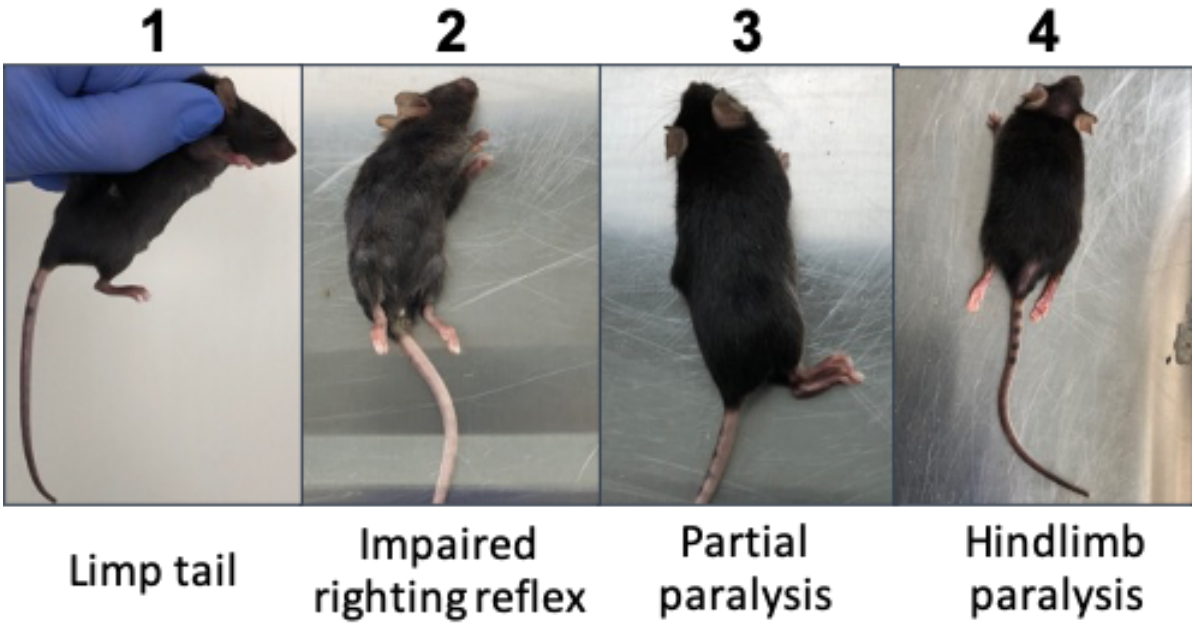

Figure 2.1 EAE neurological scoring and symptom comparison.

2.2.5.5 Carnosine efficacy in the Biozzi ABH and C57BL/6 MOG_{35-55} EAE models

Following disease induction, mice were daily administered L-carnosine (550 – 2000 mg/kg), fingolimod (3 mg/kg) or vehicle (water) control via oral gavage in a total volume of 100 µL.

2.2.5.6 Peptide 8-VLP conjugation

Peptide 8 was reconstituted in DMSO to a final concentration of 5 mM. 12.5 µL of peptide 8 was added to 50 µl Qb-VLP and left for 4 hours on the rotary shake to allow conjugation and 15 µl PBS was added to stop the reaction. Protein concentration of the P8-VLP and VLP-only were determined using the bicinchoninic acid (BCA) assay, as per manufacturers instructions. Peptide 8 conjugation to VLP was confirmed by running the samples through a 15% SDS-polyacrylamide gel – methods detailed below.

2.2.5.7 Peptide 8 immunisation

The peptide 8-VLP conjugate or VLP-only was diluted in PBS to a final concentration of 100 µg/ml. Following baseline behavioural measurements, 100 µl of P8-VLP or VLP-only solution was subcutaneously injected per mouse so that each mouse received a total of 10 µg of protein. Non-vaccinated mice received a PBS-only injection.

2.2.5.8 Behavioural assessment

2.2.5.8.1 Marble burying

Mice were individually placed in cages (19x33x21cm) filled with sawdust approximately 8-10 cm deep. 10 marbles were evenly placed on top in a 5x2 grid such that they don't disturb the sawdust (Figure 2.2A). Mice were left undisturbed for 30 minutes and then returned to their original housing cage. Marbles were included as 'buried' if over 2/3 of the marble was covered with sawdust.

2.2.5.8.2 Nest building

One 3g nestlet was placed into each cage and mice transferred and housed individually overnight (16 h), without any other source of enrichment (Figure 2.2B). Food and water was provided *ad libitum*. The following morning, nests were rated on a scale of 1 – 5 (Table 2.3).

Table 2.3 Nest building score criteria

Score	Description
1	Nestlet not noticeably touched (>90% nestlet intact).
2	Nestlet partially torn (50-90% intact).
3	Nestlet mostly shredded but often no identifiable nest site (<50% nestlet intact).
4	An identifiable but flat nest (<10% intact).
5	The nest is a crater with walls higher than the mouse body height (<10% intact)

2.2.5.8.3 Open-field test

Mice were placed in a 60x40x25 cm semi-transparent plastic box with a 3x5 grid drawn on the underside with permanent marker (Figure 2.2C). Open-field activity was recorded for 10 minutes in a semi-lit room. The number of new entrances, defined by all four paws entering a new square, was recorded.

2.2.5.8.4 Burrowing behaviour

Burrows were created by filling a 200x68 mm black plastic tube, sealed at one end, with 200 g food pellets and placed on the cage floor atop 1-2 cm sawdust (Figure 2.2D). Mice were transferred into the cage and left undisturbed for 3 h. Mice were then moved back to their home cage and the weight of food pellets displaced recorded. Mouse burrowing behaviour generally improves with practice[263], thus a practice run-through was observed before recording the first baseline measurement.

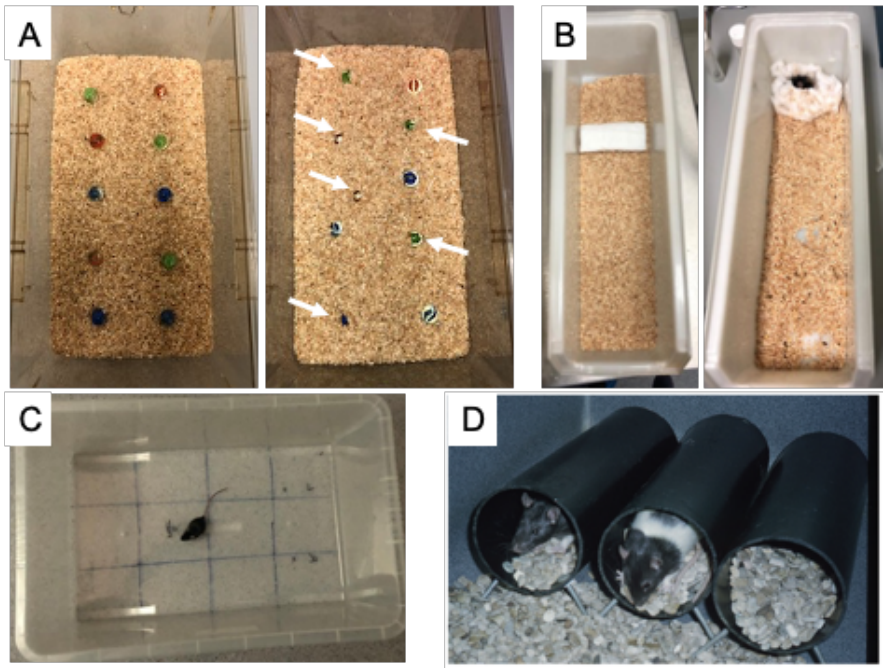

Figure 2.2 Behavioural assessment experimental setup
Example of behavioural assessment apparatus setup. A) Marble burying. Marbles counted if over 2/3 of the marble is buried (white arrow). B) nest building, C) open-field test and D) burrowing test, image from ref 244.

2.2.5.9 Peptide 8 efficacy in the C57BL/6 MOG35-55 EAE model

The peptide 8-VLP conjugate or VLP-only was diluted in PBS to a final concentration of 100 μg/ml. 2 weeks prior to disease induction, 100 μl of P8-VLP or VLP-only solution was subcutaneously injected per mouse so that each mouse received a total of 10 μg of protein. A second subcutaneous injection was given on the day of disease induction. For the non-vaccinated control group, mice received a PBS-only injection. Following

disease induction, weight and neurological score was recorded daily as previously described.

2.2.5.10 Tissue collection

At the end of the experimental procedure, mice were sacrificed through overdose of isoflurane and exsanguination. Tissue was rapidly collected, snap frozen in liquid nitrogen and stored at -80^{o}C for further analysis. Serum was obtained by collecting whole blood in a 1.5 mL Eppendorf tube and allowed to clot for 30-60 minutes. Samples were then centrifuged at 5,000 x g for 10 minutes and the supernatant transferred to a fresh tube and stored at -20^{o}C until further analysis.

2.2.6 Serum immunogenicity ELISA

The immune response was determined at 2 weeks after the first immunisation and again at the end of the study. Blood was collected through a tail-bleed, serum obtained and reactivity towards the peptide determined by ELISA. The stock 5 mM peptide 8 or VLP was diluted 1:500 in 0.05 M carbonate-bicarbonate coating buffer (pH 9.6) and 96-well plates coated at 4^{o}C overnight. Plates were washed 3x in 0.1% PBST and blocked for 1 h in 5% milk diluted in PBST. Diluted serum in milk was added (1:10, 1:20 and 1:40) and left to incubate for 2 hours at RT. Plates were again washed 3x in PBST and Anti-Mouse IgG-HRP secondary antibody in 5% milk added and left to incubate at RT for 1 hour. Plates were washed and OPD/Uric acid added (add one of each tablet to 20 ml water, 100 µL/well). The reaction was stopped by adding dilute HCL and absorbance quantified on the plate reader 492 nM absorbance.

2.2.7 Electrophysiology

Electrophysiology recordings and data analysis was performed by Dr. Ke Ning (University of Sheffield). Cortical neurons were plated onto 13mm glass coverslips and neuronal excitability was determined following overnight and 1 h incubation with serum isolated from non-vaccinated, VLP and peptide 8 immunised mice. All recordings were performed at room temperature and all reagents for solutions were purchased from Sigma. Electrodes for patch clamping were pulled on a Sutter P-97 horizontal puller (Sutter Instrument Company) from borosilicate glass capillaries (World Precision Instruments). Coverslips were placed into a bath on an upright microscope (Olympus) containing extracellular solution (150 mM NaCl, 5.4 mM KCl, 2 mM $MgCl_2$, 2 mM $CaCl_2$, 10 mM HEPES, 10 mM Glucose, osmolarity ~305 mOsm/Kg, pH 7.4). Whole-cell current clamp recordings were performed using an Axon Multi-Clamp 700B amplifier (Axon Instruments, Sunnyvale, CA, USA) using unpolished borosilicate pipettes placed at the cell soma. Pipettes had a resistance of 4-6MΩ when filled with intracellular solution (140mM K^+-gluconate, 10 mM KCl, 1 mM $MgCl_2$, 0.2mM EGTA, 9 mM NaCl, 10 mM HEPES, 0.3 mM Na^+-GTP, 3 mM Na^+-ATP, osmolarity 298 mOsm/Kg, pH 7.4. For both solutions the glucose, EGTA, Na^+-GTP, and Na^+-ATP were added fresh on each day of the experiment. To identify neurons, cells were visualised using the microscopes 40X objective, and those neurons with a triangular cell body were processed to indicate neuronal morphology were selected. The depolarised evoked action potential firing was measured in the cells using a 15-step protocol, for a duration of 500 miliseconds, injecting current from -80pA, every 10pA. Recordings were acquired at ≥10 kHz using a Digidata 1440A analogue-to-digital board and pClamp10 software (Axon Instruments). Electrophysiological data were

analysed using Clampfit10 software (Axon Instruments). A firing magnitude of 20 mV and higher was included for analysis.

2.2.8 Western Blot

2.2.8.1 Sample preparation

Spinal cords were isolated and protein extracted from the experimental groups defined in Table 2.4. Lumbar and cervical spinal cord sections were immersed in 1X RIPA buffer, 1X cOmplete protease inhibitor cocktail and 1X PhosStop phosphatase inhibitor at a ratio of 30 mg tissue per 150 μl and kept on ice throughout. 5-10 zirconium oxide beads were added per tube and tissue homogenised using the Precellys® Evolution homogeniser. Tubes were centrifuged at 10,000 x g for 30 minutes to pellet the tissue and beads, supernatant was transferred to an sterile Eppendorf tubes and protein concentration was determined using the Pierce BCA Protein Assay Kit as per manufacturers' instructions.

Table 2.4 Experimental groups for western blot and gene expression analysis

Experimental group	EAE induction?	Experimental details
Age-matched control	✗	No disease induction Tissue isolated at the same timepoint
Sham	✗	No disease induction Mice injected with complete Freund's adjuvant (CFA), but no MOG_{35-55}
Non-vaccinated (NV)	✓	EAE induction Vehicle injection only
Virus-like protein (VLP)	✓	EAE induction Non-conjugated VLP injection
Peptide 8 immunised (P8)	✓	EAE induction Peptide 8 immunisation

2.2.8.2 Electrophoresis for proteins using SDS-PAGE

Resolving gels were prepared to the desired acrylamide percentage (w/v) using a Mini-PROTEAN Electrophoresis cell (Table 2.5). Cell lysates were mixed with 4X Laemmli buffer (228 mM Tris-HCl, 28% v/v glycerol, 277 mM SDS, 0.038% w/v bromophenol blue, 5% v/v β-mercaptoethanol, pH 6.8) and boiled for 10 minutes at 95^{o}C to denature the proteins. 12% or 15% SDS-polyacrylamide gels were mounted into a Mini-PROTEAN® Tetra Vertical Electrophoresis Cell (Bio-Rad) and subsequently filled with 1X running buffer (25 mM Tris, 3.5 mM SDS. 20 mM glycine) and 20 µG of denatured protein sample was loaded per well. 2 µL pre-stained protein ladder was also loaded as a molecular weight marker. Gel electrophoresis was conducted at 100 V for 90-120 minutes until the dye front had run from the bottom of the gel. Gels were removed from the electrophoresis cell and assembled into the transfer cassettes alongside methanol-soaked polyvinylidene difluoride (PVDF) membrane and Whatman paper, loaded into the transfer cassettes and placed in the tank filled with transfer buffer (25 mM Tris, 192 mM glycine, 20% v/v methanol, pH 8.3) and an ice block. Electrophoretic transfer of the proteins was performed at 100 V for 1 h.

Table 2.5 Composition of stacking and resolving gels

Reagent	Stacking gel (ml)	Resolving gel (ml)	
		12%	15%
H2O	1.4	3.3	2.3
30% acrylamide mix	0.33	4	5
Tris-Cl (1.5 M, pH 8.8)	-	2.5	2.5
Tris-Cl (1.0 M, pH 6.8)	0.25	X	X
SDS (10%)	0.02	0.1	0.1
10% ammonium persulfate	0.02	0.1	0.1
TEMED	0.002	0.004	0.004
Total Volume	**2 ml**	**10 ml**	**10 ml**

2.2.8.3 Detection of protein

Transferred proteins were blocked (5% Milk diluted in TBS-T) for 1 h and then incubated overnight at 4°C in primary antibody diluted in blocking solution. The membrane was washed 3x for 10 minutes in TBS-T and incubated in secondary antibody for 2 h at room temperature. Membranes were again washed 3x for 10 minutes in TBS-T. Visualisation of immunoreactivity was conducted using ECL according to manufacturers instructions using the Li-Cor Odyssey Fc Imaging System. Images were compiled and band signal intensity determined using ImageStudio™ Lite Software.

2.2.9 Gene Expression Profiling

2.2.9.1 RNA extraction

RNA was extracted from thoracic spinal cord as described by Toni et al[264] from 4 different experimental groups – AMC, NV, VLP and P8 (detailed in table 2.3). Samples were placed into a 1.5 ml Eppendorf tube and 500 µL of Tri-Reagent® was added. Samples were let sit at RT for 3 minutes before being passed through a 25G needle to homogenise the tissue. 100 µL RNase-free chloroform was added to each sample and tubes were shaken vigorously for 15 seconds. Samples were let sit at RT for 3 minutes and then centrifuges at 4°C, 12,000xg for 15 minutes. 100 µL chloroform was added to a separate tube and the RNA-containing upper aqueous phase was transferred into the chloroform. Samples were shaken vigorously for 15 seconds, let sit at RT for 3 minutes and again centrifuged at 4°C, 12,000xg for 15 minutes. 250 µL RNase-free isopropanol was added to a separate tube and the RNA-containing upper aqueous phase was transferred into the isopropanol. Tubes were inverted 15 times

and let sit at RT for 10 minutes, then centrifuged at 4°C, 12,000xg for 10 minutes to precipitate and pellet RNA. Supernatant was discarded and 1 ml 75% ethanol in nuclease-free water added. Samples were centrifuged at 4°C, 7,500xg for 5 minutes to wash the RNA pellet. This RNA wash was repeated three times in total. After the final wash, samples were pulse-spinned and any remaining ethanol carefully removed with a 10 µL pipette. Tubes were left open at RT for 3 minutes and heated at 65°C for a further 3 minutes to evaporate any remaining ethanol. 20 µL of nuclease-free water was added to each RNA pellet, samples vortexed for 5-10 seconds to solubilise the RNA and stored at -80°C.

2.2.9.2 RNA Yield and Quality Assessment

RNA quantity and purity was assessed using the Nanodrop™ 1000 Spectrophotometer. RNA integrity was further determined using a Total RNA Nanochip on the Agilent 2100 Bioanalyser to assess 18S and 28S peaks, RNA degradation and provide an RNA Integrity Number (RIN).

2.2.9.3 Sample hybridisation

RNA samples were diluted to a final concentration of 20 ng/µL in a total volume of 5 µL. A hybridisation Master Mix was prepared by adding 70 µL hybridisation buffer to the Reporter CodeSet tube. The tube was inverted and briefly spun down. Hybridisation reactions were prepared by adding 8 µL Master Mix, 5 µL diluted RNA sample (100 ng in total) and 2 µL Capture ProbeSet (total volume 15 µL per sample). Tubes were inverted and briefly spun down and placed in a pre-heated 65°C thermal cycler for 19 h to let the probes hybridise to the target sequences.

Following the 19 h incubation, 15 µL RNase-free water was added to each tube to bring the total sample volume to 30 µL. The Nanostring nCounter Neuroinflammation Panel cartridge was brought to room temperature and samples were loaded. The sample port was sealed with a transparent seal and cartridge put into the SPRINT analyser for gene expression detection and quantification.

2.2.9.4 Bioinformatic analysis

2.2.9.4.1 Quality control and data normalisation

Gene CodeSets, reporter code counts (RCC) and the corresponding mouse neuroinflammation reporter library file (RLF) were loaded into nSolver Analysis Software 4.0. Firstly, quality control (QC) checks were performed to evaluate overall assay performance. Imaging QC was evaluated by reporting the field of view (FOV) number, defined as the number of FOVs successfully imaged. FOV counts lower than 75% were flagged for further inspection. Binding density QC determines the level of image saturation. A binding density outside the acceptable range of 0.1 – 1.8 were flagged for further inspection. 6 synthetic internal positive control targets are included within the gene CodeSet to measure efficiency of the hybridisation. Positive control probes A-F (0.125 fM – 128 fM) were also evaluated to check the linearity performance of the assay. 8 negative control probes are included which are not present in biological samples, which was used to determine non-specific counting.

Data normalisation was performed to minimise sources of technical variability. 13 housekeeping mRNA targets are included in the CodeSet that are known to show little-to-no variability in expression across treatment groups. These values therefore correlate with how much sample RNA was loaded. Housekeeping normalisation flags

were generated should there be an unexpectedly low gene count, which may be a result of pipetting errors, inaccurate quantification or sample degradation. Housekeeping target expression whose expression does not correlate with other housekeeping genes were excluded from normalisation, as determined by the geNorm algorithm described in the *nSolver Advanced Analysis User Manual*. Briefly, raw log counts were plotted against the raw log mean of these housekeeping probes. A large deviation from the expected line of sole 1 indicates poor normalisation quality.

2.2.9.4.2 Differential Expression Analysis

Differential expression analysis was performed to identify specific gene targets that were significantly increase or decreased between treatment groups. Volcano plots were generated by plotting -log10(p-value) against log2(fold change) with respect to the peptide 8 treated group. This identified significant differentially expressed genes between the peptide 8 group and other experimental groups - AMC, NV and VLP. Significance was determined following a Benjamini-Yekutieli p-value adjustment to minimise False Discover Rate (FDR).

2.2.10 Statistics

Data was compiled and statistically analysed using GraphPad Prism 8 software (GraphPad Software, San Diego, CA, US) with specific statistical test detailed in the figure legend. Power analysis was carried out using G*Power Version 3.1.9.6.[265] using a student's t-test, two-tailed, $\alpha = 0.05$, $\beta = 0.8$.

3 Evaluation of carnosine as a therapeutic candidate for multiple sclerosis

3.1 Introduction

As previously discussed in Chapter 1.8, carnosine is a viable therapeutic candidate for MS. The first aim of the project was to characterise the cellular specific anti-excitotoxic and antioxidant properties of carnosine in CNS-relevant cultures. To build on these cell studies, organotypic slice cultures (OSCs) were utilised to study if carnosine influenced remyelination following LPC-induced remyelination. Lastly, the effect of carnosine treatment on Biozzi ABH and C57BL/6 MOG_{35-55} EAE disease outcomes was evaluated, as determined by measuring neurological scores and disease-associated weight loss.

3.2 Aims and objectives

1) Characterise the *in vitro* properties of carnosine in CNS-relevant cultures. This will be divided into three main objectives:
    a. Characterise any cytotoxic effects of carnosine alone.
    b. Elucidate the protective effects of carnosine against excitotoxic damage and oxidative stress.
    c. Evaluate whether carnosine promotes remyelination using organotypic cerebellar slice cultures.
2) Evaluate carnosine efficacy using two animal models of MS:
    a. Biozzi ABH EAE model.
    b. C57BL/6 MOG_{35-55} EAE model.

3.3 Results

3.3.1 In vitro characterisation of carnosine

3.3.1.1 Carnosine is not cytotoxic towards primary mouse cortical neurons

Primary mouse cortical neuron and astrocyte cultures were first of all optimised to ensure high cell purity and significant axonal formation, which was important for proposed excitotoxicity studies. Representative immunocytochemical images show that primary astrocyte and neuronal cultures were highly pure and neuronal cultures had branched axons at 10 DIV, demonstrated by neurofilament staining (Figure 3.1A-B). The first *in vitro* aim was to determine any cytotoxic properties of high concentrations of carnosine using primary mouse cortical neuronal cultures. These cultures were chosen as they are CNS-relevant, widely used in neuroscience research and can be used for a wide variety of applications, including calcium imaging, electrophysiology and immunostaining.

Carnosine (0 – 30 mM) was directly added into the culture media. Cytotoxicity was quantified by measuring lactate dehydrogenase (LDH) levels in the media at 24 h. Carnosine did not show any cytotoxic properties when added to the cell culture media. Furthermore, higher concentrations of carnosine showed a trend in reducing basal cytotoxicity - absorbance values for 30 mM carnosine were 0.071 ± 0.014 compared to a value of 0.084 ± 0.017 for 0 mM carnosine (Figure 3.1). This demonstrates that high concentrations of carnosine do not affect the viability of the neuronal cultures. This was important to demonstrate before moving forward with the proposed excitotoxicity and ROS accumulation assays.

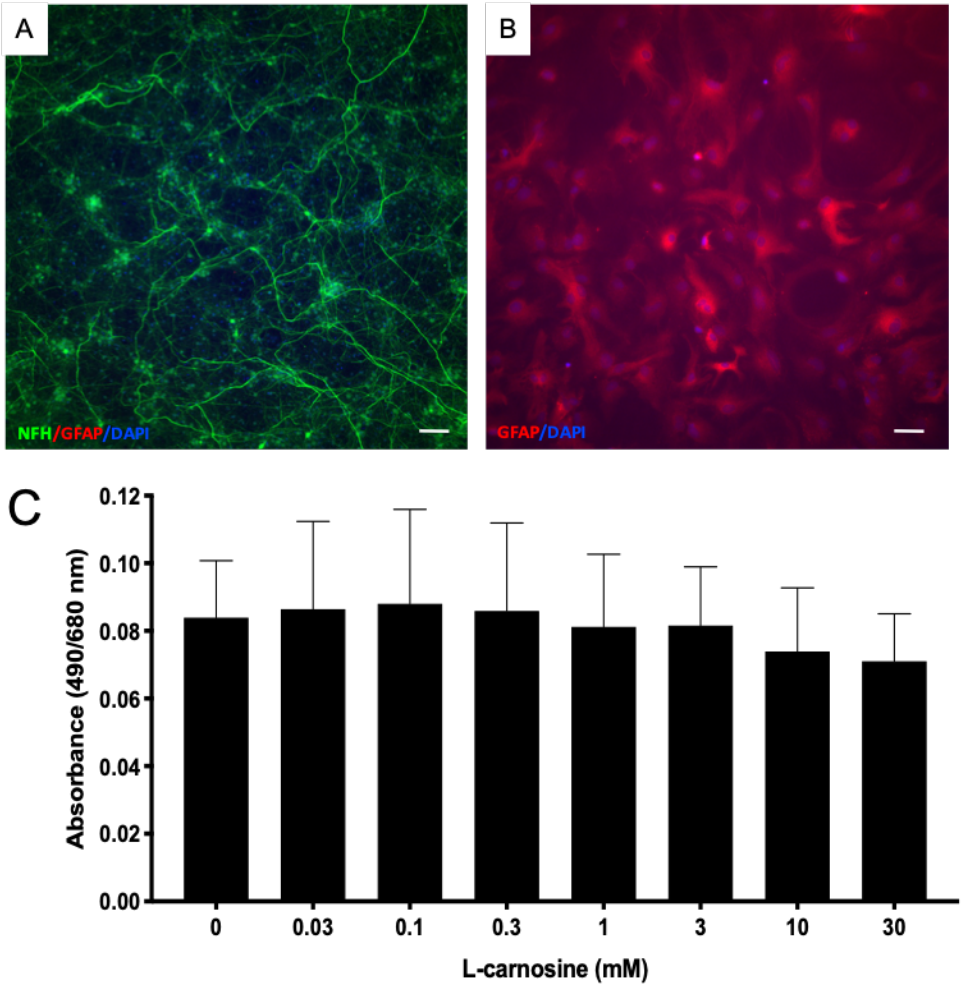

Figure 3.1 Carnosine shows no cytotoxic effects towards primary mouse neurons.
A) Primary mouse cortical neurons (10 DIV) and B) astrocytes (3 days post-passage) were cultured and cell populations characterised for purity. Representative image, scale bar = 100 µm. C) Primary mouse cortical neurons (10-14 DIV) were cultured for 24 hours in the present of L-carnosine (0 – 30 mM) and cytotoxicity measured using the LDH assay. Data represented as mean ± SD, n=2 experiments, 3 wells/condition/experiment..

3.3.1.2 Carnosine reduces NMDA-induced excitotoxicity in primary mouse cortical neurons

Initially, an LDH assay was performed on neurons exposed to increasing doses of N-methyl-D-aspartate (NMDA). This was to determine the range of NMDA concentrations that induce significant, but not lethal, excitotoxic damage. Neurons were exposed to NMDA (0 – 1000 μM) for 30 minutes and the LDH levels in the media was measured at 24 h.

NMDA exposure significantly increased LDH levels in the cell culture media in a dose-dependent manner (Figure 3.2A). LDH absorbance values increased from 0.080 ± 0.002 (0 μM NMDA) and LDH release peaked at around 100 μM NMDA with an absorbance of 0.391 ± 0.135 and did not further increase at higher doses of NMDA. For future experiments it was determined that 30 minutes exposure to 30 μM NMDA would provide a sufficient window to evaluate any anti-excitotoxic effects of carnosine. Thus, neurons were incubated for 24 h in the presence of carnosine (0 – 300 μM) and then exposed to 30 μM NMDA for 30 minutes. Wells were washed and media replaced ± carnosine (0 – 300 μM). Absorbance values at 24 h were greatly increased following NMDA exposure and absorbance values increased from 0.0978 ± 0.032 (0 μM NMDA) to 0.2697 ± 0.0811 (30 μM NMDA, 0 μM carnosine). This increase in absorbance was in line with the previous dose-response experiment and gave a sufficient experimental window (Figure 3.2B). The raw absorbance data was then normalised by subtracting the average '0 μM NMDA' absorbance from each individual value to remove background absorbance values. These values were then expressed as a percentage relative to the 0μM L-carnosine control. Incubation with 300 μM carnosine significantly

reduced NMDA-induced excitotoxicity, 100 ± 5.037% (0 μM carnosine) v 87.9 ± 6.67% (300 μM L-carnosine, *P = 0.0307) (Figure 3.2C).

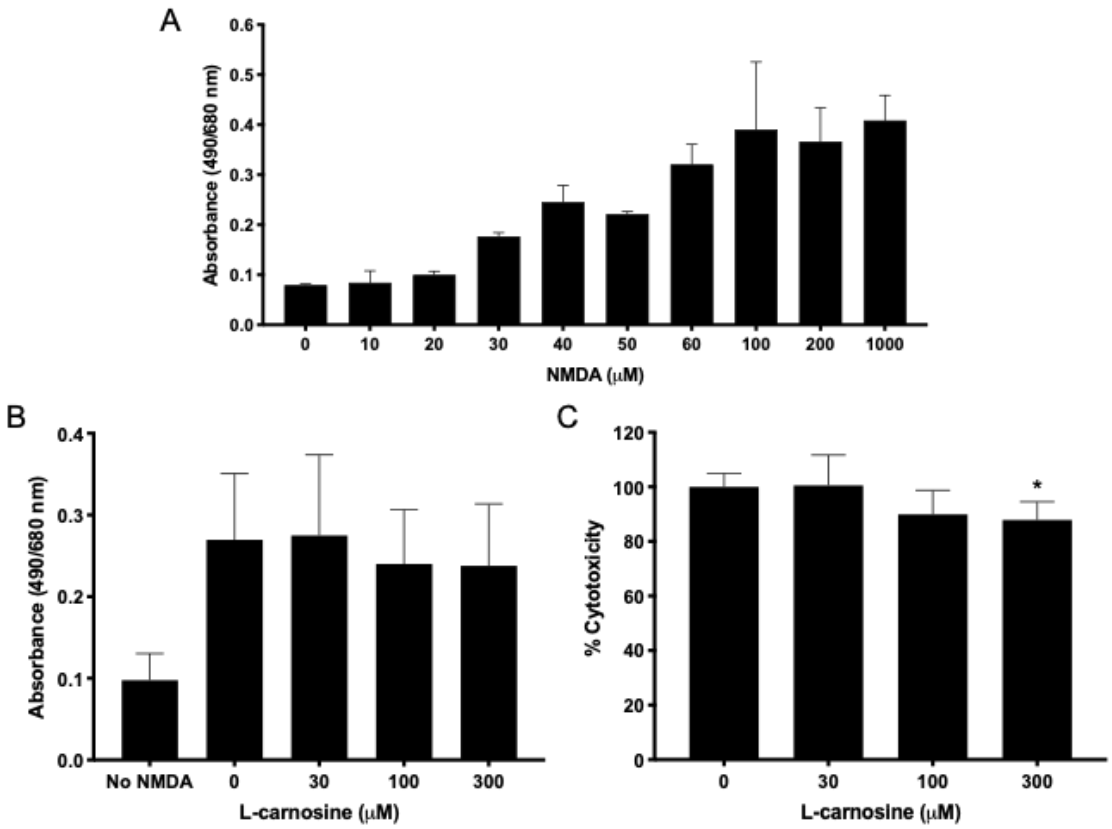

Figure 3.2 Anti-excitotoxic effects of carnosine in mouse cortical neuron cultures.
A) 24 h LDH absorbance values of neurons stimulated with NMDA (0 – 100 μM) for 30 minutes. n = 2 biological replicates from separate culture preparations, n = 3 wells/condition/experiment. B) 24 h LDH absorbance values of neurons pre-incubated with carnosine (0 – 300 μM), stimulated with 30 minutes exposure to 30 μM NMDA and media replaced ± carnosine (0 – 300 μM). n = 4 biological replicates, n = 3 wells/condition/experiment. C) Data normalised to 0 μM L-carnosine control. *P < 0.05 v 0 μM L-carnosine, one-way ANOVA with Tukey's multiple comparison test. All data presented as mean ± SD.

3.3.1.3 Carnosine reduces reactive oxygen species (ROS) accumulation in primary mouse cortical neurons

The cell permeant dye 6-carboxy-2',7'-dichlorodihydrofluorescein diacetate (DCFDA) diffuses through the plasma membrane and is deacetylated by intracellular esterases to make DCF. The removal of this acetyl group makes the compound lipid impermeant and therefore trapping it within the cell. The presence of intracellular ROS activates the DCF compound to make it fluoresce. Therefore, DCF is a measure of intracellular ROS accumulation.

Neurons were loaded with DCFDA (20 μM) for 45 minutes, wells washed to remove any excess DCFDA and media replaced without B27-supplement to facilitate ROS accumulation ± carnosine (0 – 300 μM). Fluorescence intensity was measured at 24 h. ROS accumulation was greatly increased following B27-supplement removal. Fluorescence intensity increased from 13734 ± 313 (with B27-supplement present in the media) to 38363 ± 6770 (no B27-supplement, 0 μM carnosine), evidencing that B27-supplement removal is sufficient enough to induce significant ROS accumulation within the cell (Figure 3.3A). The raw fluorescence intensity data was then normalised by subtracting the average control absorbance (with B27 present in the media) from each individual value to remove background measurements. Each value was then expressed as a percentage relative to the average 0 μM carnosine value. ROS accumulation was significantly reduced in the presence of 30 μM carnosine (66.48 ± 15.83%, *P = 0.0226), 100 μM carnosine (70.68 ± 14.89%, *P = 0.043) and 300 μM carnosine (67.48 ± 19.15%, *P = 0.0266) when compared to the control (0 μM carnosine, 100 ± 25.19%) (Figure 3.3B).

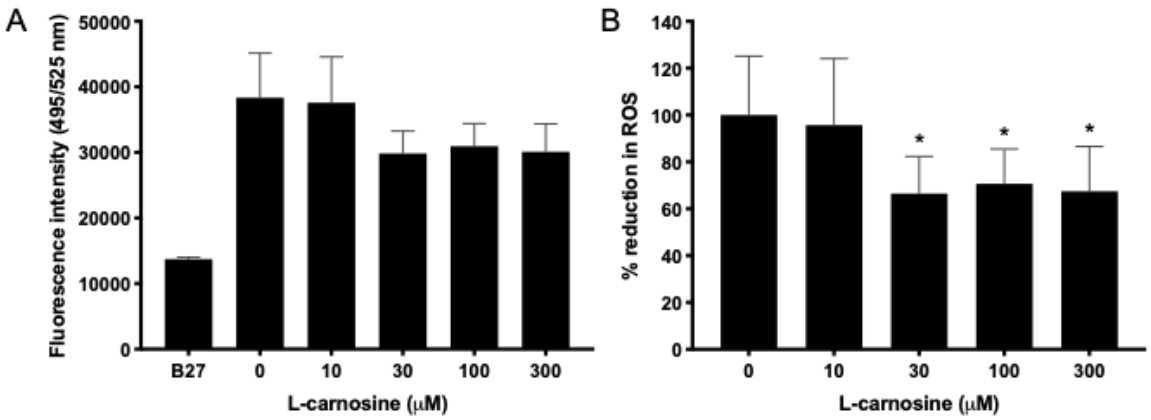

Figure 3.3 Antioxidant properties of carnosine in mouse cortical neurons. A) Fluorescence intensity measurements in neurons following 24 h B27-supplement withdrawal ± carnosine (0 – 300 μM). n = 4 biological replicates from separate culture preparations, n = 8-10 wells/condition/experiment. B) Data normalised to 0 μM carnosine control. *P < 0.05 v 0 μM carnosine control, one-way ANOVA with Tukey's multiple comparison test. All data presented as mean ± SD.

3.3.1.4 Carnosine reduces ROS accumulation in primary mouse cortical astrocytes

To build on the previous experiment, astrocytes were loaded with DCFDA (20 μM) for 45 minutes, wells were washed and media replaced without FBS to facilitate ROS accumulation ± carnosine (0 – 300 μM). Fluorescence intensity was measured at 24 h.

FBS withdrawal significantly increased intracellular ROS accumulation. Fluorescence intensity increased from 27228 ± 1264 (with FBS present) to 66448 ± 11630 following FBS withdrawal (Figure 3.4A). Data was normalised by subtracting the mean FBS-supplemented control from each individual value to remove background signal. Each value was then expressed as a percentage relative to the average 0 μM carnosine value. Carnosine reduced ROS accumulation in a dose-dependent manner. Normalised fluorescence intensity values were reduced through the addition of 10 μM carnosine (71.09 ± 24.62%, *P = 0.0183), 30 μM carnosine 62.04 ± 23.91%, **P =

0.0013), 100 µM carnosine (56.33 ± 13.25%, ***P = 0.003) and 300 µM carnosine (49.18 ± 19.33%, ****P < 0.0001), relative to the 0 µM control (100 ± 20.98%) (Figure 3.4B).

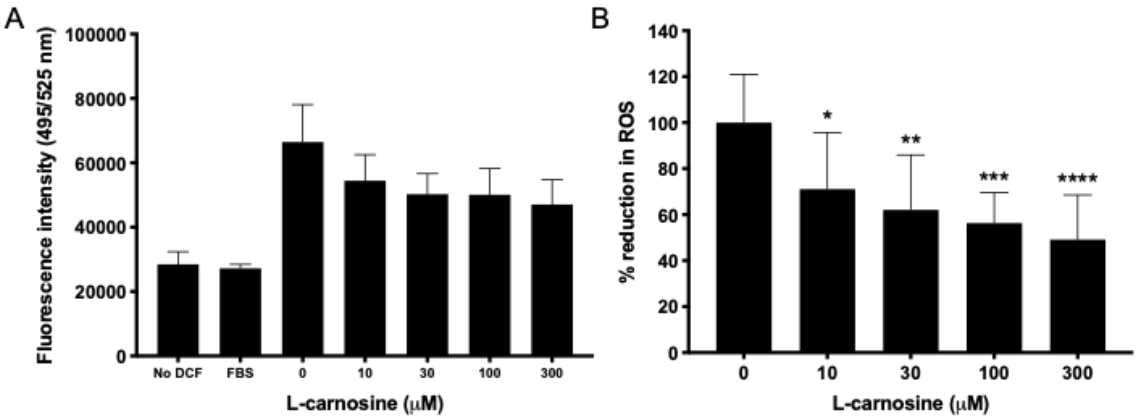

Figure 3.4 Antioxidant properties of carnosine in mouse cortical astrocytes. A) Fluorescence intensity measurements in astrocytes following 24 h FBS withdrawal ± carnosine (0 – 300 µM). n = 4 biological replicates from separate culture preparations, n = 4-6 wells/condition/experiment. B) Data normalised to 0 µM carnosine control. *P < 0.05, **P < 0.01, ***P < 0.001, ****P < 0.0001 v 0 µM carnosine control, one-way ANOVA with Tukey's multiple comparison test. All data presented as mean ± SD.

3.3.1.5 Carnosine does not influence (re)myelination in organotypic cerebellar slice cultures

Cell culture models are homogenous cell populations that are important for gaining insights into cell-specific effects and interrogating basic biology. However, these models are far removed from the *in* vivo complexity of an organism and do not replicate the cellular diversity of a living organism. Organotypic brain slice cultures can be used to bridge this gap in neuroscience research by preserving the three-dimensional structural integrity, cell-cell interactions, microenvironment, neurotransmitter release and synaptic transmission[266–268]. OSCs show spontaneous remyelination following LPC-induced demyelination[221,269,270], therefore the effect of carnosine treatment on remyelination was assessed.

Cerebellar slices were cultured for 10 days and then incubated for 24 h with 300 μM carnosine. Slices were subsequently demyelinated by the addition of lysophosphatidylcholine (LPC, 0.5 mg/ml) to the media for 16 h. Slices were subsequently washed and culture media replaced ± carnosine for 72 h. Slices were then fixed and stained for neurofilament-H (NFH) and myelin basic protein (MBP) (Figure 3.5A-C). Colocalisation between NFH and MBP, a measure of myelinated axons, was determined using ImageJ (Figure 3.5D-F). Data is presented using the Manders' coefficient, where 1 represents total colocalisation and 0 represent no colocalisation[271].

LPC induces significant demyelination in the cerebellar slices. The Manders' coefficient decreased from 0.778 ± 0.17 to 0.372 ± 0.07 at 24 h post-demyelination. Following demyelination, cerebellar slices showed spontaneous remyelination over the next 14 days, which is typical of the model[272] (Manders' coefficient 0.907 ± 0.09). This experiment concluded that in our hands, cerebellar slices showed significant demyelination following LPC addition, as well as robust remyelination over the next 14 days (Figure 3.5G).

For the next experiment we wanted to elucidate whether carnosine could promote remyelination. Therefore, slices were demyelinated, washed and media replaced ± 300 μM carnosine. 5 days after demyelination, before complete spontaneous remyelination had occurred, slices were fixed and stained to quantify (re)myelination. Mean Manders' coefficient calculation showed that 300 μM carnosine does not significantly promote remyelination following LPC-induced demyelination (control 0.417 ± 0.23 versus 300 μM carnosine 0.508 ± 0.25) (Figure 3.5H).

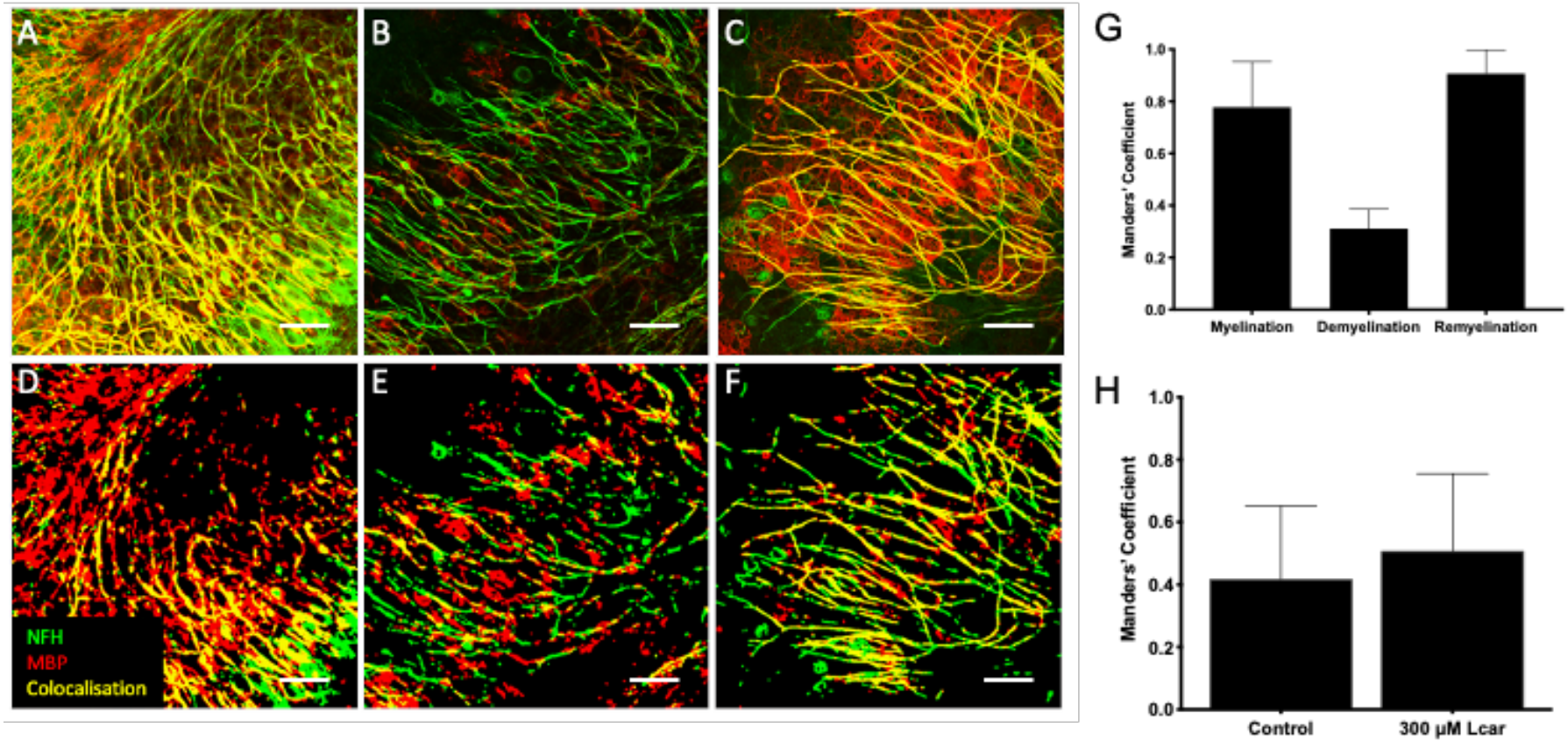

Figure 3.5 The influence of carnosine on remyelination in an organotypic cerebellar slice culture model of remyelination. Representative immunofluorescent images of cerebellar slices were fixed and stained with NFH (green) and MBP (red). A) Before demyelination, B) 24 h post-demyelination and C) 14 days after demyelination (remyelination). D-F) Representative image after ImageJ processing. G) Quantification of colocalization shows robust demyelination following LPC addition followed by significant remyelination. n = 2 biological replicates from separate culture preparations, 3 slices/condition/experiment, 2 x 10 image z-stacks per slice. H) Colocalisation quantification 5 days post-demyelination ± 300 µM carnosine. n = 3 experiments, 3-4 slices/condition/experiment, 2 x 10 image z-stacks/slice. All data presented as mean ± SD.

3.3.2 Carnosine efficacy in the Biozzi ABH EAE model

3.3.2.1 Carnosine shows a trend in reducing the first relapse disease severity in the Biozzi ABH EAE model

To further build on these *in vitro* experiments, carnosine was tested using the Biozzi ABH EAE model. This model most closely resembles the typical clinical disease course observed in MS patients, which firstly presents with a relapsing-remitting disease course followed by a secondary progressive phase, where neurological deficits slowly accumulate. Therefore, this model offers the advantage of having both immune-mediated relapsing-remitting disease and neurodegenerative progressive disease[273].

The aim of this first *in vivo* study came in three parts. The first aim was to induce disease in a small cohort of mice to ensure we could successfully induce disease. Data variance was used for future power calculations. The second was to elucidate whether carnosine administration influenced the EAE disease course. Lastly, to use a positive control (fingolimod) to demonstrate dosing competency and provide an internal control.

Immediately following disease induction, mice were administered water control, fingolimod (3 mg/kg) or L-carnosine (550 mg/kg) via daily oral gavage, in a total volume of 100 µL. Previous work in our lab demonstrated that carnosine showed significant efficacy at this dose in the tMCAO stroke mouse model, therefore the same dose was used in this study. Mice were neurologically scored and weighed daily for signs of disease. As previously shown[195], fingolimod completely inhibits the onset of disease throughout the whole 90-day monitoring period. During the first acute phase

of disease, no significant difference in neurological score (Figure 3.6A) or disease-associated weight loss (Figure 3.6B) was seen between control and carnosine groups.

Following this first acute phase, mice recovered and entered a period of remission before entering the relapsing-remitting phase of disease at around 33-34 days post-induction (dpi). Carnosine showed a trend in reducing the overall disease severity during the first relapse of disease compared to vehicle control (Figure 3.6C). The overall first relapse disease severity was calculated by quantifying the area under the curve (AUC) of the neurological score from each mouse from day 30 to day 55, before the onset of the second relapse (control AUC 45.75 ± 5.66 v carnosine AUC 32.54 ± 5.38, $P = 0.14$).

The time it took for each mouse to reach a specific neurological score or experimental endpoint was also calculated. Carnosine seemed to delay the onset of more severe neurological symptoms during the relapsing-remitting phase (Figure 3.7A-D). Furthermore, the time it took mice to reach an experimental endpoint also seemed to be delayed (Figure 3.7E).

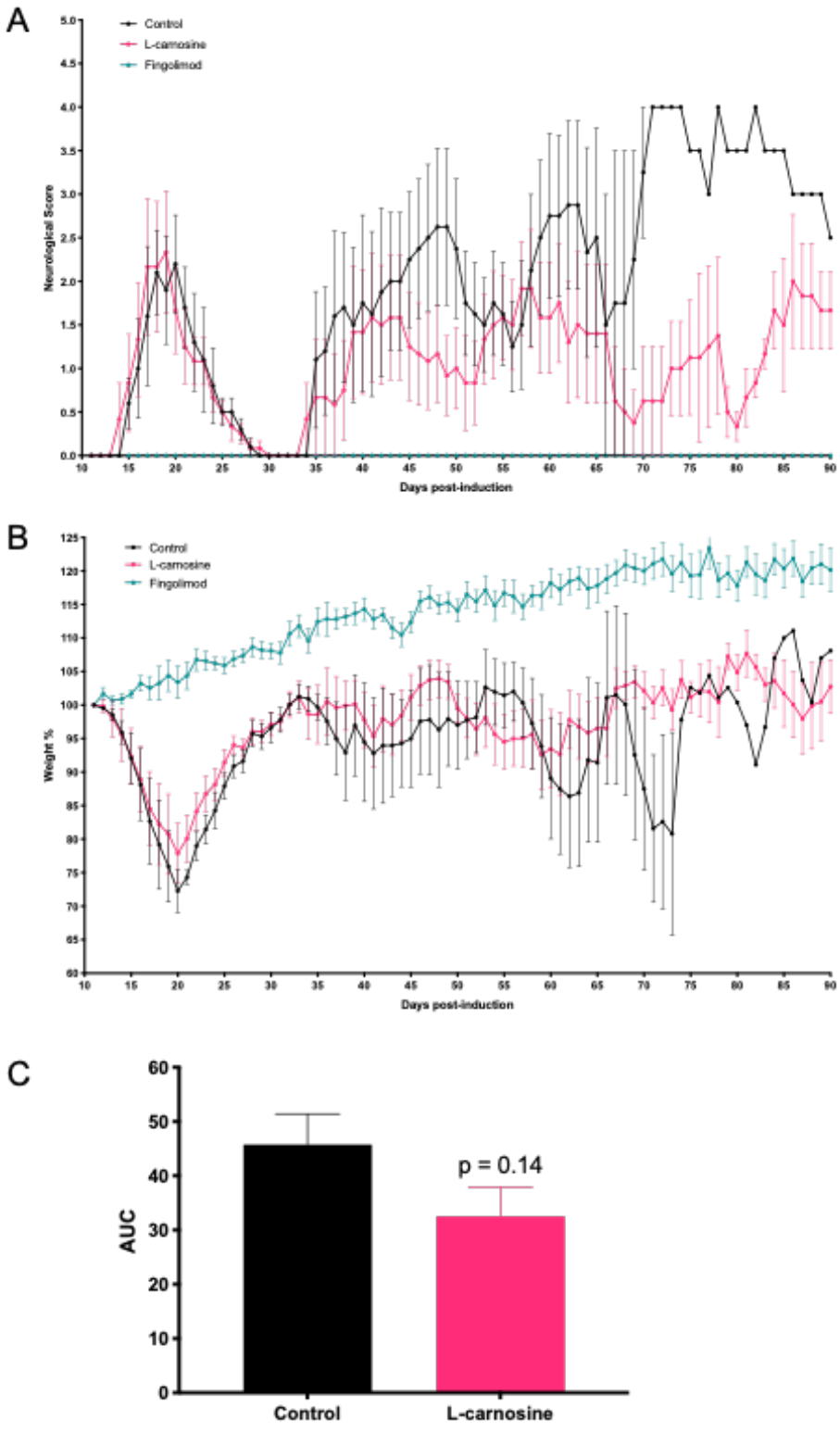

Figure 3.6 Efficacy of 550 mg/kg carnosine in the Biozzi ABH model.
A) Neurological scores and B) percentage weight change were measured throughout the 90-day monitoring period. n = 6 fingolimod, n = 6 control, n = 6 carnosine. Data presented at mean ± SEM. C) Area under the curve (AUC) analysis during the first relapse of disease showed no significant difference. Student's t-test, data presented as mean ± SD.

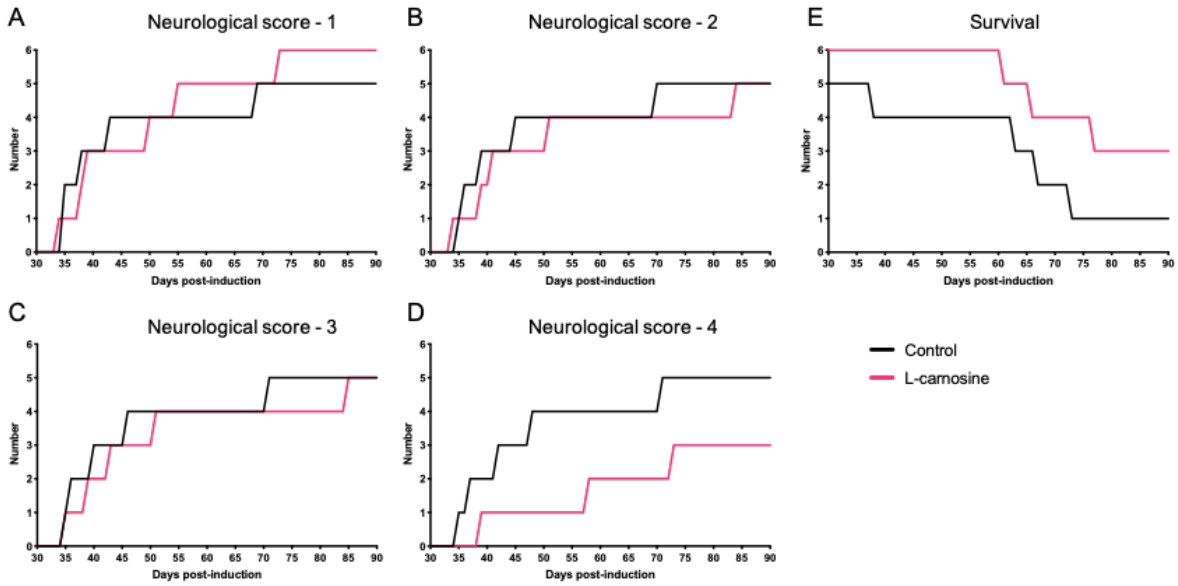

Figure 3.7 Neurological scores and survival following the first relapse.
The time taken to reach a neurological score of A) 1, B) 2, C) 3, D) 4 or E) to reach a clinical endpoint was calculated. n = 6 control, n = 6 carnosine.

Our next aim was to repeat this first *in vivo* experiment to interrogate model repeatability and to also increase our confidence from the first study by completing experiments to the correct statistical power. However, following disease induction a number of mice displayed a very severe disease phenotype during the first acute phase. This resulted in a number of mice dying overnight (4/20) or rapidly reaching an experimental endpoint (11/20). No clear trend was evident between age, sex or treatment group with disease severity. Although some mice exhibited the expected disease course, statistical power was too low to warrant carrying on with the study. The details of these mice can be found in Table 3.1.

Following contact with researchers at QMUL, we discovered that they were experiencing the same problems. They advised us that varying the inoculum composition, spinal cord homogenate concentration or dose of bacteria made no

difference to the severity of the outcome. We managed to source a second cohort of Biozzi ABH breeding mice from the University of Edinburgh. However, despite extensive efforts we were unable to successfully breed these mice. Therefore, to continue our *in vivo* studies, we proceeded to amend our Home Office Project License so that all of our future EAE studies would utilise the C57BL/6 MOG_{35-55} model.

Table 3.1 Table summarising experimental outcomes following EAE induction in Biozzi ABH mice.
A number of mice rapidly reached an experimental endpoint (11/20) or died overnight (4/20) during the acute phase of disease. No trend can be seen between sex, starting weight or treatment group.

Animal ID	Sex	Starting weight (g)	Treatment group	Day of death (dpi)	Comments
219052	M	33.1	Control	18	Endpoint reached
219046	F	27	L-carnosine	17	Endpoint reached
219057	M	35.4	L-carnosine	15	Died overnight
219060	M	32.9	Control	16	Died overnight
219062	M	34.5	Control	18	Died overnight
220647	M	26.7	L-carnosine	17	Endpoint reached
219063	F	28.8	Control	18	Endpoint reached
219044	M	35.3	Control	19	Died overnight
220649	F	29.3	Control	18	Endpoint reached
219050	M	35.4	L-carnosine	19	Endpoint reached
219045	F	29.4	L-carnosine	19	Endpoint reached
219051	M	33.1	L-carnosine	-	Normal disease
219053	F	25.2	L-carnosine	-	No Disease
219054	F	29.6	Control	21	Endpoint reached
219055	F	29.5	Control	21	Endpoint reached
219047	F	25.3	Control	-	Normal disease
219058	M	33.2	L-carnosine	20	Endpoint reached
219059	M	35.8	L-carnosine	20	Endpoint reached
219061	M	34.9	Control	-	Normal disease
220648	F	27.3	L-carnosine	-	Normal disease

3.3.2.2 Carnosine does not reduce disease severity in the C57BL/6 MOG_{35-55} EAE model

Our first aim was to assess carnosine efficacy in this EAE model by using a dose response experimental design. Following disease induction, mice were administered water, or L-carnosine (550, 1000 and 2000 mg/kg) via daily oral gavage, in a total volume of 100 µL. Previous studies have shown these higher doses to be safe and efficacious in the mouse tMCAO stroke model[243], therefore this higher dosing regime was implemented for this study in order to maximise therapeutic potential. Mice were neurologically scored and weighed daily for signs of disease. Mice were sacrifice at 28 dpi once they had partially recovered.

Disease symptom onset occurred at 11 dpi in all groups. Neurological scores and disease-associated weight loss progressively worsened over the following days and peaked at 15 – 18 dpi. Mice showed partial recovery over the next 10-12 days with residual neurological deficits remaining (Figure 3.8A-B). The overall disease severity, calculated by the AUC, showed no significant difference between the vehicle group (31.3 ± 2.9) and carnosine groups (550 mg/kg 29.0 ± 3.3 v 1000 mg/kg 31.1 ± 2.75 v 2000 mg/kg 30.5 ± 2.7) (Figure 3.8C). The disease-associated weight loss showed the same trend and no significant difference was observed between the vehicle group (142.1 ± 30.5) and carnosine groups (550 mg/kg 124.9 ± 26.1 v 1000 mg/kg 148.7 ± 24.5 v 2000 mg/kg 117.3 ± 23.7) (Figure 3.8D).

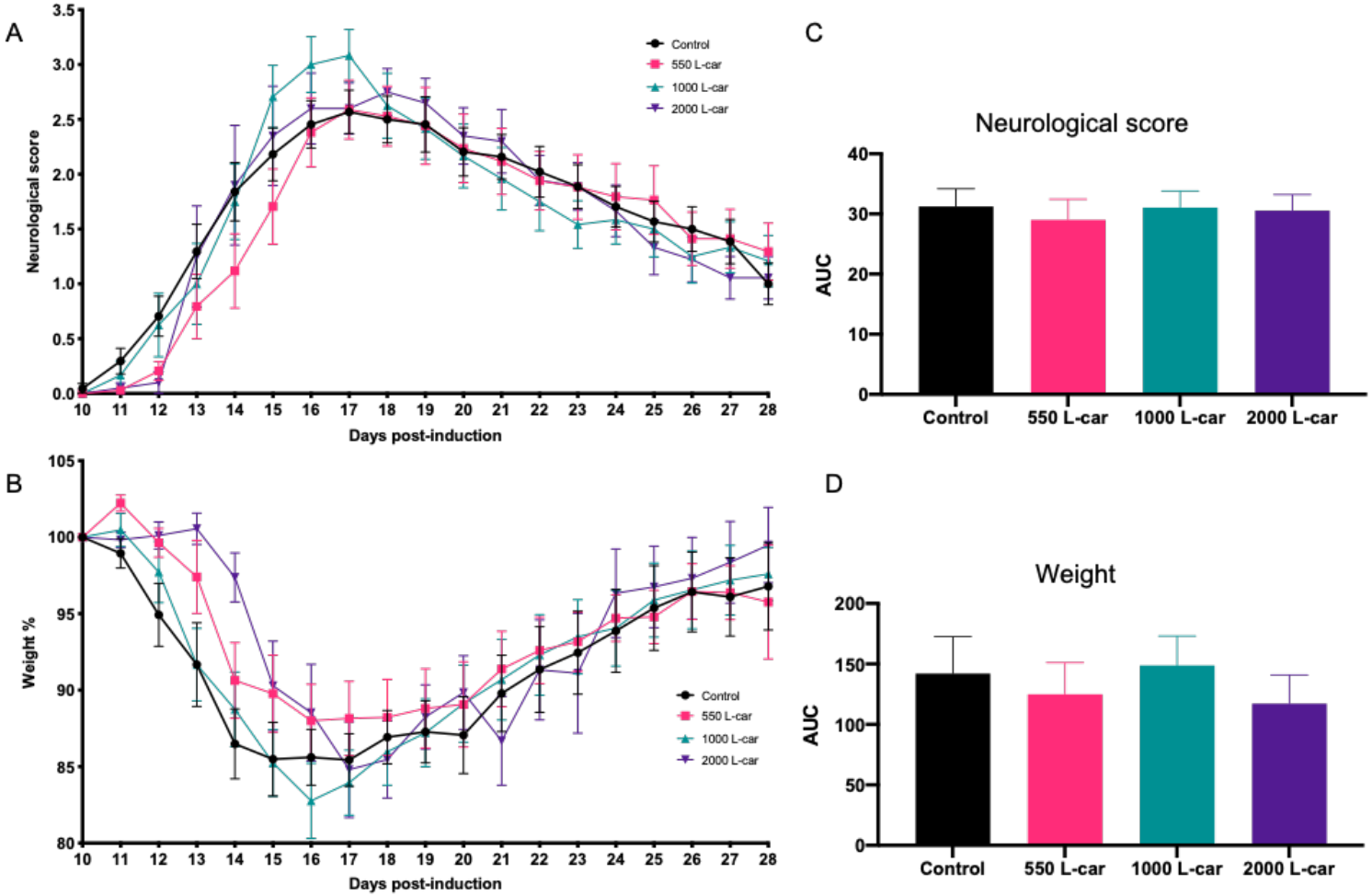

Figure 3.8 Carnosine efficacy in the C57BL/6 MOG35-55 EAE model.
A) Neurological scores and B) percentage weight change were measured throughout the 28-day monitoring period. Data presented at mean ± SEM. Area under the curve (AUC) analysis calculated for C) neurological score and D) weight showed no significant difference between treatment groups. One-way ANOVA, Tukey's multiple comparison test. Data presented as mean ± SD. n = 20 control, n = 17 550 mg/kg, n = 12 1000 mg/kg, n = 12 2000 mg/kg.

3.4 Discussion

The first aim of this thesis was to evaluate carnosine as a potential therapeutic for MS. As discussed in Chapter 1.8, carnosine shows multiple properties that leave it a viable candidate to explore further. This was done by utilising *in vitro* and *in vivo* models to mimic MS pathological mechanisms.

3.4.1 Carnosine shows no cytotoxicity towards primary mouse cortical neurons

The first aim of this chapter was to determine the *in vitro* neurotoxic effects of carnosine by exposing primary mouse cortical neurons to log-fold increases of carnosine. This was to characterise whether carnosine would contribute towards any observed toxicity in future ROS accumulation and excitotoxicity assays. Carnosine showed no significant cytotoxicity towards primary mouse neurons (0-30 mM) as measured by lactate dehydrogenase (LDH) release (Figure 3.1). This information provided evidence that carnosine was not contributing towards any observed toxicity in future excitotoxicity and ROS accumulation assays.

A number of techniques have been developed to measure *in vitro* cell viability and cytotoxicity. These include measuring LDH in the media, which is released following loss of plasma membrane integrity. Another method is measuring the enzymatic reduction of 3-[4,5-dimethylthiazole-2-yl]-2,5-diphenyltetrazolium bromide (MTT). This results in the formation of dark blue coloured MTT-formazan and this colorimetric change is quantified. This reduction into MTT-formazan is dependent on the mitochondrial enzyme succinate dehydrogenase, thus is a measure of mitochondrial function. Literature has highlighted distinct differences between the LDH and MTT

assays. A paper by Lobner found that the MTT assay is less sensitive for detecting changes in apoptosis as mitochondrial dysfunction likely happens upstream of caspase activation and therefore may be less useful for assaying neuroprotective strategies. LDH release is a marker of irreversible cell death and is a long-established method for measuring cell death in cortical neuron cultures[274]. Thus, the LDH assay was utilised for *in vitro* studies to quantify cytotoxicity and neuroprotective strategies, an assay in which our lab has extensive previous experience.

Primary mouse cortical neurons were utilised as a pre-clinical tool to support the proposed *in vivo* studies. Neuronal cultures are widely used throughout neuroscience research to evaluate the effects of drugs and/or toxic insults on cellular responses[275]. Cultures were optimised and characterised to ensure high purity, viability and axonal integrity (Appendi 1). Primary mouse cortical neurons are sensitive to environmental changes[276], therefore careful and consistent inter- and intra-experimental practice is vital to minimise these effects.

3.4.2 Carnosine is protective against NMDA-induced excitotoxicity

Excitotoxicity, especially through NMDARs, is implicated in exacerbating tissue damage and neuronal death in MS[174,182]. NMDA-induced excitotoxicity is widely used in the literature to study neuronal excitotoxic death. NMDA stimulation results in excess calcium flux through NMDARs, specifically through NMDAR1, which is lethal to cortical neuron cultures[277]. Experimental protocols differ and the extent of excitotoxic damage is dependent on a number of factors, including neuronal maturity, density and purity. A dose response curve was first of all generated by exposing primary mouse neurons to escalating concentrations of NMDA for 30 minutes. The

aim of this was to elucidate a concentration that would produce a significant LDH response, without completely killing all cells in the well. 30 minutes exposure to 30 μM NMDA was sufficient to generate significant LDH release (Figure 3.2A). This stimulation protocol was maintained throughout the subsequent anti-excitotoxicity experiments with carnosine.

Pre-treatment with carnosine 24 h prior to NMDA exposure significantly reduced NMDA-induced excitotoxicity at 300 μM when compared to the 0 μM carnosine control (Figure 3.2B-C). Other literature supports these findings, although the majority of these are in the context of stroke. Bae et al. found that carnosine at both 10 μM and 100 μM concentrations was sufficient to significantly reduce transition of mitochondrial membrane potential (MMP) and propidium iodide (PI) staining following both NMDA-induced excitotoxicity and oxygen glucose deprivation (OGD) in cortical neuron cultures[243]. This experiment builds on this work by showing that carnosine can also reduce LDH release, a marker of irreversible cell death, albeit at higher concentrations than stated by Bae et al. The potent anti-excitotoxic effects of carnosine have also been highlighted in rodent models of stroke. Carnosine treatment significantly decreases glutamate levels within the infarct zone by improving mitochondrial function in the ischemic brain and reducing glutamate transporter-1 (GLT-1) expression on cortical astrocytes, a key transporter involved in glutamate homeostasis[278]. Another study demonstrates that carnosine protective effects against ischaemic insults may be due to carnosine decreasing the binding capacity of NMDARs to NMDA[279].

3.4.3 Carnosine reduces ROS accumulation in neurons and astrocyte

The antioxidant effects of carnosine were next assessed using primary mouse cortical neuronal cultures. Trophic factor withdrawal is widely used in cell studies to induce oxidative stress and intracellular ROS accumulation. The cell culture microenvironment plays a profound role in cellular stress and survival. B27-supplement is utilised in neuronal cultures to improve neuronal survival, longevity and neurite outgrowth[280]. B-27 supplement contains several antioxidants, including catalase, superoxide dismutase, selenium and vitamin E. Selenium and Vitamin E are particularly important for neuronal health and survival[281]. B27-suplement removal for 24 h induced significant ROS accumulation in neuronal cultures, as measured by DCF fluorescence intensity. In order to investigate the antioxidant capabilities of carnosine, neuronal cultures were cultured in the presence of carnosine, following B27-supplement withdrawal. Carnosine significantly reduced ROS accumulation at 24 h (30 – 300 μM) (Figure 3.3). Similar experiments conducted in rat neurons have shown that carnosine reduced ROS accumulation by nearly 50% following rotenone treatment[282].

To build on this, the effects of carnosine on ROS accumulation was also assessed in primary mouse cortical astrocytes. ROS release from infiltrated immune cells and local astrocytes and microglia contribute towards further glial reactivity, disease progression and neuronal death[104,148]. Astrocyte cultures require serum as a source of many nutrients, hormones and growth factors to maintain a favourable cell culture environment[283]. Serum withdrawal removes these supportive factors, which triggers ROS accumulation and cell death[284]. ROS accumulation within astrocytes affects their function and drives astrocytes towards a pro-inflammatory state. Serum withdrawal for

24 h significantly increases ROS accumulation in astrocyte cultures. Carnosine treatment significantly reduced ROS accumulation at concentrations on 10 – 300 μM, when compared to 0 μM control (Figure 3.4). Serum withdrawal triggers mitochondrial ROS release, specifically complex III of the mitochondrial respiratory chain[284]. Further work could characterise the mitochondrial response following serum withdrawal, given that carnosine is known influence mitochondrial membrane potential[243].

The effect of carnosine on the antioxidant system is well documented. This data, as well as previously published literature demonstrates carnosine's ability to dampen ROS accumulation through modulation of antioxidant pathways, as well as direct scavenging of excess reactive oxide and carbonyl species[234,282,285]. These anti-excitotoxic and antioxidant properties of carnosine have led to numerous reviews highlighting its therapeutic potential[235,286–288]. To date, the influence of carnosine on remyelination had not been explored.

3.4.4 Carnosine does not influence remyelination

The aim of the next experiment was to elucidate whether carnosine influenced remyelination in an organotypic cerebellar slice culture (OSC) model of demyelination. We hypothesised that the aforementioned pleiotropic properties of carnosine may enhance remyelination. Demyelination causes significant neuronal stress, ROS accumulation, metabolic imbalance and eventual death[289–291]. Carnosine may limit this by reducing excitotoxic and oxidative damage, thus producing a more regenerative environment for remyelination.

Cerebellar brain slices were obtained from postnatal day 8-12 mouse neonates. Slices cultured from this age show the distinct morphological characteristics while still maintaining neuronal plasticity, regenerative capacity and injury resistance, thus leading to increased survival and viability in culture[292]. Marked axotomy is observed in OSCs and this results in a loss of target innervation and can contribute towards neuronal death, although this can be somewhat overcome through supplementation[292]. Development in culture allows the differentiation and maturation of the myelin sheath, resulting in similar morphology and tissue organisation as *in vivo* tissue[292]. Although OSCs do not fully replicate the adult CNS, they maintain much of the tissue complexities such as the three-dimensional architecture, cell-cell interactions, microenvironment, neurotransmitter release and synaptic transmission[266–268]. Activated macrophages are also present in cerebellar slices and are thought to clear myelin debris[222], similar to what is seen in EAE[293,294] and MS lesions[295,296]. Furthermore, OSCs maintain a strong network of brain capillaries, which survive despite the loss of circulation[297]. OSCs provide a more complex platform to study multicellular interactions whilst still maintaining sufficient throughput and biological relevance and are widely cited in MS research to both aid in animal studies and better understand complex mechanisms of remyelination[298–303].

Lysophosphatidylcholine (LPC) was used to induce widespread demyelination. LPC is specifically toxic to the myelin sheath, whilst neuronal axons remain intact. LPC has a specific affinity for myelin proteins causing myelin lamellae to fuse, transform into spherical vesicles and progressively reduce in size until they are eventually phagocytosed[304,305]. Following LPC-induced demyelination, brain slices show spontaneous remyelination, which has been cited in the literature to be complete at

14 days-post-demyelination (dpd)[222]. The process of remyelination requires numerous sequential steps, involving cross-talk between neurons and glial cells. Signalling molecules released from neurons control the proliferation, differentiation and survival of oligodendrocytes.

The aim of this experiment was to elucidate whether carnosine could modulate early remyelination, where most of the excitotoxic and oxidative damage occurs. Following LPC-induced demyelination, media was replaced with or without carnosine (300 μM) and the extent of remyelination was quantified 5 dpd. Carnosine showed a trend in increasing remyelination at 5 dpd, however this was not significant (Figure 3.5). Further temporospatial characterisation could quantify (re)myelination at other timepoints that are later in the remyelination process.

Further work could also assess carnosine in a more pathologically relevant cell culture model to assess neuroprotective and remyelinating strategies. Lysolecithin is quite an artificial way of inducing demyelination and is far removed from the pathology of EAE and MS. A splenocyte cell culture mediated demyelination model has recently been published. Splenocytes isolated from EAE mice can be re-stimulated by CNS peptides in culture and induce significant demyelination[298]. Remyelination can be improved through the addition of fingolimod which is seen in the lysolecithin model[299], which further supports the validity of this model and could be used as a positive control.

3.4.5 Carnosine efficacy evaluation in the Biozzi ABH EAE model

This promising *in vitro* data as well as previously highlighted literature provided evidence that carnosine may reduce neurological deficits in the EAE mouse model of

MS. The Biozzi ABH EAE model offers a number of advantages over other EAE models as it offers a reproducible relapsing-remitting disease course where relapses are easy to distinguish. This relapsing disease is followed by a slow, progressive accumulation of neurological disease, thus making it a good model for neuroprotective assessment[306]. Both oxidative stress and excitotoxicity exacerbate tissue damage during inflammatory disease as well as drive neurodegenerative disease progression. Therefore, we chose the Biozzi ABH model to conduct our *in vivo* evaluation of carnosine. The first aim of these experiments was to establish baseline parameters of disease onset, severity and progression as determined by neurological scores and disease-associated weight loss. Secondly, to use a positive control fingolimod, which has been previously been shown to significantly reduce neurological deficits in this model[195]. This was to ensure that *in vivo* data could be compared to other literature as well as confirm therapeutic interventions could be effectively administered and assessed. Lastly, carnosine efficacy was assessed in a small cohort of mice. This initial EAE study aimed to quantify the model variability in our hands so future studies could be accurately powered.

Carnosine was administered via oral gavage to minimise animal discomfort and ensure accurate dosing. Carnosine is easily absorbed from the gut into the bloodstream where it can cross the BBB. Further BBB breakdown that occurs during EAE will further allow carnosine entry into the CNS. Carnosine was administered on the day of induction, prior to the onset of disease and doses ranged from 550 – 2000 mg/kg. This dose range was chosen, as previous work in our lab demonstrated that this was the therapeutic range in a mouse ischaemic model of stroke[245].

Disease onset and progression was primarily monitored through neurological scoring and weight loss. Neurological scoring is the most widely used parameter in EAE research to measure disease disability. Close monitoring of ascending paralysis from the tail, hindlimbs and forelimbs has proved to be the most robust and reproducible method[307]. There is no international standard scoring system, which leaves it difficult to compare between studies and clinical assessment scales can range from 0-3[308], 0-4[309], 0-5[195] and 0-6[310] points. Recent efforts have aimed to refine this clinical scoring by including other parameters such as grid walk, a righting test and a hanging test alongside a 5.5-point neurological scale. However this study found that this system was no more sensitive than a 3-point scale[311]. A 5 point scoring scale was used in this study, which is widely used in the Biozzi ABH EAE model[273,312,313]. Neurological score was plotted against time (days) and the area under curve (AUC) was quantified as a measure of overall neurological disability over time. Carnosine-treated mice showed a mild improvement during the first relapse of disease when compared to vehicle treated control, although this did not reach significance. The reason for this trend in reduced neurological score may be due to the anti-excitotoxic and antioxidant capabilities of carnosine, as illustrated by previous *in vitro* studies.

Disease-associated weight loss is a typical feature of a number of EAE models and is another useful indicator of disease onset, progression, recovery and experimental endpoints. Expressing weight loss as a percentage reduces the effect of starting weight and allows comparison between mice. This disease-associated weight loss occurs even when animals are given fluids and food via oral gavage[306] and correlates with infiltration of T cells and monocytes into the CNS parenchyma[314]. No significant

difference in disease-associated weight loss was observed between control and carnosine treatment groups (Figure 3.6).

To build on this we designed a second study to further explore these preliminary findings to the correct statistical power. However, following disease induction, a significant number of mice rapidly reached experimental endpoints or died during the first acute phase of disease (Table 3.1). Experiments conducted at QMUL, from whom we sourced the mice, found that adjusting the experimental protocol did not reduce this severity, which indicates a change in the strain itself and therefore concluded the cohort may be too inbred for robust disease induction. Following close consultation with other researchers, the Home Office Inspector and the University of Sheffield Named Animal Care & Welfare Officer (NACWO) the license was amended so that future EAE studies will be conducted in the C57BL/6 MOG_{35-55} model.

3.4.6 Carnosine efficacy evaluation in the C57BL/6 MOG_{35-55} EAE model

The C57BL/6 MOG_{35-55} model offers a highly reproducible and robust EAE model that is widely cited in the literature. Disease is induced through the subcutaneous injection of MOG peptide, constituting amino acids 35 to 55 of the protein (MOG_{35-55}). Immune cell infiltration is seen as early as 7dpi, which peaks at 12 dpi. This correlates with axonal demyelination and loss. Demyelination peaks and plateaus at 15-19 dpi, with a trend in increased demyelination in lumbar spinal cord regions. Axonal loss still continues after inflammation has significantly receded, indicating other mechanisms contribute towards this neuronal death[191]. Previous studies have shown efficacy in this model with both antioxidant[315] and metal chelating agents[316]. The pleiotropic properties of carnosine leave it a viable candidate to screen in this model.

Carnosine did not significantly alter disease, as measured by neurological scores and disease-associated weight loss (Figure 3.8). This may be for a number of reasons. Although carnosine is readily taken up in the gut[244], carnosinases present in the blood readily break carnosine down into its constituent amino acids, β-alanine and L-histidine[317]. Mouse studies using high-performance liquid chromatography-mass spectrometry (HPLC-MS) to study carnosine pharmacokinetics found that a single intraperitoneal injection (1000 mg/kg) resulted in a peak brain carnosine concentration of 20.3 μG/g in 6 hours. Not reaching the therapeutic concentrations achieved in the *in vitro* cultures may be a reason for lack of efficacy. One way to increase tissue availability would be to pack carnosine into nanoparticles, as demonstrated by a recent publication[318]. In this study, carnosine was encapsulated in a polymerosome with oligopeptide angiopep-2 incorporated onto the surface, which targets lipoprotein receptor related protein-1 (LRP-1) expressed on the BBB. This decreased the therapeutic dose needed by at least three orders of magnitude in a mouse model of stroke[318].

Further tissue analysis may reveal a beneficial effect at the cellular and tissue level, that may not result in an observed neurological improvement in the model. Nrf2 is a transcription factor that plays a major role in regulating antioxidant genes to protect against oxidative stress[143]. Nrf2 analysis could elucidate if carnosine is eliciting an antioxidant effect in the tissue, either directly or through ROS scavenging.

In this study, the natural isomer L-carnosine was used. D-carnosine is the non-natural isomer of L-carnosine. D-carnosine is considered carnosinase resistant[224,225], can

cross the BBB and our recently published data shows that D-carnosine shows similar *in vitro* efficacy in excitotoxicity and ROS accumulation assays. However, pharmacokinetic analysis showed that pharmacokinetic parameters (area under curve, peak serum concentration and serum half-life) were similar between L- and D-carnosine between 5 and 360 minutes post intravenous injection of 1000 mg/kg[240], which goes against this hypothesis. Studies analysing stroke efficacy evaluated carnosine and analogues N-acetyl carnosine and anserine found that carnosine was the most neuroprotective[319]. These comparisons haven't been explored in the EAE model.

4 Evaluation of peptide 8 immunisation as a therapy for multiple sclerosis

4.1 Introduction

Excitotoxicity has been evidenced to exacerbate tissue injury in MS and EAE and this is mediated through calcium influx through NMDARs, specifically NMDAR1. As detailed in Chapter 1.8, previous work in our lab has developed a therapeutic vaccine by generating an immune response against a short peptide sequence (peptide 8) that is expressed on NMDAR1. Peptide 8 immunisation significantly reduced infarct volume in a mouse model of ischaemic stroke. Building on this, the overall second aim of this project was to determine if immunisation against peptide 8 resulted in improved neurological outcome in the C57BL/6 MOG_{35-55} EAE model. Underlying mechanisms of action will be investigated through analysis of protein and gene expression in spinal cord as well as *in vitro* assays.

4.2 Aims and objectives

1) Characterise any behavioural changes in mice as a result of peptide 8 immunisation.
2) Determine if peptide 8 immunisation improves neurological outcomes in the C57BL/6 MOG_{35-55} EAE model.
3) Investigate the mechanism of action:
    i. Use electrophysiology to study neuronal excitability following peptide 8 serum incubation.
    ii. Use immunocytochemistry to quantify neuronal NMDAR1 expression following peptide 8 serum incubation.

iii. Spinal cord analysis using western blot to investigate glial reactivity and NMDAR1 downstream pathways.

iv. Determine gene expression signature changes following EAE induction and peptide 8 immunisation.

4.3 Results

4.3.1 Behavioural characterisation following peptide 8 immunisation

4.3.1.1 Peptide 8 conjugation

In order to induce a significant immune response, peptide 8 was conjugated to a virus-like protein (VLP). Western blotting was used to determine successful peptide conjugation. VLP and VLP-peptide 8 conjugates (10 μG protein) were loaded onto a 15% resolving polyacrylamide gel to ensure successful conjugation. A slightly higher molecular weight band can be observed in the conjugated peptide 8 lane compared to the VLP only lane, indicating successful conjugation (Figure 4.1).

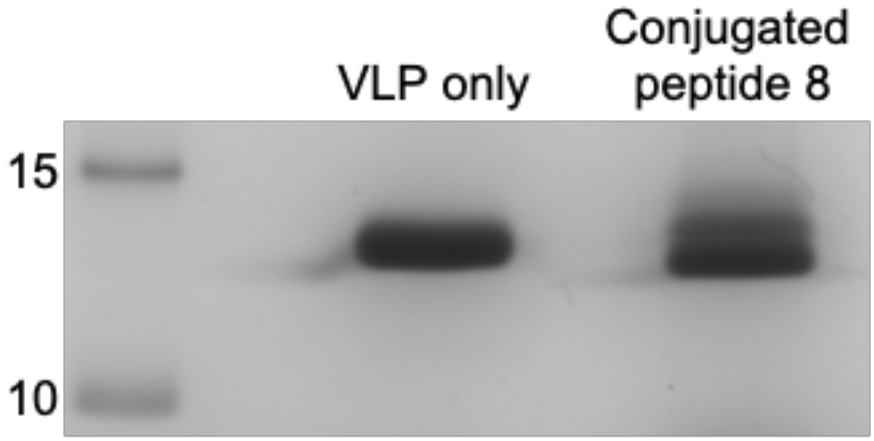

Figure 4.1 Peptide 8 conjugation to VLP
A representative immunoblot shows that peptide 8 conjugation results in a second band at a higher molecular weight. This indicates successful conjugation.

4.3.1.2 Peptide 8 immunisation does not alter normal behavioural parameters

Before determining efficacy in the MOG_{35-55} EAE model, mice were monitored for 8 weeks following peptide 8 immunisation. PBS and VLP only treated groups were included as controls. All baseline and 8-week measurements are summarised in Table 4.1. Marble burying behaviour is generally considered to be indicative of foraging behaviour, which is considered normal, habitual behaviour[320]. The data showed, over the 8-week testing period, no significant change in marble burying behaviour following peptide 8 immunisation (Figure 4.2A). Nest building behaviour is an important mouse behaviour for heat conservation, reproduction and shelter[321]. The data showed no significant difference in nest building behaviour between treatment groups (Figure 4.2B). The open field test is mainly used to quantify general movement, exploratory behaviour or anxiety-mediated fear[322]. The data showed no significant difference in open field activity between treatment groups. However, there was a significant time-dependent reduction in open field test values when comparing baseline and 8-week values (Figure 4.2C).

Mice, and rodents in general, are known for their burrowing behaviour, which can offer protection, defence against predators or simply a measure of foraging/hoarding behaviour[263,320]. The data showed no significant difference in burrowing behaviour between treatment groups. Temporal changes were significantly reduced in non-vaccinated and VLP only groups (Figure 4.2D). Weight was monitored as an indicator of normal development and feeding behaviour. Mice showed normal weight gain through the assessment period, with no significant differences between the treatment

groups (Figure 4.2E). Taken together, this data indicates that peptide 8 immunisation does not significantly change these behavioural outcomes.

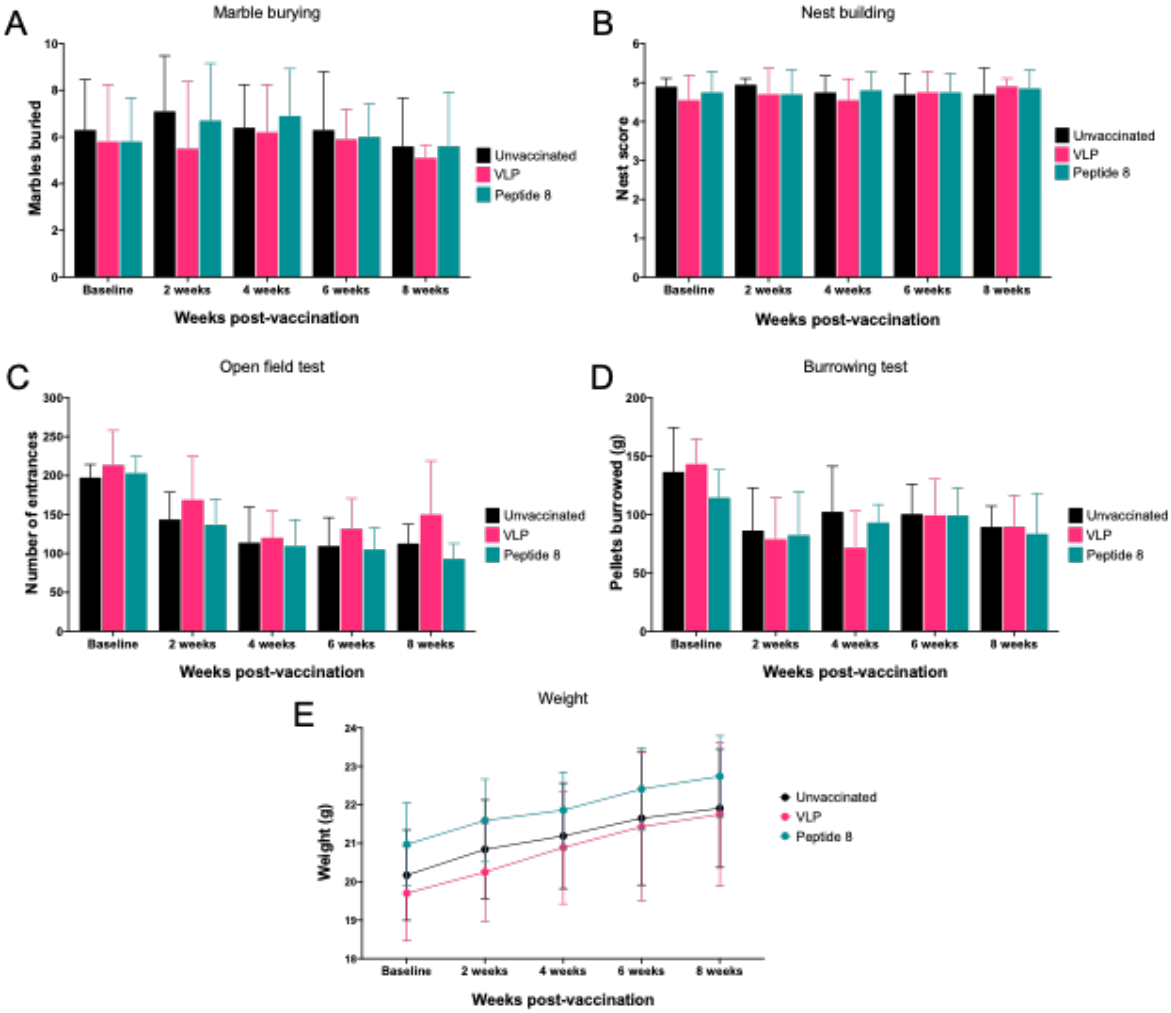

Figure 4.2 Long-term behavioural outcomes following peptide 8 immunisation Baseline measurements taken prior to PBS, VLP or peptide 8 administration. Measurements taken every other week for 8 weeks after immunisation for A) marble burying, B) nest building, C) open field test, D) burrowing test and E) weight. No significant differences was seen between the treatment groups in any of the behavioural assessments. Two-way ANOVA with Tukey's multiple comparison test. n = 10 unvaccinated, n=10 VLP, n = 10 peptide 8. All data presented as mean ± SD.

Table 4.1 Summary table of statistics for long-term behavioural assessments. No significant difference was seen between treatment groups in any of the behavioural assessments. In all groups, a significant time-dependent decrease was seen in the open field and burrowing tests when comparing baseline v 8-week measurements. *P < 0.05, **P < 0.01, ***P < 0.001, ****P < 0.0001, Two-way ANOVA with Tukey's multiple comparison test. n = 10 unvaccinated, n=10 VLP, n = 10 peptide 8. All data presented as mean ± SD.

Behavioural test	Group	Baseline	8 Weeks
Marble Burying	Non-vaccinated	6.3 ± 2.16	5.6 ± 2.07
	VLP	5.8 ± 2.44	5.1 ± 0.57
	Peptide 8	5.8 ± 1.87	5.6 ± 2.14
Open Field Test	Non-vaccinated	197.5 ± 16.7	112.8 ± 24.6***
	VLP	213.5 ± 44.4	150.0 ± 68.8*
	Peptide 8	203.1 ± 21.7	92.9 ± 19.7****
Burrowing	Non-vaccinated	136.4 ± 38.0	89.4 ± 17.9*
	VLP	143.2 ± 21.5	89.5 ± 26.8**
	Peptide 8	114.4 ± 23.9	83.4 ± 34.7
Nest Building	Non-vaccinated	4.90 ± 0.21	4.70 ± 0.68
	VLP	4.55 ± 0.64	4.90 ± 0.21
	Peptide 8	4.75 ± 0.54	4.85 ± 0.48

4.3.2 Peptide 8 efficacy in the MOG_{35-55} EAE model

4.3.2.1 Peptide 8 immunisation significantly reduces neurological deficit and disease-associated weight loss in the MOG_{35-55} EAE model

The aim of our next experiment was to determine the efficacy of peptide 8 immunisation using the MOG_{35-55} EAE model. Mice were immunised against either peptide 8 or administered VLP-only or PBS vehicle control 2 weeks prior to disease induction. On the day of disease induction, mice were administered another immunisation injection. Following EAE induction, mice were weighed and neurologically scored daily for signs of disease for 28 dpi.

Disease onset occurred from 10 dpi, evidenced by an increase in neurological score and the onset of disease-associated weight loss. As summarised in Table 4.2, both the neurological score and disease-associated weight loss were significantly reduced in peptide 8 immunised mice when compared to both non-vaccinated and VLP-only groups (

Figure 4.3A-B). The AUC, a measure of total disability, showed a significant reduction in neurological deficit in the peptide 8 group (29.88 ± 3.52) versus non-vaccinated (41.42 ± 5.56, #P = 0.0132) and VLP-only (42.25 ± 4.92, **P = 0.0077) (

Figure 4.3C). Additionally, the overall disease-associated weight loss was also significantly decreased in the peptide 8 group (225.1 ± 82.22) versus non-vaccinated (332.7 ± 62.46, ##P = 0.0036) and VLP-only groups (343.4 ± 59.64, **P = 0.0014) (

Figure 4.3D).

Additionally, this experiment demonstrated no significant difference between the non-vaccinated and VLP-only groups. Therefore, for our next experiment non-vaccinated mice were removed as a control group in order to implement the 3R's framework. The aim of the next experiment was to determine longer term neurological outcomes in this model up to 45 dpi.

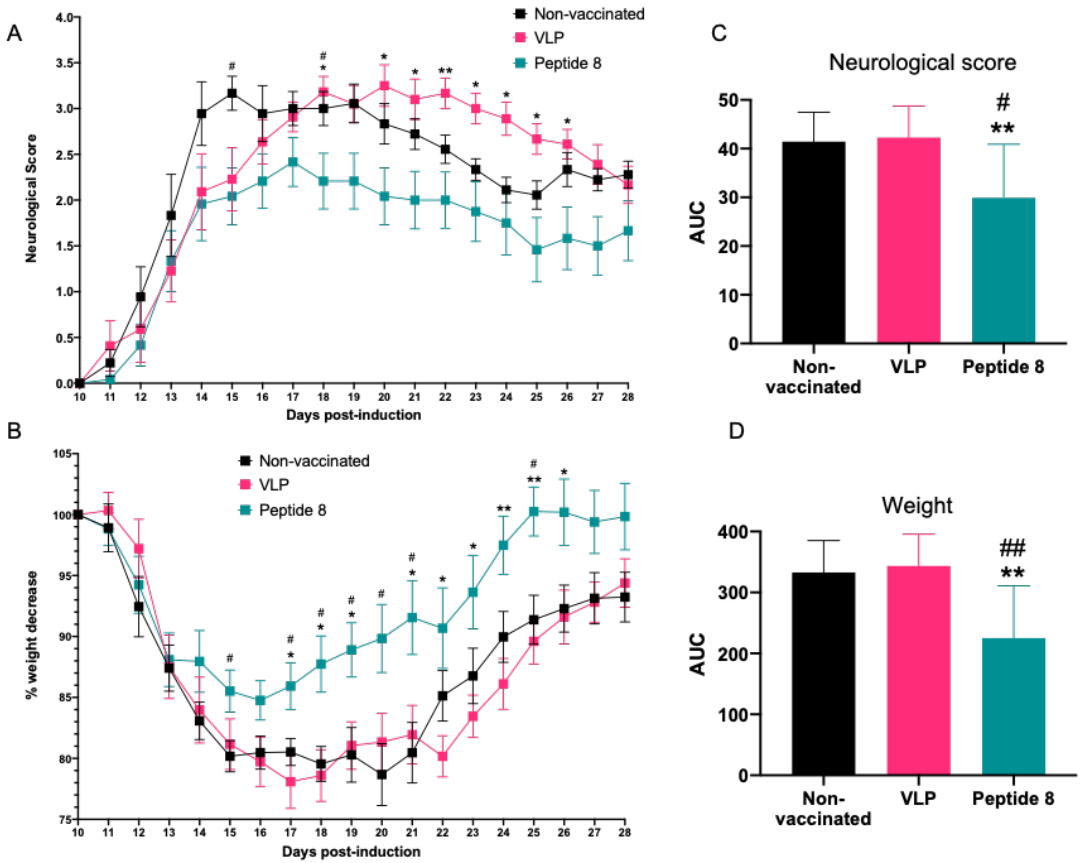

Figure 4.3 Peptide 8 efficacy in the C57BL/6 MOG_{35-55} EAE model.
A) Neurological scores and C) disease-associated weight loss were significantly reduced in the peptide 8 group on specific days when compared to VLP and n-m-vaccinated groups. Two-way ANOVA with Tukey's multiple comparison test. *P < 0.05, **P < 0.01 versus VLP. #P < 0.05 versus non-vaccinated. Data represented as mean ± SEM. Area under the curve (AUC) analysis calculated for B) neurological score and D) weight showed a significant reduction when comparing peptide 8 with both VLP and non-vaccinated groups. One-way ANOVA, Tukey's multiple comparison test. Data presented as mean ± SD. n = 10 non-vaccinated, n = 10 VLP, n = 12 peptide 8.

Table 4.2 Summary table of statistical values for neurological score and percentage weight decrease

Overview of specific P values on specific days comparing peptide 8 group versus VLP and non-vaccinated groups. *P < 0.05, **P < 0.01, Two-way ANOVA with Tukey's multiple comparison test. All data presented as mean ± SD.

Day	Group	Neurological Score		% Weight Decrease	
		Significance	Adjusted P Value	Significance	Adjusted P Value
11	Non-vaccinated	ns	0.428	ns	0.9989
	VLP	ns	0.3567	ns	0.6795
12	Non-vaccinated	ns	0.343	ns	0.824
	VLP	ns	0.8904	ns	0.5961
13	Non-vaccinated	ns	0.5899	ns	0.9609
	VLP	ns	0.9653	ns	0.9795
14	Non-vaccinated	ns	0.1402	ns	0.2056
	VLP	ns	0.9632	ns	0.4722
15	Non-vaccinated	*	0.012	*	0.0414
	VLP	ns	0.8941	ns	0.2127
16	Non-vaccinated	ns	0.1779	ns	0.1004
	VLP	ns	0.4512	ns	0.1174
17	Non-vaccinated	ns	0.1585	*	0.0474
	VLP	ns	0.2292	*	0.0265
18	Non-vaccinated	ns	0.073	*	0.0143
	VLP	*	0.0232	*	0.0157
19	Non-vaccinated	ns	0.0632	*	0.0258
	VLP	ns	0.0613	*	0.0289
20	Non-vaccinated	ns	0.094	*	0.0154
	VLP	*	0.0101	ns	0.0565
21	Non-vaccinated	ns	0.1068	*	0.0204
	VLP	*	0.0187	*	0.0415
22	Non-vaccinated	ns	0.2199	ns	0.2934
	VLP	**	0.0078	*	0.0227
23	Non-vaccinated	ns	0.3477	ns	0.1507
	VLP	*	0.0139	*	0.0175
24	Non-vaccinated	ns	0.5538	ns	0.0528
	VLP	*	0.0204	**	0.0038
25	Non-vaccinated	ns	0.2419	*	0.0108
	VLP	*	0.0131	**	0.002
26	Non-vaccinated	ns	0.128	ns	0.0529
	VLP	*	0.0291	*	0.0445
27	Non-vaccinated	ns	0.0961	ns	0.1363
	VLP	ns	0.0618	ns	0.0839
28	Non-vaccinated	ns	0.1917	ns	0.1218
	VLP	ns	0.3546	ns	0.215

Mice were immunised against either peptide 8 or administered VLP-only or PBS vehicle control 2 weeks prior to disease induction. On the day of disease induction, mice were administered another immunisation injection. Following EAE induction, mice were weighed and neurologically scored daily for signs of disease until 45 dpi.

Similar to the previous experiment, the onset of neurological symptoms presented from day 10 onwards, peaking at 18 dpi (VLP only 3.15 ± 0.52, peptide 8 2.022 ± 1.13) (Figure 4.4A). Peptide 8 immunised mice showed a significant reduction in neurological score on specific days, detailed in Table 4.3. However, the overall neurological disability over the 45 days, calculated by the AUC, was not significantly lower (VLP only 65.72 ± 3.1, peptide 8 54.53 ± 4.5) (Figure 4.4C).

A significant reduction in the disease-associated weight loss was also seen in the peptide 8 treated group on a number of days (Figure 4.4B). This resulted in a significant overall reduction in disease-associated weight loss in the peptide 8 group, calculated by the AUC (peptide 8 AUC 451.2 ± 36.5 v VLP only AUC 606.5 ± 31.72, **P = 0.0063) (Figure 4.4D).

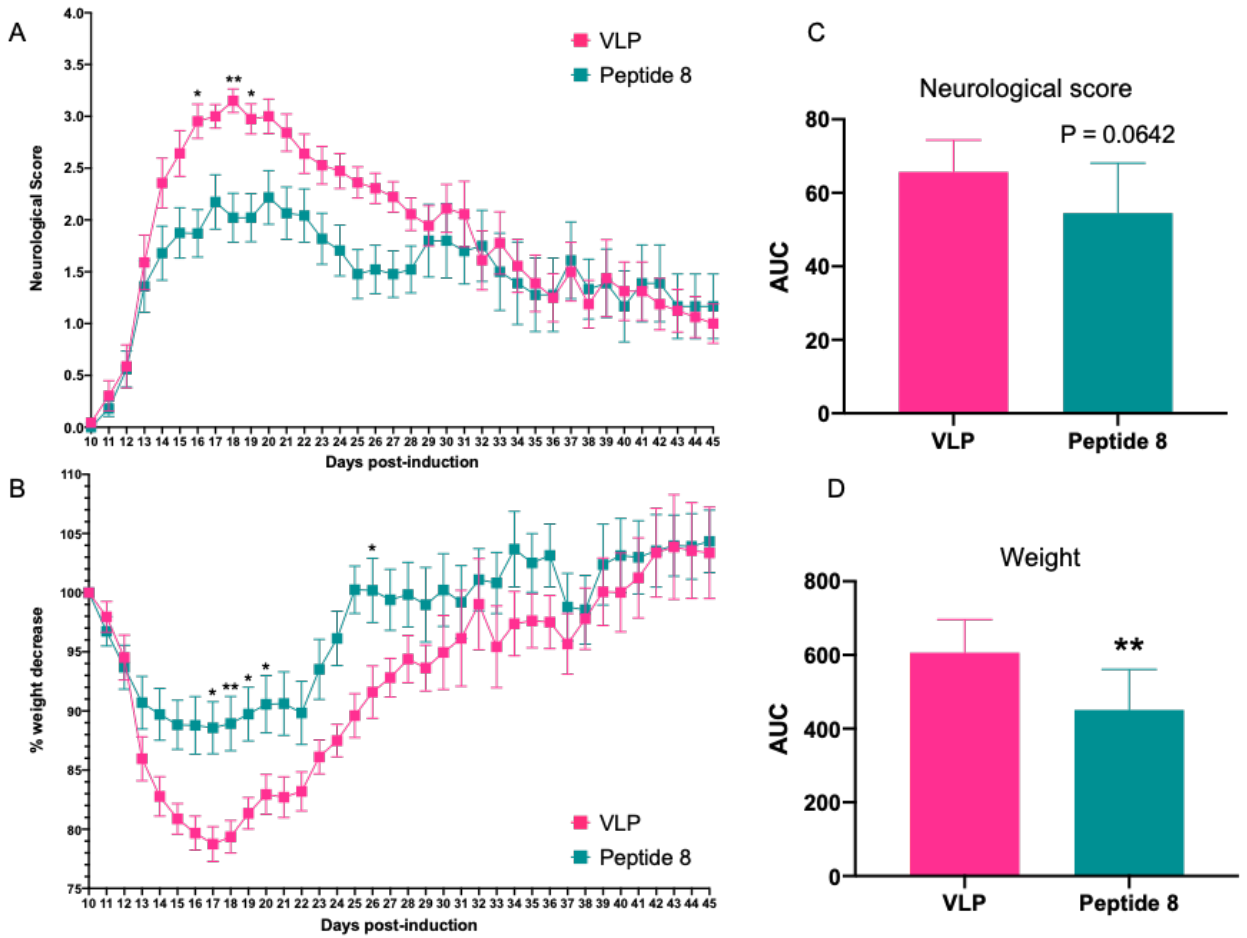

Figure 4.4 Long-term peptide 8 efficacy in the C57BL/6 MOG_{35-55} EAE model.
A) Neurological scores and C) disease-associated weight loss were significantly reduced in the peptide 8 group on specific days when compared to VLP Group. One-way ANOVA with Tukey's multiple comparison test. *P < 0.05, **P < 0.01 versus VLP. Data represented as mean ± SEM. Area under the curve (AUC) analysis calculated for B) neurological score and D) weight showed a significant reduction when comparing peptide 8 with VLP group. n = 10 VLP, n = 10 peptide 8. Student's t-test. Data presented as mean ± SD.

Table 4.3 Summary table of statistical values comparing neurological scores and percentage weight decrease between peptide 8 and VLP groups.
Overview of specific P values, on specific days, comparing peptide 8 v VLP. *P < 0.05, **P < 0.01, Two-way ANOVA with Tukey's multiple comparison test. All data presented as mean ± SD.

Day	Neurological Score		% Weight Decrease	
	Significance	Adjusted P Value	Significance	Adjusted P Value
11	ns	>0.9999	ns	>0.9999
12	ns	>0.9999	ns	>0.9999
13	ns	>0.9999	ns	>0.9999
14	ns	>0.9999	ns	>0.9999
15	ns	0.8729	ns	0.2479
16	*	0.0162	ns	0.1183
17	ns	0.2582	*	0.0279
18	**	0.0056	**	0.008
19	*	0.0485	*	0.0114
20	ns	0.5554	*	0.0496
21	ns	0.5918	ns	0.1256
22	ns	>0.9999	ns	0.0882
23	ns	0.966	ns	0.5409
24	ns	0.5137	ns	0.3031
25	ns	0.1183	ns	0.0767
26	ns	0.273	*	0.0435
27	ns	0.3145	ns	0.2985
28	ns	>0.9999	ns	>0.9999
29	ns	>0.9999	ns	>0.9999
30	ns	>0.9999	ns	>0.9999
31	ns	>0.9999	ns	>0.9999
32	ns	>0.9999	ns	>0.9999
33	ns	>0.9999	ns	>0.9999
34	ns	>0.9999	ns	>0.9999
35	ns	>0.9999	ns	>0.9999
36	ns	>0.9999	ns	>0.9999
37	ns	>0.9999	ns	>0.9999
38	ns	>0.9999	ns	>0.9999
39	ns	>0.9999	ns	>0.9999
40	ns	>0.9999	ns	>0.9999
41	ns	>0.9999	ns	>0.9999
42	ns	>0.9999	ns	>0.9999
43	ns	>0.9999	ns	>0.9999
44	ns	>0.9999	ns	>0.9999
45	ns	>0.9999	ns	>0.9999

4.3.2.2 Immune response towards peptide 8 continues up to 45 days post-induction

Serum was collected from both VLP only and peptide 8 groups on the day of disease induction via a tail-bleed, and then again at 45 dpi during tissue collection. Serum immunoreactivity against peptide 8 and VLP was quantified using an ELISA. Serum collected from both groups elicited a significant response against VLP (Figure 4.5A), whereas only serum collected from peptide 8 immunised mice showed significant immunoreactivity against peptide 8 (Figure 4.5B) . This data demonstrates that an immune response against peptide 8 was maintained throughout the whole study period.

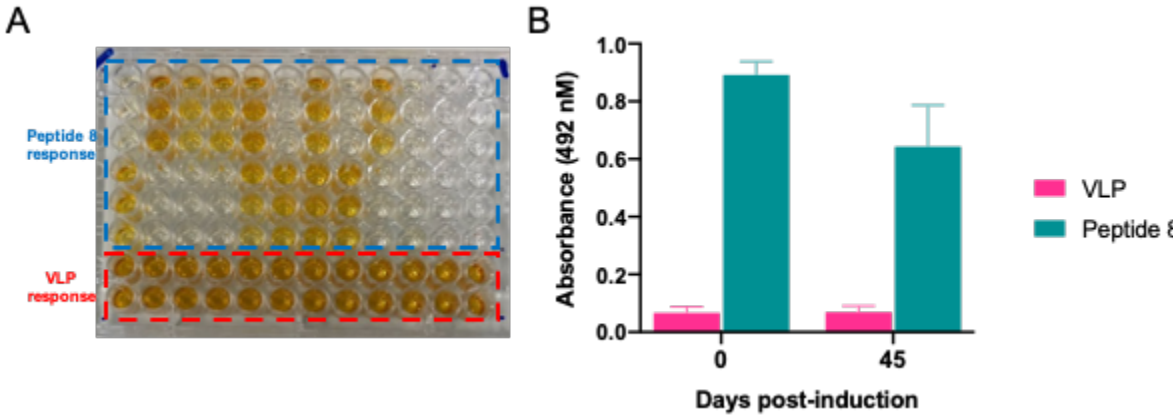

Figure 4.5 Peptide 8 ELISA serum immunoreactivity.
A) A representative image of a typical ELISA plate showing a strong immune response from peptide 8 immunised serum (yellow) and o response in VLP-only group. All serum samples were also tested for immunoreactivity against VLP as a control. B) Quantified absorbance at 492 nm.

4.3.3 *In vitro* characterisation of peptide 8 immunised serum

4.3.3.1 Overnight incubation with serum from peptide 8 immunised mice significantly increases cortical neuron firing and NMDAR1 expression

Our *in vivo* studies showed that peptide 8 immunisation significantly reduced both neurological deficits and disease-associated weight loss in the MOG_{35-55} EAE model. Therefore, the aim of the next experiment was to elucidate a potential mechanism of action.

Serum isolated from peptide 8 immunised mice contains polyclonal antibodies targeting NMDAR1, which may influence neuronal excitability. Primary mouse cortical neurons (10-14 DIV) were cultured on coverslips and incubated with serum from non-vaccinated, VLP-only or peptide 8 immunised mice (overnight, 1:100). Whole-cell current clamp recordings were taken to measure neuronal excitability, with serum present (1:100) in the extracellular solution (Figure 4.6A). Neurons incubated overnight with peptide 8 immunised serum showed a significant increase in neuronal firing versus non-vaccinated and VLP control (**$P < 0.01$, Figure 4.6B). Coverslips were then immediately fixed and then stained for NMDAR1 expression. Coverslips were co-stained with anti-mouse monoclonal antibody (mAb) to quantify co-localisation with NMDAR1 (Figure 4.7A). NMDAR1 expression was significantly increased following overnight incubation with peptide 8 immunised serum when compared to non-vaccinated and VLP control (Figure 4.7B). Furthermore, this correlated with increased staining for anti-mouse mAb (Figure 4.7C). Taken together this data demonstrates that cortical neurons that are incubated overnight with peptide

8 immunised serum show increased neuronal firing likely due to an increase in NMDAR1 expression.

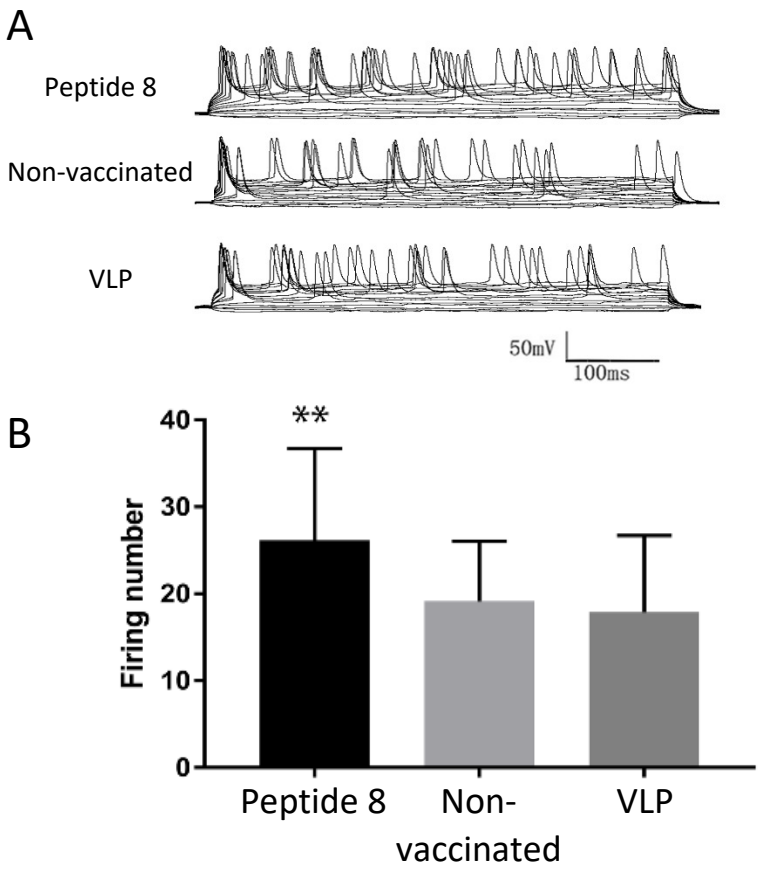

Figure 4.6 Primary mouse cortical neuron firing following overnight serum incubation.
A) Whole-cell current clamp recordings taken from cortical neurons incubated overnight with non-vaccinated, VLP and peptide 8 immunised serum. Whole-cell current clamp recordings were performed at room temperature and injected with 15 steps (10pA increase) of currents from -80pA to 60pA. B) Total firing (action potential) number with magnitude of 20mV or higher were counted for analysis. **P<0.01 vs non-vaccinated and VLP. n = 24 recordings/condition. Data presented as mean ± SD. One-way ANOVA with Tukey's multiple comparison test.

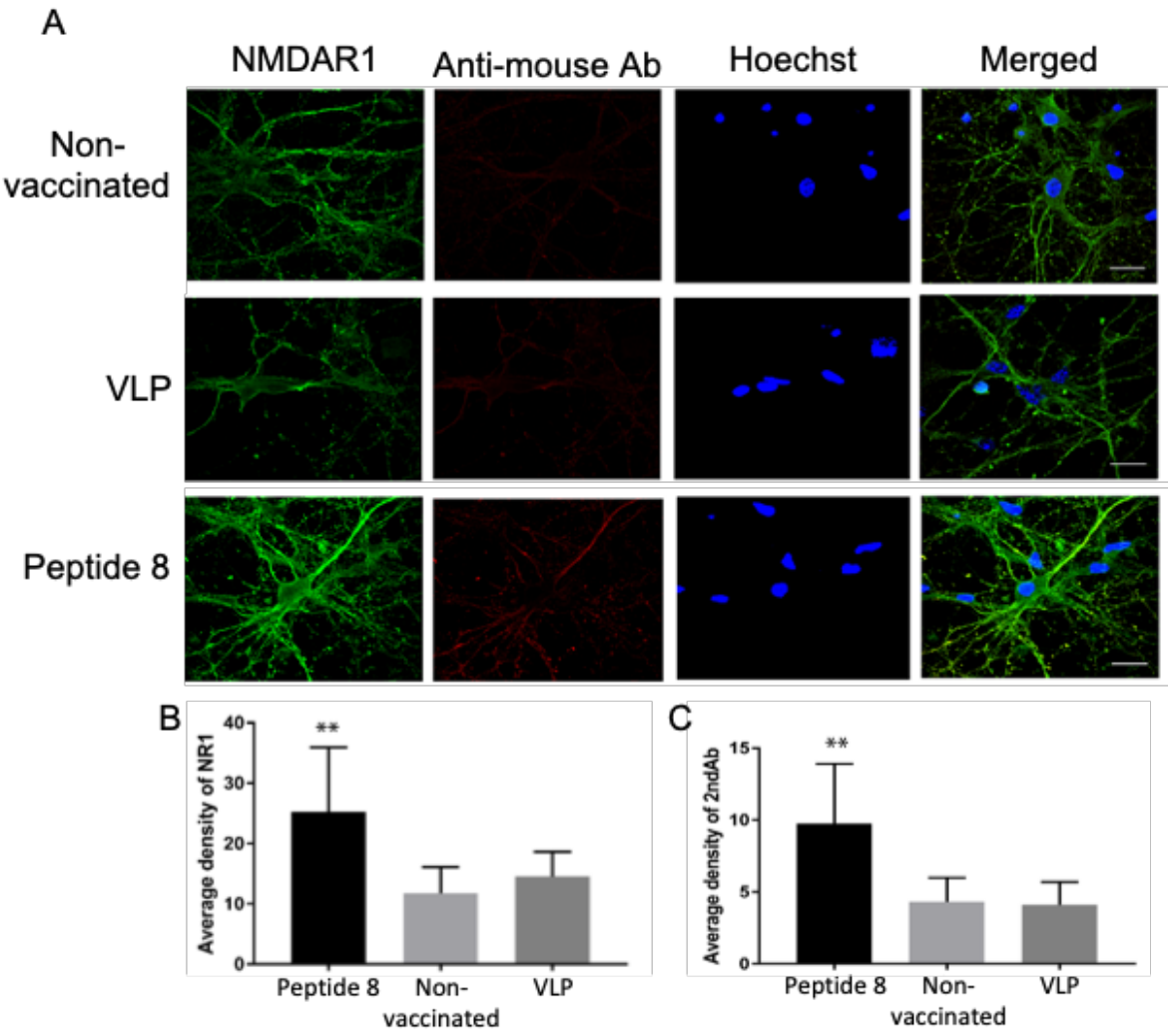

Figure 4.7 Primary mouse cortical neuron NMDAR1 expression following overnight serum incubation.
A) Cortical neurons used for electrophysiological recordings were stained with goat anti-rabbit NMDAR1 (green) and goat anti-mouse secondary antibody (red). Co-localisation of NR1 and anti-mouse secondary antibody in yellow can be seen in neurons treated with vaccine serum, but not in non-vaccinated or VLP-treated neurons. Scale bar=20μm. Average density of B) NMDAR1 and C) anti-mouse secondary antibody were significantly increased in neurons treated with vaccine. **P<0.01 vs non-vaccinated and VLP. n = 25 images/condition. One-way ANOVA with Tukey's multiple comparison test.

4.3.3.2 Short-term incubation with peptide 8 serum treatment does not significantly change cortical neuron firing or NMDAR1 expression

Following the previous experiment, we wanted to elucidate whether immediate treatment with peptide 8 immunised serum also altered cortical neuron excitability and/or NMDAR1 expression. Primary mouse cortical neurons were cultured (10-14 DIV) on coverslips and whole-cell current clamp recording were performed 1 h after the addition of non-vaccinated, VLP and peptide 8 immunised serum (1:100) into the extracellular solution (Figure 4.8A). This was done to determine if immediate binding of serum antibodies could influence neuronal excitability. Both cortical neuronal firing (Figure 4.8B) and NMDAR1 expression (Figure 4.9A-B) were not significantly altered. This experiment demonstrated that short term incubation with peptide 8 serum does not alter neuronal firing and is also not sufficient to change NMDAR1 expression.

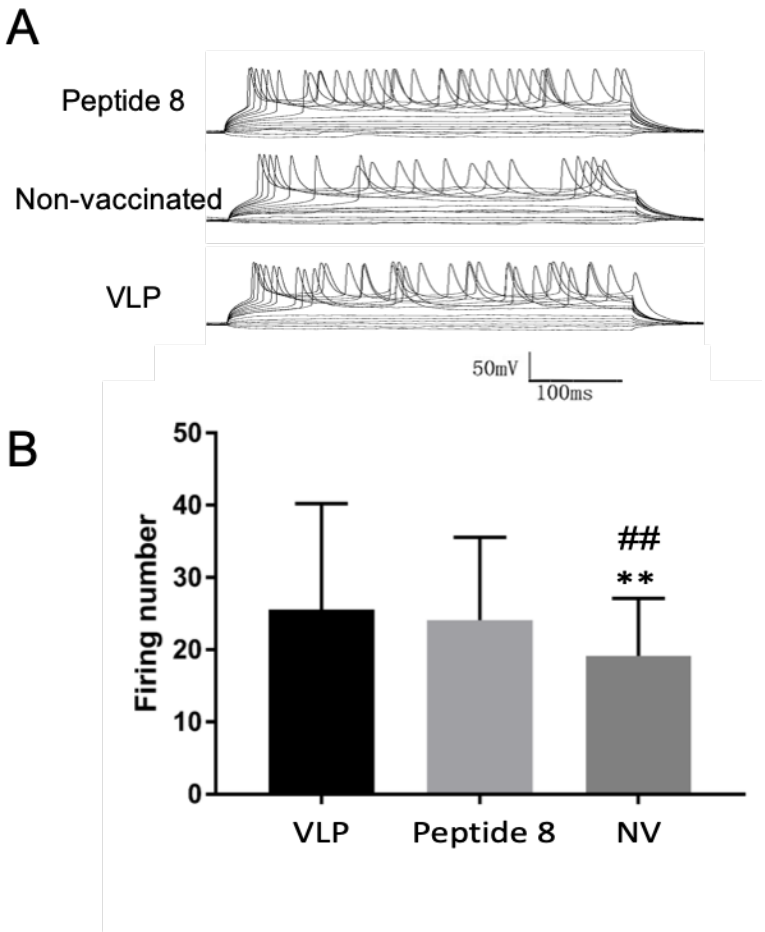

Figure 4.8 Primary mouse cortical neuron firing following short-term serum incubation.
A) Whole-cell current clamp recordings taken from cortical neurons in the presence of non-vaccinated, VLP and peptide 8 immunised serum. Whole-cell current clamp recordings were performed at room temperature and injected with 15 steps (10pA increase) of currents from -80pA to 60pA. B) Total firing number was significantly lower in non-vaccinated groups compared to both VLP and peptide 8 groups. **P<0.01 vs non-vaccinated and VLP. n = 21 recordings/condition. Data presented as mean ± SD. One-way ANOVA with Tukey's multiple comparison test.

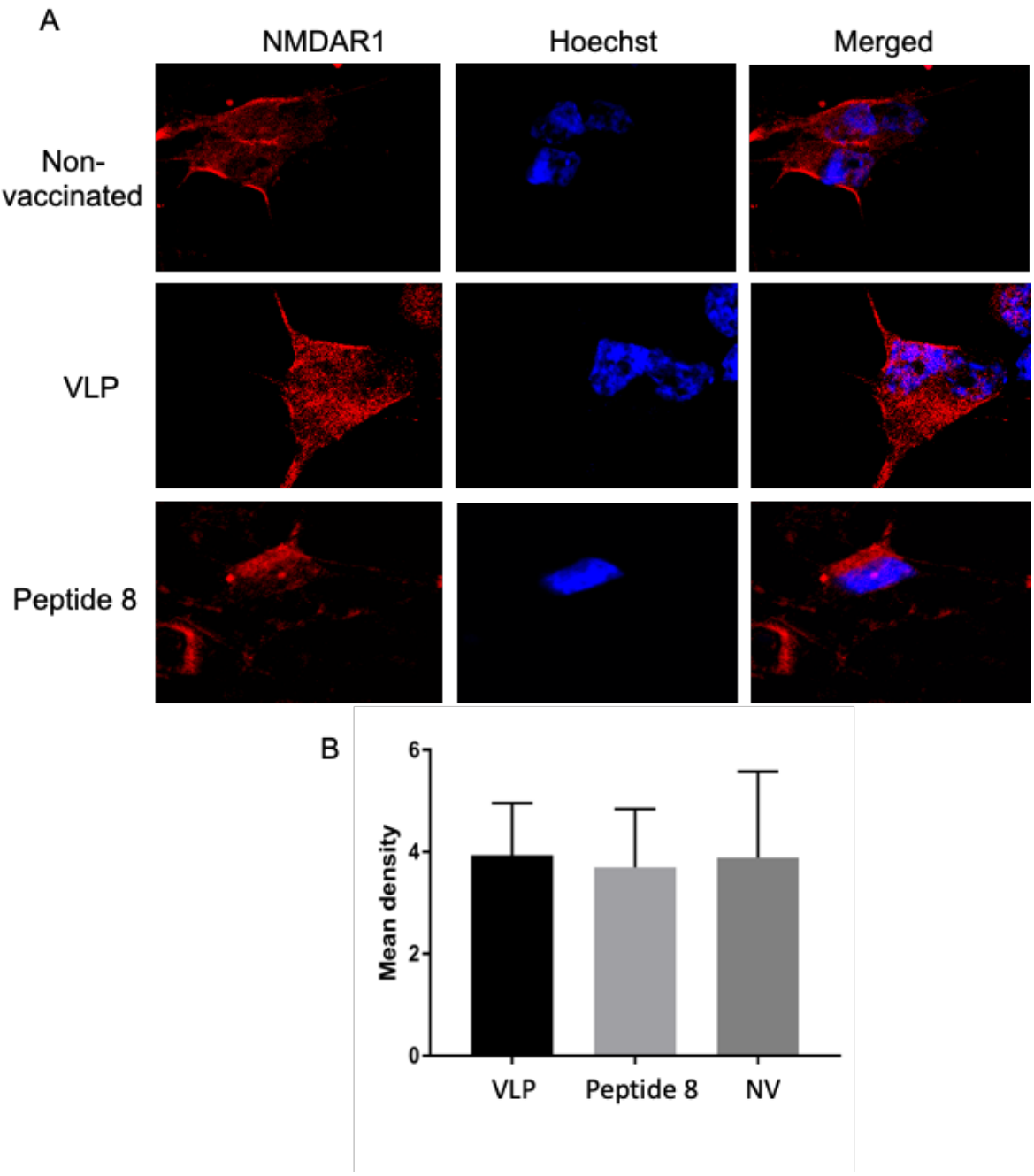

Figure 4.9 Primary mouse cortical neuron NMDAR1 expression following short-term serum incubation.
A) Cortical neurons used for electrophysiological recordings were stained with goat anti-rabbit NMDAR1 (red). Scale bar = 20 μm. B) Mean density of NMDAR1 was unchanged following short-term serum incubation. n = 22 images/condition. One-way ANOVA with Tukey's multiple comparison test.

4.3.4 Spinal cord western blot analysis

Western blot analysis of lumbar and cervical spinal cord EAE samples was next performed. Glial fibrillary acidic protein (GFAP) expression was quantified to determine glial reactivity and phosphorylated extracellular-regulated kinase 1/2 (pErk1/2) expression was used as a downstream marker for ionotropic NMDAR activation, particularly NMDAR1, excitotoxic injury and axonal transection[323]. Cervical and lumbar spinal cord were isolated at two timepoints – peak disease (14 days post-induction) and following partial disease recovery (28 days post-induction) to characterise the temporospatial changes of these markers between experimental groups. Experimental groups for western blot analysis are defined in Table 2.4.

GFAP and pERK1/2 expression were first of all quantified at peak disease (14 dpi) in cervical and lumbar spinal cord. No significant difference was observed between treatment groups in cervical spinal cord (Figure 4.10A-C). However, analysis of lumbar spinal cord showed a significant increase in GFAP expression in non-vaccinated (NV) mice compared to sham control (Figure 4.10E, NV 0.181 ± 0.0575 v sham 0.0678 ± 0.0119, $p = 0.0201$). Interestingly, peptide 8 samples show reduced GFAP expression when compared to NV mice, however this trend is also observed in VLP samples. Lumbar spinal cord pERK1/2 showed a similar expression pattern to GFAP expression at 14dpi. Peptide 8 immunised mice showed a trend in reduced pERK1/2 expression when compared to NV mice, however this did not reach significance (Figure 4.10F).

GFAP and pERK1/2 expression was also quantified following partial disease recovery (28dpi) in cervical and lumbar spinal cord. No significant difference was observed between treatment groups in cervical spinal cord GFAP or pERK1/2 expression

(Figure 4.11A-C). However, lumbar GFAP expression was significantly increased in VLP (P = 0.0018) and peptide 8 (P=0.025) groups versus AMC group (Figure 4.11E, AMC 0.803 ± 0.061, VLP 1.531 ± 0.306, peptide 8 1.78 ± 0.008). Furthermore, lumbar pERK1/2 expression was significantly increased in the non-vaccinated group versus both AMC (P = 0.042) and sham (P = 0.023) groups (Figure 4.11F, AMC 0.07174 ± 0.007, sham 0.0967 ± 0.019, NV 0.0843 ± 0.008). The peptide 8 group showed a trend in decreased pERK1/2 expression, similar to the 14dpi lumbar pERK1/2 data.

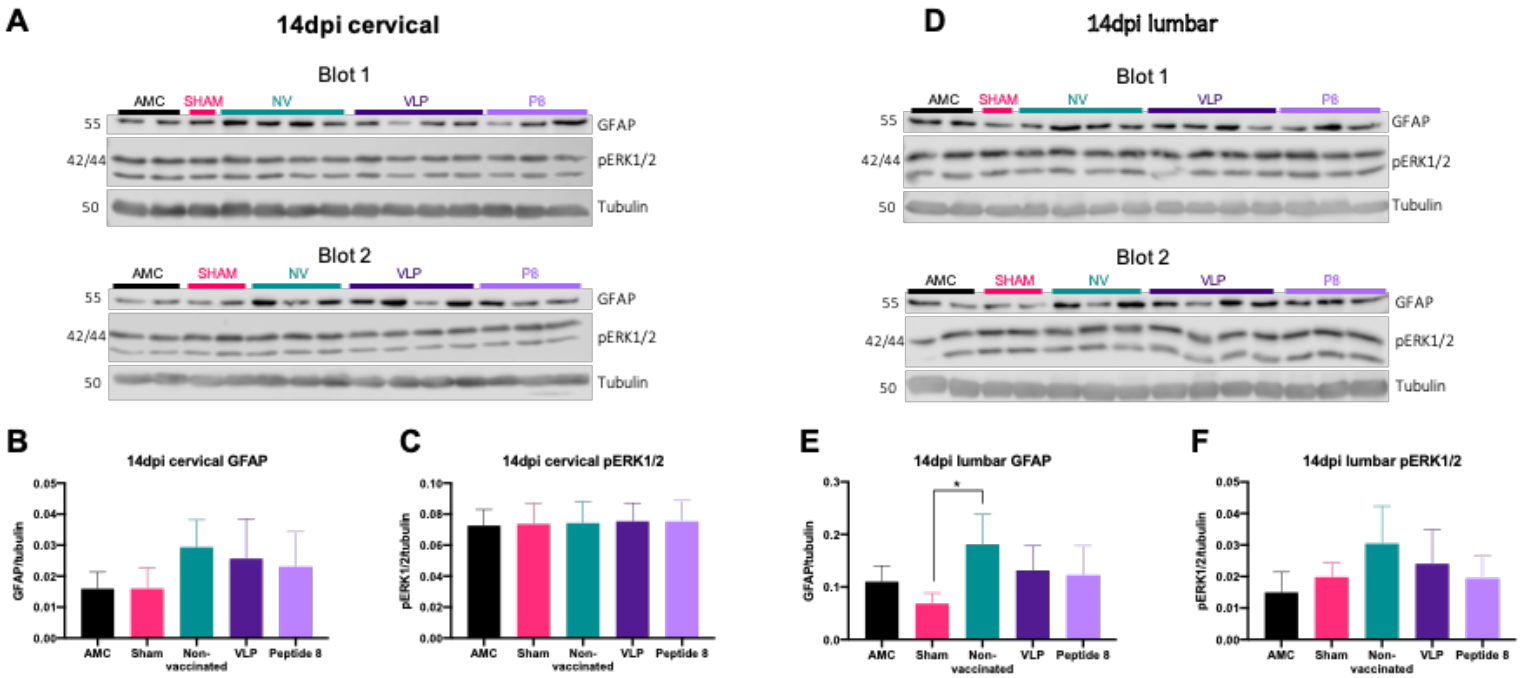

Figure 4.10 Lumbar and cervical spinal cord GFAP and pERK1/2 expression at peak disease (14dpi).
Western blot analysis of glial fibrillary acidic protein (GFAP) and phosphorylated extracellular-regulated kinase 1/2 (pErk1/2) of cervical and lumbar spinal cord isolated at peak disease (14dpi). A/D) Chemiluminescent immunoreactivity was visualised using the Li-Cor Odyssey Imaging System and signal intensity was quantified using ImageStudio™ Lite. Data represented as normalised signal intensity relative to tubulin control. B) GFAP or C) pERK1/2 expression was not significantly different between treatment groups in cervical spinal cord. E) GFAP expression was significantly increased in non-vaccinated mice when compared to sham control. F) No significant difference in pERK1/2 expression was observed. One-way ANOVA, Tukey's multiple comparison test. * $p < 0.05$. One-way ANOVA, Tukey's multiple comparison test. Data presented as mean ± SD. n = 4 AMC, n = 3 sham, n = 7 NV, n = 8 VLP, n = 6 Peptide 8.

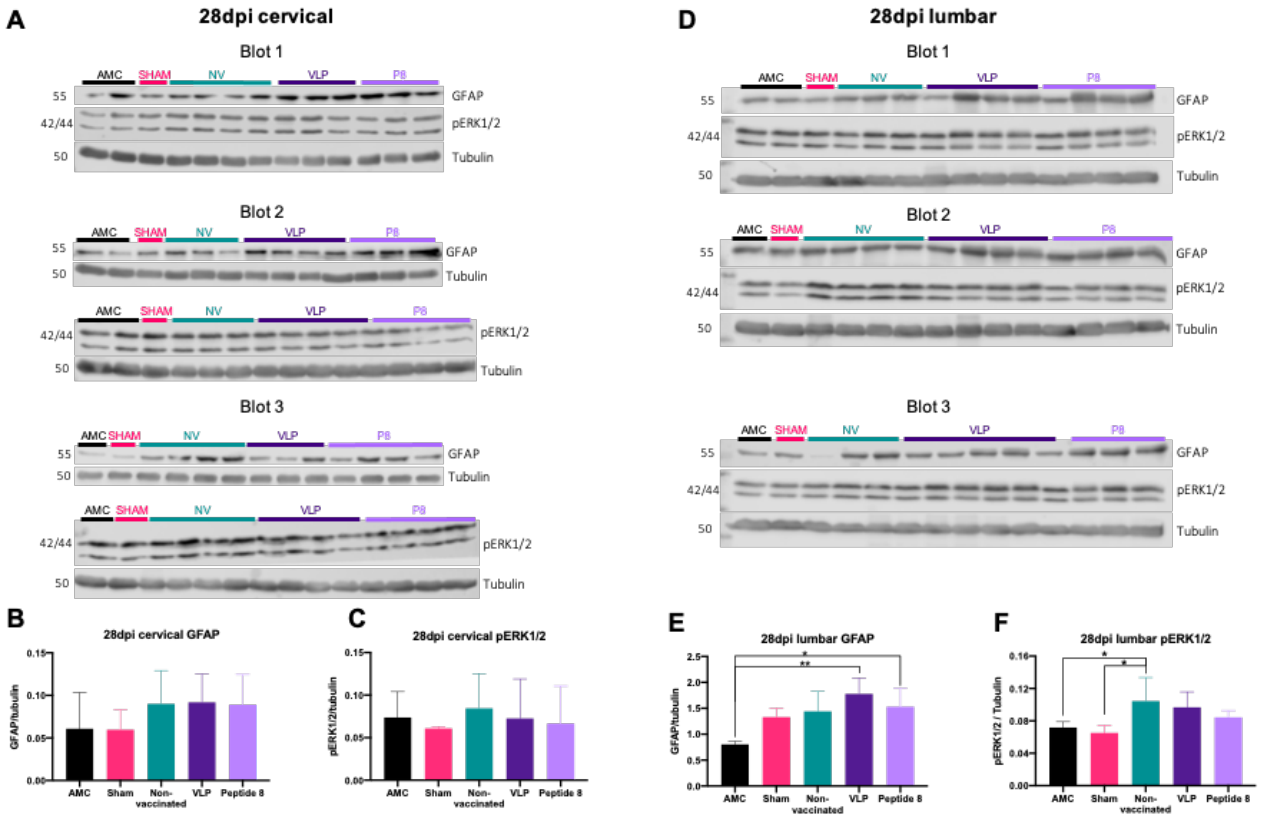

Figure 4.11 Lumbar and cervical spinal cord GFAP and pERK1/2 expression following partial disease recovery (28dpi). Western blot analysis of glial fibrillary acidic protein (GFAP) and phosphorylated extracellular-regulated kinase 1/2 (pErk1/2) of cervical and lumbar spinal cord isolated following partial disease recovery (28dpi). A/D) Chemiluminescent immunoreactivity was visualised using the Li-Cor Odyssey Imaging System and signal intensity was quantified using ImageStudio™ Lite. Data represented as normalised signal intensity relative to tubulin control. B) There was no observed difference in cervical spinal cord GFAP or C) pERK1/2 expression between treatment groups E) Lumbar spinal cord GFAP expression was significantly increased in VLP and peptide 8 treated mice when compared to age-matched control (AMC). F) Lumbar spinal cord pERK1/2 expression was significantly increased in non-vaccinated mice when compared to age-matched control and sham groups. One-way ANOVA, Tukey's multiple comparison test. * $P < 0.05$, **$P < 0.01$. One-way ANOVA, Tukey's multiple comparison test. Data presented as mean ± SD. n = 4-5 AMC, n = 3 sham, n = 10-11, n = 10-13 VLP, n = 10-11 Peptide 8.

4.3.5 Nanostring nCounter gene expression analysis

4.3.5.1 RNA yield and integrity

Following spinal cord RNA extraction, sample RNA yield and purity was determined using the NanoDrop™ spectrophotometer. All samples had a A260/280nm value of 2.0 ± 0.2 and a 260/230 ratio of 2.2 ± 0.2 (Table 4.4). RNA integrity was determined using the Agilent 2100 Bioanalyzer. Gel electrophoresis of total RNA show distinct bands at 18S and 28S ribosomal (rRNA) (Figure 4.12A-B). Corresponding electropherograms for each sample were generated to calculate an RNA integrity number (RIN), where RIN 0 is completely degraded and RIN 10 is completely intact RNA (Table 4.5). Although some values were considered low, previous experimental characterisation deemed these RIN values suitable for further analysis using the Nanostring nCounter system.

Table 4.4 Extracted RNA quality and yield.

Animal ID	Group	Experimental ID	ng/ul	A260	A280	260/280	260/230
255430	Age-matched control	AMC1	594.28	14.96	7.77	1.91	1.93
255432		AMC2	43.81	1.10	0.59	1.85	1.85
255431		AMC3	349.64	8.74	4.51	1.94	1.94
255410	Non-vaccinated	NV1	325.37	8.13	4.22	1.93	1.93
255402		NV2	107.77	2.69	1.59	1.7	1.70
255403		NV3	367.08	9.18	4.67	1.96	1.96
255425	Virus-like protein	VLP1	146.36	3.66	1.99	1.84	1.84
255409		VLP2	116.15	3.30	1.71	1.69	1.93
255411		VLP3	178.02	4.55	2.51	1.78	1.82
255414	Peptide 8	P81	262.38	6.56	3.54	1.85	1.85
255404		P82	437.65	10.94	6.08	1.8	1.80
255423		P83	155.37	3.88	2.28	1.7	1.70

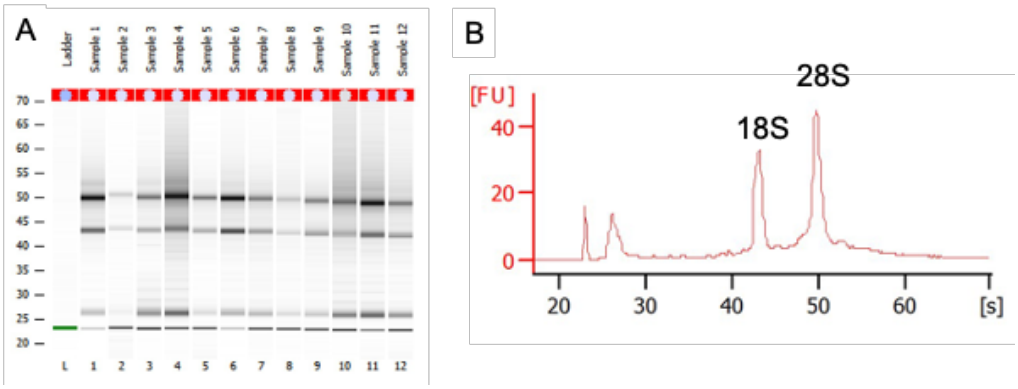

Figure 4.12 RNA integrity assessment.
A) Electrophoresis gels of each sample produced by the Agilent 2100 Bioanalyzer used to asses RNA integrity of extracted samples. B) Example electropherogram with labelled peaks corresponding to 18S and 28S rRNA.

Table 4.5 Extracted RNA integrity.
RNA integrity number (RIN) was determined using the Agilent 2100 Bioanalyzer.

Experimental ID	RNA integrity number (RIN)
AMC1	9.4
AMC2	2.4
AMC3	8.2
NV1	7.5
NV2	9.3
NV3	9.4
VLP1	8.4
VLP2	7.8
VLP3	9.4
P81	N/A
P82	2.5
P83	8.9

4.3.5.2 Heatmap of raw gene expression data and quality control

RNA samples were hybridised to the target sequence probes and loaded into the cartridge of the Nanostring nCounter Neuroinflammation panel. Corresponding gene CodeSet reporter code counts (RCC) were loaded into nSolver Analysis for quality control (QC) and differential expression analysis.

Firstly, QC checks were conducted to ensure assay performance. No samples were flagged for QC anomalies, therefore all gene codes were successfully imaged, including internal positive and negative controls (Figure 4.13A.). Heatmaps of raw gene counts were generated by plotting z-scores for each probe ID, with blue showing low expression and orange showing high expression. The heatmap provides an overview of how robust the raw expression levels are across samples and gene sets and highlights samples that fell below the detection limit of the assay. It is evident that all samples follow a general gene expression pattern, however further analysis aimed to identify differentially expressed genes.

In order to calculate differential expression (DE) between groups, gene counts were normalised against reference housekeeping genes to account for differences in RNA loading and minimise technical errors that may influence DE analysis. Mean signal was plotted against variance for each probe ID and housekeeping target gene expression whose expression did not correlate with other housekeeping genes were excluded from normalisation, of which two genes were excluded (highlighted in orange, Figure 4.13B), as determined by the geNorm algorithm. P-value plots were generated to evaluate overall differential expression between samples. This p-value plot shows a rightward shift, indicating that the majority of genes analysed were not differentially expressed (Figure 4.13C).

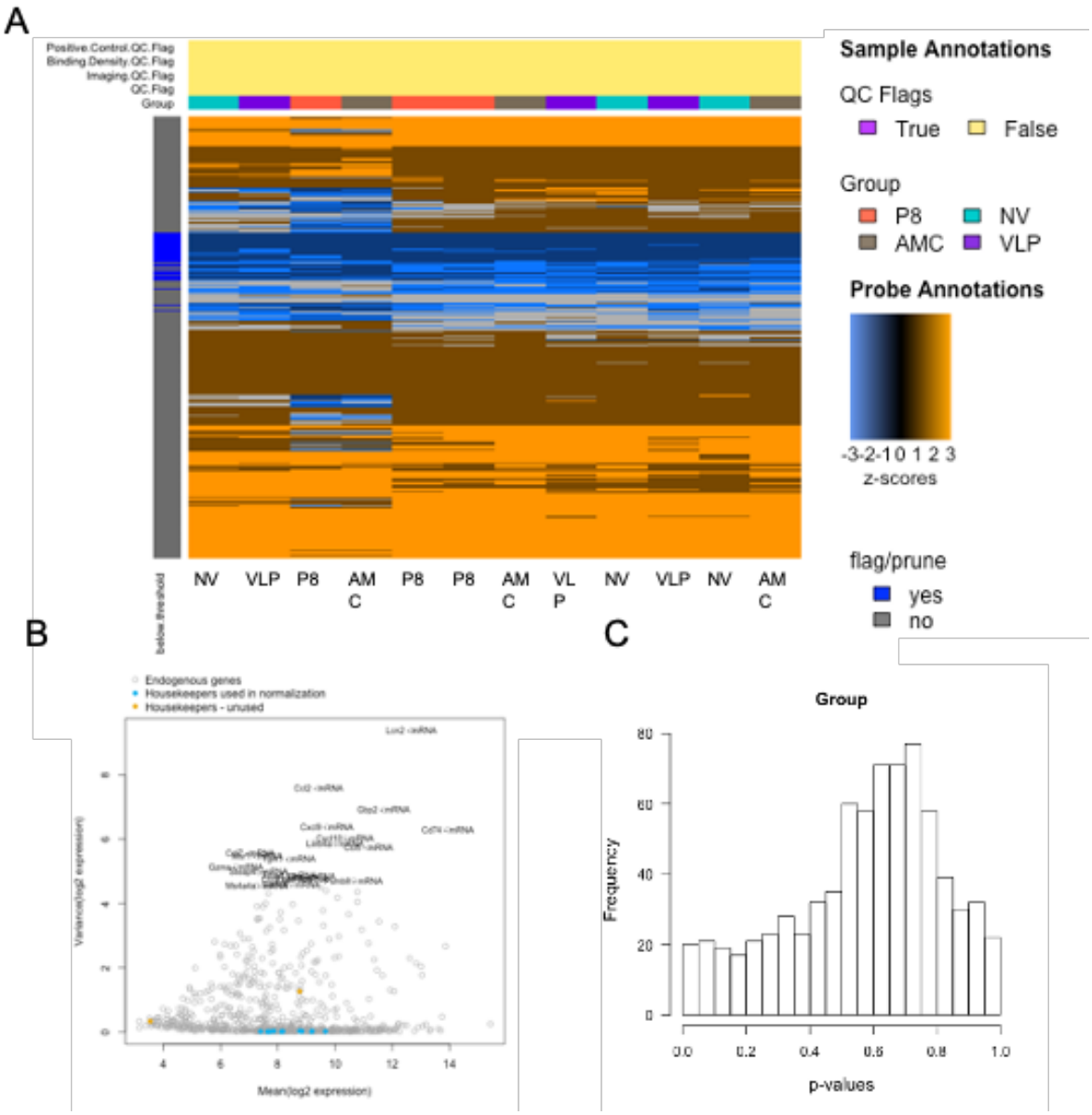

Figure 4.13 Nanostring raw data overview.
A) QC flag status of each sample indicates all samples fall within the acceptable QC values. Heatmap of the raw counts shows the z-score of each probe. Blue bars on the left indicate probes whose counts fell below the threshold in all samples and were removed for further analysis. Blue – low expression, black – average expression, orange – high expression. B) Variance vs. Mean normalized signal plot across all targets/probes. Each gene's variance in the log-scaled, normalized data is plotted against its mean value across all samples. Highly variable genes are indicated by gene name. Housekeeping genes are colour coded according to their use in (or omission from) normalisation. C) p-value distribution plot for each group included in the analysis. Left-weighted histograms indicate high differential expression between groups.

4.3.5.3 Global gene expression pathway signatures versus peptide 8 samples

Heatmaps showing global significance scores within specified gene sets show changes in gene expression in multiple pathways in the peptide 8 group (Figure 4.14). This broad view of the data highlights changes in grouped pathway signatures, allowing identification of further gene sets to explore. Analysis aimed to compare peptide 8 samples against the other experimental groups to investigate gene sets that may be contributing towards the observed neuroprotection. All gene pathways included in the panel showed decreased expression in the AMC samples when compared to peptide 8 samples. This was expected as neuroinflammation is significantly increased following EAE induction and AMC samples were used to determine baseline expression values.

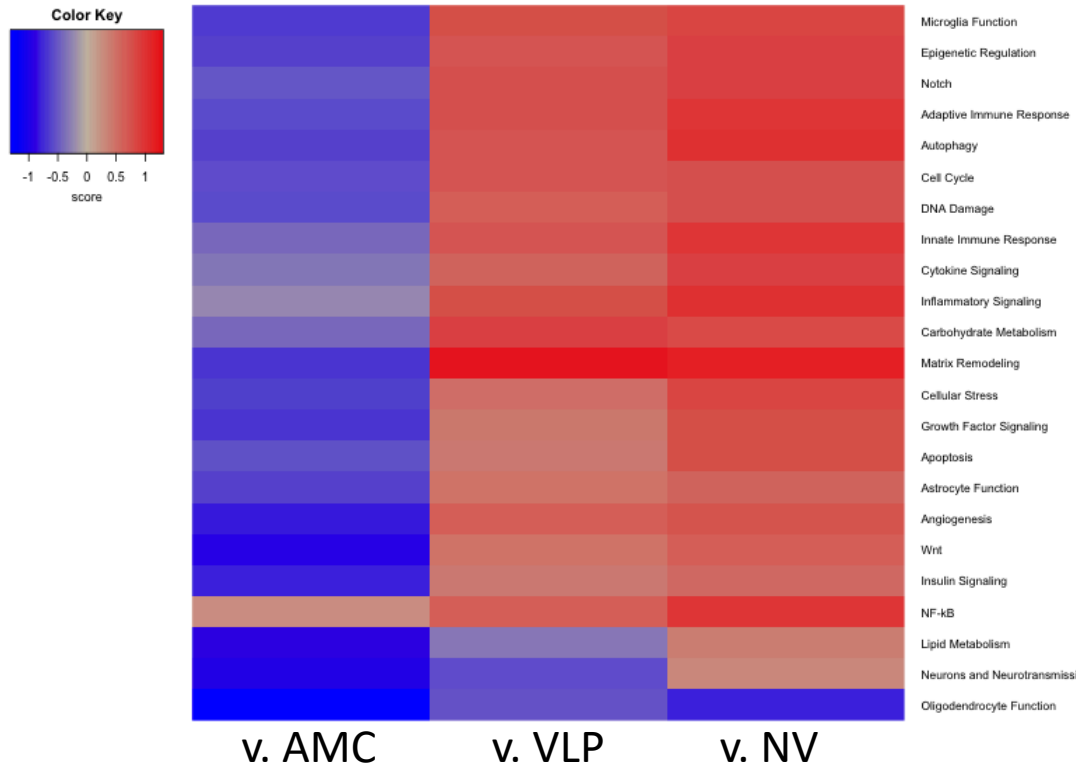

Figure 4.14 Directed global significance scores relative to peptide 8 group. Heatmap displaying each sample's directed global significance scores within specified gene sets. Red denotes gene sets whose genes exhibit extensive over-expression with the covariate, blue denotes gene sets with extensive under-expression relative to the peptide 8 group.

4.3.5.4 Differential expression versus peptide 8 group

Volcano plots aimed to identify specific differentially expressed genes relative to the peptide 8 samples. Generated volcano plots display each gene's -log10(p-value) versus the normalised log2 fold change relative to the peptide 8 samples. Therefore, highly statistically significant genes fall at the top of the graph and highly differentially expressed genes fall to either side (Figure 4.15).

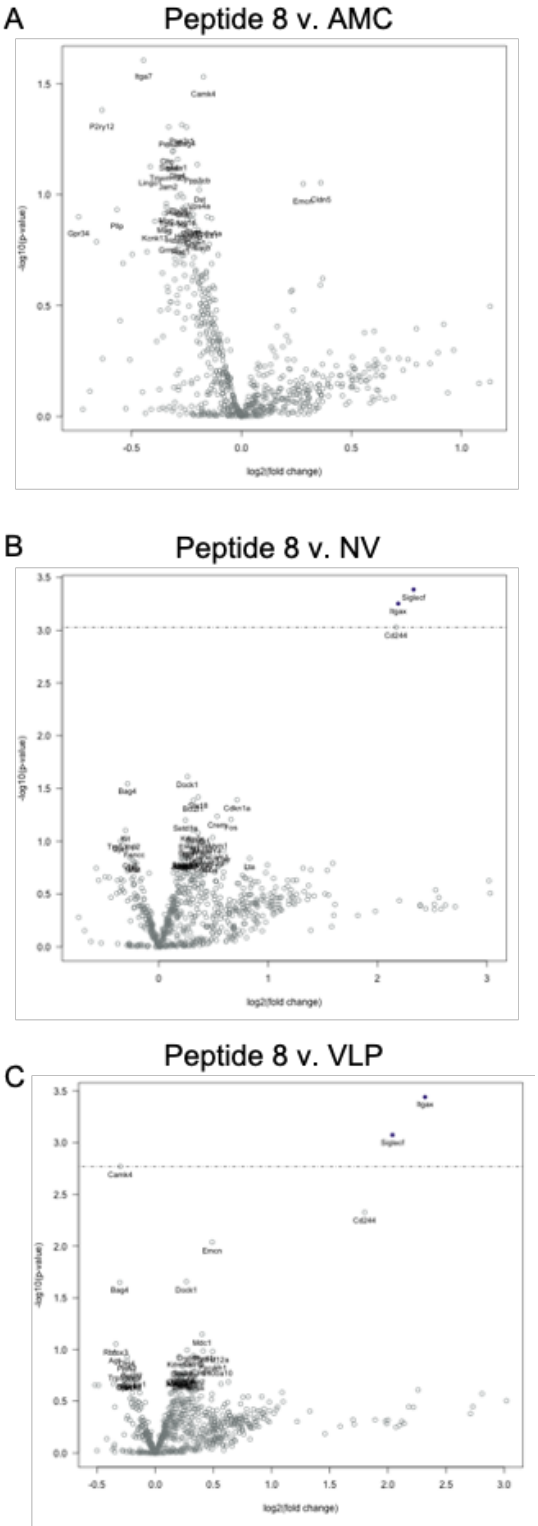

Figure 4.15 Volcano plots of Nanostring gene expression data
Volcano plot displaying each gene's -log10(p-value) and log2 fold change versus the peptide 8 group. Highly statistically significant genes fall at the top of the plot above the horizontal lines, and highly differentially expressed genes fall to either side. The 40 most statistically significant genes are labelled.

4.3.5.5 Peptide 8 cervical spinal cord shows differential expression in genes involved in calcium signaling, immune regulation and cell death

The most differentially expressed genes and their respective significance values are summarised in Table 4.6. Figure 4.16 visualises normalised log2p peptide 8 values expressed against each experimental group to identify the top six highly differentially expressed genes.

Bag4 expression was significantly lower in AMC, NV and VLP groups compared to peptide 8 samples (Figure 4.16A). Furthermore, lower expression of Camk4 (Figure 4.16B) was seen in AMC and VLP samples (Figure 4.16C). Expression of Cd244, Dock1, Itgax and Siglecf were significantly higher in both NV and VLP samples when compared peptide 8 samples (Figure 4.16D-F). No significant difference was seen between peptide 8 samples and AMC samples in these genes, indicating that peptide 8 may return these genes back to baseline levels. The potential significance of these results are discussed in Chapter 4.4.6.

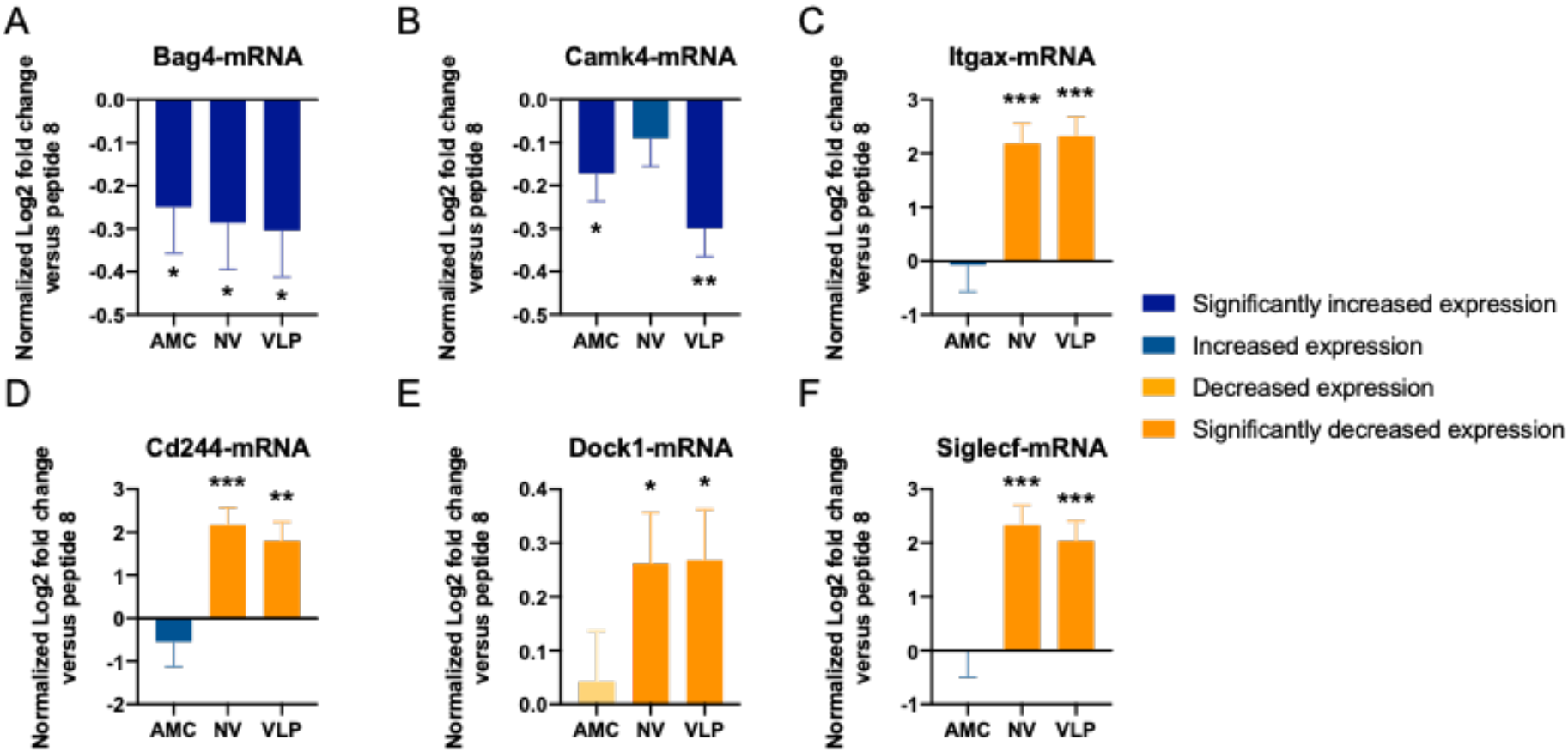

Figure 4.16 Differential expression analysis versus peptide 8 group
Log2 fold-changes show most differentially expressed genes. Data presented as mean ± SEM. One-way ANOVA followed by Benjamini-Yekutieli adjustment. *P < 0.05, **P < 0.01, ***P < 0.001.

Table 4.6 Summary of most differentially expressed genes versus peptide 8 group

Overview of specific P values comparing specified gene log2 changes relative to the peptide 8 group. *P < 0.05, **P < 0.01, ***P < 0.001. One-way ANOVA followed by Benjamini-Yekutieli adjustment.

Gene	Probe ID	Peptide 8 versus.	Log2 fold change	std error	Sig.	Adj. p-value
Bag4	NM_026121.3:3735	AMC	-0.249	0.108	*	**0.0497**
		NV	-0.287	0.108	*	**0.0286**
		VLP	-0.304	0.108	*	**0.0224**
Camk4	NM_009793.3:3280	AMC	-0.172	0.0649	*	**0.0294**
		NV	-0.0905	0.0649	ns	0.201
		VLP	-0.3	0.0649	**	**0.0017**
Cd244	NM_018729.2:262	AMC	-0.551	0.575	ns	0.37
		NV	2.17	0.396	***	**0.000935**
		VLP	1.8	0.442	**	**0.00472**
Dock1	NM_001033420.2:405	AMC	0.0423	0.0946	ns	0.666
		NV	0.262	0.0946	*	**0.0244**
		VLP	0.268	0.0946	*	**0.022**
Itgax	NM_021334.2:327	AMC	-0.0767	0.496	ns	0.881
		NV	2.19	0.367	***	**0.00056**
		VLP	2.32	0.362	***	**0.000363**
Siglecf	NM_145581.1:355	AMC	-0.00869	0.489	ns	0.986
		NV	2.33	0.371	***	**0.000412**
		VLP	2.04	0.367	***	**0.000843**

4.4 Discussion

4.4.1 VLP conjugation and immunogenicity quantification

VLPs can be produced in a multitude of systems, including yeast, bacteria and mammalian cells[257]. The VLP utilised in this project uses a bacteriophage to couple Qβ-VLP to peptide 8 using an succinimidyl 6-(beta-maleimidopropionam (SMPH) cross-linker. SMPH cross-linkers express maleimide and ester groups, that react with thiol and amino groups, respectively. This method allows VLPs to display several copies of the peptide[324]. This structure renders them highly immunogenic vaccine templates. VLPs are taken up by APCs, including macrophages, DCs, CD8 T cells and B cells[324]. VLPs have no viral genetic material and have been shown to be a safe and effective method of eliciting an antibody immune response[260].

Successful conjugation was determined by SDS-page (Figure 4.1). Following immunisation, serum was collected from each experimental group and an ELISA against peptide 8 was used to quantify serum antigenicity. ELISA was used due to their simplicity, high sensitivity and their amenability for high throughput serological screening[325,326]. Furthermore, assays can be automated to increase throughput of immunogenicity screening, which is paramount for clinical translation. In the context of this project, immunogenicity quantification is important to ensure that a sustained immune response is achieved and that this is consistent between experiments. An immune response against peptide 8 was maintained up until 45 days post-induction when the mice were sacrificed (Figure 4.5A-B). These experiments determined that peptide 8 was successfully conjugated to VLP and that this conjugate induced a significant antibody response against the peptide 8 sequence.

In this ELISA, the B cell response is quantified as generated antibodies are largely responsible for mediating the immune effects. Although peptide conjugates were designed to minimise a T cell response, the generation of peptide 8 specific T cells has not been determined. The enzyme-linked immunosorbent spot (ELISpot) assay has been widely used in both mouse and human studies to measure antigen-specific T cells by detecting cytokine secretion following peptide stimulation[327,328] and could be used to measure and T cell-specific response.

4.4.2 Peptide 8 immunisation does not change behavioural outcomes

Peptides were designed to minimise the chance of encephalitis by synthesising short peptide sequence that are highly specific to the NR1 subunit of NMDAR1. These peptide sequences were profiled using an online B cell immunogenicity predictor so that peptide sequences would elicit a B cell response but avoid a T cell response to prevent the risk of anti-NMDAR T cell mediated encephalitis. Anti-NMDAR encephalitis is a reported syndrome consisting of psychosis, dyskinesia, anxiety, depression, cognitive decline and autonomic dysregulation[329,330]. With this in mind, behavioural measurements were chosen to measure habitual behaviour (marble burying, burrowing and nest building) as well as anxiety and locomotion alterations (open-field test). These behavioural analyses did not result in any observed changes in peptide 8 immunised mice when compared to both VLP and non-vaccinated mice. Furthermore, mouse weight did not differ between groups, indicating no changes in eating behaviour either (Figure 4.2A-E). This said, onset of encephalitis is dependent on the breakdown of BBB integrity which allows CNS infiltration of encephalitic antibodies[331]. BBB breakdown is observed in MS pathogenesis[332] and in EAE, evidenced by the necessity of pertussis toxin for robust disease induction[333]. Further

experiments characterising these behavioural parameters following peptide 8 immunisation during BBB breakdown and EAE induction will further characterise behavioural outcomes in a more clinically relevant model. The open field test can be used to evaluate general locomotor activity and willingness to explore. A significant reduction in distance travelled, quadrant changes and number of rearings can be seen in symptomatic EAE animals when compared to control[191]. However, this is likely due to a reduced mobility because of hindlimb paralysis and not any changes in willingness to explore. Memory dysfunction is also observed in EAE animals. MOG_{35-55} induced EAE mice are unable to discriminate between a familiar and new object[334], indicating a lack of ability to form and retain memories. Other observable differences have been shown in EAE models, including impaired spatial memory[335,336], the development of allodynia[334,337] and behavioural changes such as anxiety and depression[338,339]. Further characterising these cognitive and functional parameters would allow us to better understand the influence of peptide 8 immunisation on innate and learned behaviour.

4.4.3 Peptide 8 immunisation efficacy in the C57BL/6 MOG_{35-55} EAE model

Literature has highlighted the role of glutamate excitotoxicity in a number of neurodegenerative diseases, including Parkinson's disease, Alzheimer's disease and amyotrophic lateral sclerosis (ALS)[177,340–342]. Dysregulation of glutamate homeostasis is also observed in MS[343] and EAE[182], including the C57BL/6 MOG_{35-55} EAE model used in this experiment[344]. EAE vastly increases excitatory transmission of glutamatergic synapses, particularly in striatal neurons[345]. Excessive calcium entry through NMDARs mainly mediates the pathological effects of glutamate overload in EAE[346,347] and facilitates downstream mitochondrial dysfunction and oxidative

stress[164,182,343]. Peptide 8 immunisation significantly reduced both neurological scores and disease-associated weight loss in the MOG_{35-55} EAE model compared to both non-vaccinated and VLP groups. Overall disability, as measured by area under the curve (AUC), showed a significant reduction in both of these parameters. This data shows for the first time the efficacy of a therapeutic vaccine targeting the NMDAR1 receptor in the EAE model (Figure 4.3A-D).

Other studies support our data and show that pharmacologically inhibiting NMDARs significantly reduces EAE neurological deficits. Pharmacological blockade of NR2B-containing NMDARs with highly selective inhibitor RO25-6981 significantly reduces EAE neurological deficits in a dose-dependent manner[346]. Other therapeutic strategies targeting excitotoxic mechanisms have used well characterised small molecules to inhibit NMDA receptors to great effect, including non-competitive selective NMDAR antagonists memantine and MK-801[346,348]. The limit with this pharmacological approach is that drug dose and timing is critical for therapeutic efficacy and to minimise adverse effects. This is supported by research showing that MK-801 can induce impairments in spatial memory, memory deficits and acute psychosis in mice[349]. Furthermore, visual hallucinations have been reported to worsen or precipitate in Alzheimer's disease patients treated with memantine[350]. Therapeutic vaccination aims to circumvent these challenges of small molecule inhibition. Large molecules, such as the antibodies generated following peptide 8 immunisation, can only enter the CNS following BBB breakdown. In the context of MS, antibody infiltration would only occur during BBB dysfunction during a relapse and is therefore not dependent on the dose timing and in turn reduce the probability of adverse events. However, further characterisation of synaptic plasticity and memory[349], as discussed previously in

Chapter 4.4.2, would be needed to confirm this claim. In these studies, MK-801 could provide a useful control when investigating cognitive parameters so that data can be compared to previous literature.

4.4.4 Peptide 8 serum modulates cortical neuronal firing and NMDAR1 expression

The next experimental aim was to determine if the antibodies produced following peptide 8 immunisation could influence *in vitro* neuronal excitability. As discussed previously, EAE studies show increased glutamate release in the striatum that is associated with increased NMDAR function[345]. The therapeutic effect of peptide 8 immunisation is hypothesised to be through modulation of endogenous NMDAR1 function by direct binding of generated antibodies. In order to investigate this, primary cortical neurons (10-14 DIV) were incubated with serum isolated from non-vaccinated, VLP and peptide 8 immunised mice. Serum samples were first of all screened using an ELISA to ensure a significant immune response had been induced in the peptide 8 samples. Whole-cell patch clamp electrophysiology showed that overnight serum treatment increased neuronal firing (Figure 4.6). This correlated with increased NMDAR1 expression and mouse secondary mAb expression in peptide 8 serum treated neurons, indicating the binding of peptide 8 antibodies to NMDAR1 (Figure 4.7). Elegant work by Zue et al. demonstrated that NMDA application to mouse hippocampal neurons could induce GABAergic spontaneous inhibitory postsynaptic currents (sIPSCs) in CA1 pyramidal neurons. Furthermore, this increase in GABAergic transmission was suppressed by MK-801 and was associated with the nitric oxide signalling pathway[351]. Pharmacological NMDAR inhibition leads to a loss of this feedforward NMDA-mediated inhibitory GABAergic transmission and therefore

increased neuronal firing by disinhibited glutamatergic neurons[352]. This loss of GABAergic inhibitory transmission, as well as increased NMDAR1 expression, may be a reason for the observed increased firing following peptide 8 serum incubation. Further electrophysiology experiments, similar to those used by Xue et al., could further investigate the influence of peptide 8 serum on GABA receptor mediated currents.

Our next aim was to determine whether a shorter incubation time with peptide 8 serum would also influence neuronal excitability. Primary cortical neurons were pre-treated with serum for 1 h to allow antibody binding and whole-cell patch clamp recordings were taken. Neither neuronal firing (Figure 4.8) nor NMDAR1 expression (Figure 4.9) were significantly altered following this short-term incubation with peptide 8 serum. This data indicates that a long-term incubation is required to modulate NMDAR excitability and therefore the initial binding of peptide 8 antibodies is not sufficient to do this.

Taken together these results indicate that antibodies present in peptide 8 immunised serum can directly influence neuronal biology by increasing neuronal firing and NMDAR1 expression when compared to both non-vaccinated and VLP control serum groups. Further work aims to determine target specificity and whether this change in excitability is directly through NMDAR1 receptors or via another mechanism. Current work aims to validate antibody target specificity by utilising a more simplistic *in vitro* model. Human embryonic kidney 293 (HEK) cells are widely used in cell biology studies as they are easy to maintain and grow and are very efficient for protein production and nucleic acid transfection experiments[353]. Transfection of a functional

NMDAR1 protein into HEK293 cells has previously been reported in previous literature[354].

4.4.5 Western blot analysis of glial reactivity and cell survival signalling

Glial fibrillary acidic protein (GFAP) is an intermediate filament protein that is mainly expressed in astrocytes and is a marker of astrogliosis[355]. Astrocytes react to CNS injury by increasing GFAP transcription[356]. In the context of the MOG_{35-55} EAE model, astrocyte activation is seen even prior to immune cell infiltration and GFAP expression correlates with axonal injury[357] and onset of clinical symptoms[358]. Increased GFAP expression is also positively correlated with neurological deficits in chronic EAE models, including the Biozzi ABH[359] and C57BL/6 MOG_{35-55} model[360]. Thus, GFAP expression was quantified in lumbar and cervical spinal cord at peak and post disease in order to allow temporospatial characterisation of glial reactivity.

No significant difference was observed in GFAP expression between treatment groups in cervical spinal cord in either peak disease (Figure 4.10A-B) or post disease (Figure 4.11A-B) timepoints. However, analysis of lumbar spinal cord showed a significant change in GFAP expression between experimental groups. This was hypothesised as previous literature has demonstrated a trend in increased demyelination, axonal loss and inflammation is increased towards the lumbar regions of the spinal cord[191]. At peak disease, lumbar GFAP expression was significantly increased in non-vaccinated mice when compared to the sham control group (Figure 4.10E), however this may be due to the low sample number of the sham group, therefore analysis of more samples would increase the confidence of this result. Furthermore, post-disease (28dpi) GFAP expression is significantly decreased in VLP and peptide 8 treated groups when

compared to age-matched controls, however no significant difference is seen in the non-vaccinated group (Figure 4.11E). These results suggest that peptide 8 immunisation may be delaying GFAP expression as no significant difference is observed at peak disease, but expression is significantly increased post-disease. The opposite trend is seen in non-vaccinated mice, with significance at peak disease and not at post disease. GFAP expression analysis using other techniques may further elucidate spatial expression and these timepoints, including immunocytochemical staining, which is often used in EAE studies to quantify GFAP expression[361]. Fixing and staining spinal cords at multiple timepoints (pre-, peak and post-disease) could help us understand if glial reactivity modulation may be contributing towards the observed efficacy of peptide 8.

The extracellular signal-regulated kinases 1 and 2 (ERK1/2) are part of the mitogen-activated protein kinase (MAPK) superfamily and are the most studied of this group[362]. Following binding of growth factors, c-Raf phosphorylate and activate MAPK/ERK1 and 2 (MEK1/2) which in turn activate ERK1/2 through phosphorylation (pERK1/2). pERK1/2 translocates to the nucleus and phosphorylates multiple targets involved in cell proliferation, migration and survival[362,363]. ERK1/2 signalling is mediated by numerous extracellular signals[364] including NMDAR activation[365,366]. Thus, pERK1/2 was used as a marker of the MAPK, activated ERK cell signalling and NMDAR activation. Interestingly, pERK1/2 shows a similar temporospatial expression pattern as GFAP expression. First of all, no significant difference is seen between any of the treatment groups in cervical spinal cord at either timepoint. No significant difference in pERK1/2 expression is seen in lumbar spinal cord at 14 dpi (Figure 4.10C), however pERK1/2 is significantly increased in non-vaccinated mice when compared to both

age-matched controls and sham mice at 28 dpi (Figure 4.11F). Characterising pERK1/2 expression at a later timepoint would reveal if pERK1/2 is delayed by peptide 8 immunisation. This said, VLP and peptide 8 groups show the same trend across all groups, despite significant efficacy differences. This highlights that other pathways are likely at play or a more sensitive experimental approach was required.

4.4.6 Nanostring gene expression analysis

Limitations in this project so far fail to show direct binding of generated antibodies against the NMDAR1 sequence in the CNS and the observed efficacy may be a result of other pathways, either directly or indirectly. Therefore, in order to widen our search for therapeutic efficacy, the Nanostring mouse neuroinflammation gene expression panel technology was utilised to look at major neuroinflammatory pathways that may be influenced.

Gene expression analysis highlighted a number of differentially expressed targets in the thoracic in peptide 8 immunised mice when compared to the other groups (Figure 4.16). This said, heterogeneity of the *in vivo* model left few of the genes significantly expressed in the panel. Increasing the number of animals per group will increase confidence in this data set and may highlight other genes of interest. The possible implications of the most differentially expressed genes are discussed below.

4.4.6.1 Calcium/calmodulin-dependent protein kinase IV (CaMK4)

Calcium/calmodulin-dependent protein kinase IV (CaMK4) is a multifunctional serine/threonine kinase that regulates a number of cellular processes. CaMK4 is found in a number of tissues, mainly in the brain, thymus bone marrow and adrenal glands[367].

In the immune system, CaMK4 is expressed in immature and mature T cells and acts by activating transcription factor expression downstream of T cell receptor signalling[367]. Following calcium influx, calcium binds to form a complex with calmodulin, a messenger protein sensitive to changes in intracellular calcium levels. Calmodulin induces conformational changes in its protein targets, including CaMK4[368]. Activated CaMK4 subsequently translocates to the nucleus and regulates TF activity, including cyclic-AMP-response-element-binding protein (CREB), cyclic-AMP response element modulator α (CREMα), histone deacetylase 4 and monocyte enhancer factor 2A (MEF2). These play a key role in immune function and T cell cytokine and chemokine expression signatures[369,370].

The implications of CaMK4 expression have been explored in the context of EAE. Increased CaMK4 expression is associated with worse EAE outcome and CaMK4 inhibition improves neurological outcome in the C57BL/6 MOG_{35-55} model[371]. Increased CaMK4 expression correlates with decreased T cell IL-2 production. IL-2 is necessary for CD4 T cell differentiation into T_{regs}, which play a major role in immune regulation and tolerance. Therefore, decreased IL-2 expression decreases T_{reg} populations and increases Th17 cell number[371].

In the context of this project, spinal cord CaMK4 expression was increased in peptide 8 samples versus all other experimental groups, despite peptide 8 immunisation improving neurological scores. Therefore this data does not align with the aforementioned study[371]. Future work could characterise peripheral and central T cell populations, as well as chemokine/cytokine quantification could elucidate if peptide 8 is having an immune effect and working peripherally.

Increased neuronal firing was observed in previous electrophysiology studies, following overnight incubation with peptide 8 serum. This increase in firing was correlated with an increase in neuronal NMDAR1 expression. Both of these indicate increase calcium influx and excitability. The major mechanisms that mediate neuronal calcium signalling are calcium influx through voltage-gated calcium channels (VSCCs) and NMDARs as well as activation of downstream calcium/calmodulin dependent protein kinases, particularly CaMK4[372]. Further work to characterise CaMK4 expression in neuronal cultures following serum incubation could provide support for this EAE gene expression data. Further quantification of calcium signalling pathways, including NMDAR expression are needed for this.

4.4.6.2 Bcl-2 associated athanogene-4 (Bag-4)

Bcl-2 associated athanogene-4 (Bag-4), also known as silencer of death domains (SODD) is one of six family members identified. Bag proteins influence a number of biological processes, including apoptosis, neuronal differentiation and stress responses[373]. Increased Bag-4 expression has been extensively researched in the context of cancer and is associated as an anti-apoptotic marker in ovarian[374], breast[375], pancreatic[376] and skin cancer[377].

Bag-4, in combination with heat shock protein 70 kDa (Hsp70) negatively regulates tumour necrosis factor 1 (TNFR1) and death receptor 3 (DR3) by preventing trimerization of the receptor death domain subunits. Bag-4 retains TNFR1 in an inactive monomeric state. Bag-4 dissociates following ligand binding to TNFR1,

allowing receptor trimerization, recruitment of adapter proteins, including TRADD, FADD and TRAF, and the initiation of cell death pathways[378,379].

TNFR1 has been shown to have a detrimental role in EAE[380,381] and TNFR1 signalling has been shown to exacerbate demyelination and oligodendrocyte apoptosis[382]. In the context of this study, Bag-4 expression is significantly increased in peptide 8 samples relative to all other samples. A decrease in Bag-4 expression may indicate decreased TNFR1 trimerization and decreased activation of downstream death pathways. Further work to characterise TNFR1 or apoptotic marker expression could elucidate if this pathway is a key mediator of neurological improvement.

4.4.6.3 Integrin alpha-X (Itgax)

Integrins are a range of heterodimeric cell surface receptors involved in cell adhesion and are involved in bi-directional communication between the extracellular environment and intracellular signalling molecules[383]. Twenty-four integrin family members have been identified, each with a unique combination of two α-subunits and two β-subunits[384]. Integrin alpha-X (Itgax), also known as cd11c, play an important role in dendritic cell (DC) and microglial function.

Itgax is a widely used marker to identify DCs. Functionally, Itgax helps DCs capture integrin associated protein (IAP)-deficient (non-self) cells, necessary to induce the adaptive immune response and their subsequent destruction[385]. Studies have demonstrated the role of Itgax in DCs during EAE development. Treatment with intravenous MOG peptide significantly improves neurological outcomes in the C57BL/6 MOG_{35-55} model. This therapeutic effect was determined to be due to an

increase in Itgax+ DC population, as this tolerant phenotype was removed following selective depletion of these cells[386,387].

Itgax+ microglia are also increased in EAE and act as APCs to induce proliferation of MOG-specific CD4 T cells. However, these Itgax+ microglia only weakly induce Th1, Th2 and Th17 cytokine expression[388]. The complexity of the Itgax+ microglial response is yet to be fully elucidated, and both pathological and protective roles have been reported[388,389].

Lastly, increased Itgax+ CD8 T cell populations have been reported in a number of inflammatory disorders, including acute viral infection[390,391], lung transplant recipients[392] and respiratory syncytial virus[393] and therefore present an important subset of T cells in the adaptive immune response. *In vivo* characterisation of Itgax+ CD8 T cells have found both regulatory, immunosuppressive[394] and effector functions[394–396]. The function of Itgax+ CD8 T cells has not been explored in EAE or MS.

The specific role of Itgax/CD11c in the adaptive immune response differs between cell types and may present an important pathway in the context of this project. Further characterising cell populations between experimental groups, either through immunostaining of fluorescent-activated cell sorting (FACS), could highlight subtle immune and CNS cell population changes that occur following EAE induction and peptide 8 immunisation.

4.4.6.4 CD244

Cluster of differentiation 244 (CD244), or 2B4, is an immunoregulatory transmembrane receptor and is part of the Signalling Lymphocyte Activation Molecule (SLAM) family. CD244 expression is found in a number of immune cell types, but mainly in NK cells, CD4 T cells and a subset of memory CD8 T cells[397–399].

The function of CD244 has been most widely studied in NK cells, as it is expressed in all NK cells[400]. CD244 binds a variety of intracellular adapter molecules, which propagates both inhibitory and activating signals[401], thus signal outcome is dependent on specific adapter molecule binding. *In vitro* studies have shown that CD244 expression negatively correlates with NK cell activation, indicating an inhibitory role of CD244 on NK cells, however the specific pathway that leads to this change in expression was not determined[402].

CD244 is also expressed on a subset of memory CD8 T cells and this subtype play an important role in chronic infection. CD244 expression is decreased in CD8 T cell population in a mouse model of chronic viral infection and this expression negatively correlates with IFNγ production. CD48 is the preferred co-stimulation ligand of CD244[403] and blocking the actions of CD244 with an anti-CD48 mAb significantly increases IFNγ release from CD8 T cells[404], indicating a pivotal inhibitory role for CD244 in infection. Studies in EAE have found that treatment with this anti-CD48 mAb reduces EAE incidence and severity. Further analysis found anti-CD48 treatment significantly reduced pathogenic CD4 T cell proliferation and CD4 T cell expression of IFNγ, TNFα and il-17A[405].

These findings demonstrate a deleterious role of CD244 in EAE as blocking CD244 co-stimulation with an anti-CD48 mAb improves EAE outcome, likely through the actions of NK cells, CD4 and CD8 T cells. CD244 spinal cord expression was significantly increased in both VLP and NV samples versus peptide 8 samples. This pathway could play a role in the protective role of peptide 8 immunisation.

4.4.6.5 Dock1

The dedicator of cytokinesis (DOCK) family contains 11 proteins (DOCK1-11) that mainly mediate the activation of the GTPases Rac and CDC42. This modulates various B and T cell functions including adhesion and chemotaxis.

Dock1, also known as Dock180, forms a complex with ELMO adapter proteins, which activates the Rho GTPase Rac, promoting cell migration[406]. Dock1 also stimulates the phosphorylation of p130Cas to form the p130Cas-Crk complex, which is a key mediator of cell adhesion, chemotaxis to growth factors and cell migration[407]. The role of Dock1 in EAE or MS has not been explored in the literature. One paper by researchers at QMUL demonstrated that micro-RNA 155 negatively regulates BBB dysfunction in the Biozzi ABH EAE model. Researchers found that this was associated with differential gene and protein expression of a number of factors, including decreased Dock-1 expression. They propose that Dock-1 may contribute towards the observed BBB dysfunction by modulating the Rho GTPase Rac that regulate epithelial permeability[408].

Decreased Dock1 gene expression is observed in peptide 8 samples versus both NV and VLP samples. Further work could quantify Dock1 levels in BBB epithelial cells to

see if gene and protein expression correlates with spinal cord expression. This work has focussed on CNS-specific mechanisms, however peripheral mechanisms may be influenced, including BBB permeability.

4.4.6.6 Sialic acid-binding immunoglobulin-type lectin-F (Siglec-F)

Siglecs are sialic acid-binding lectins that are highly expressed the cell surface of immune cells. There are 15 members of the Siglec family which each have different expression patterns, intracellular domains and pathways[409]. Siglec-F, also know as CD170, is the mouse functional paralog of human Siglec-8, and is highly expressed eosinophils and microglia[410,411]. Siglec-F null mice show increased eosinophil and NFκB activation following induced lung inflammation[412]. Furthermore, elevated eosinophil counts are seen in a number of immune conditions, including asthma[413] and neuromyelitis optica[414], which has only recently been clinically differentiated from MS[415,416]. The role of Siglec-F is not documented in EAE or MS and may provide a novel pathway in which peptide 8 immunisation influences. Peripheral and central eosinophil count may determine if this is influenced.

Further experiments aim to validate this Nanostring gene expression data through qPCR and subsequent western blot to correlate with protein expression.

5 Limitations and future work

5.1 Carnosine pre-clinical evaluation – experimental limitations and future work

This project shows promising data and limitations can be overcome in future experimental work. Oxidative stress plays a detrimental role in a number of neurodegenerative diseases[417,418]. The C57BL/6 MOG_{35-55} model is a useful model for investigating therapeutic intervention during a monophasic relapse of disease. However, neurodegeneration is limited in this model and mice show partial recovery following the first acute relapse with no subsequent worsening of disease. Further *in vivo* studies evaluating carnosine in an EAE model that shows marked neurodegeneration, such as the Biozzi ABH EAE model, would determine if carnosine influences neurodegenerative disease mechanisms. Unfortunately, these could not be completed to the correct statistical power for this project.

The pharmacokinetic profile and CNS distribution of intravenous carnosine administration has been previously reported[243], however these have not been studied following oral gavage administration as is used in this project. Failing to reach the therapeutic concentrations achieved in the *in vitro* assays may be a reason for lack of efficacy and this needs to be investigated further. As discussed in Chapter 3.3.2.2, one way to increase tissue availability would be to encapsulate carnosine into polymerosomes that targets LRP-1 expressed on the BBB epithelial cells[318].

In this study, the natural isomer L-carnosine was used. D-carnosine is the non-natural isomer of L-carnosine and is considered carnosinase resistant[224,225], can cross the BBB and our recently published data shows that D-carnosine shows similar *in vitro*

efficacy in excitotoxicity and ROS accumulation assays. However, pharmacokinetic analysis showed that pharmacokinetic parameters (area under curve, peak serum concentration and serum half-life) were similar between L- and D-carnosine between 5 and 360 minutes post intravenous injection of 1000 mg/kg[240]. Studies analysing stroke efficacy evaluated carnosine and analogues N-acetyl carnosine and anserine found that carnosine was the most neuroprotective[319]. These comparisons have not been explored in the EAE model.

5.2 Peptide 8 immunisation – experimental limitations and future work

VLPs have recently been suggested to be the ideal candidate for therapeutic vaccine development due to their high immunogenicity and safety profile[419]. This is supported by our data, demonstrating no behavioural changes following VLP administration. This said, the role of VLP has not been evidenced in EAE. Although VLP groups did not show any significant therapeutic benefit when compared to their NV counterparts, an additional control group of VLP conjugated to a non-immunogenic peptide would add further confidence to these results.

One of the concerns raised regarding this approach was the risk of encephalitic disease. This risk has been minimised during peptide design to ensure a B cell response and not a T cell response is elicited. Further safety studies looking for encephalitic disease and BBB breakdown in wildtype immunised and non-immunised mice would further strengthen our understanding of the safety profile of peptide 8 immunisation. Initial behavioural evaluation following peptide 8 immunisation showed no significant alterations in mouse behaviour, however further work needs to characterise these behavioural and other cognitive parameters during active disease

where there is significant BBB breakdown. This will ensure generated antibodies can enter the CNS and reach their CNS target and allow us to further evaluate the safety and efficacy of peptide 8 immunisation in more detail. Demonstration of an effective, but also safe treatment is paramount when translation is the ultimate aim.

The Biozzi ABH model offers a useful tool for evaluating the effect of therapeutic intervention on both immune-mediated and neurodegenerative disease. Further neurological and behavioural evaluation of peptide 8 immunisation in the Biozzi ABH model would advance our knowledge on changes in disease onset, progression and time to reach experimental endpoints. This will allow us to identify specific disease phases that peptide 8 immunisation influences and will further narrow down the pathological processes that are being affected.

The mechanistic work detailed in this is limited to CNS-related mechanisms that peptide 8 may be influencing. The Nanostring neuroinflammatory panel highlighted a number of interesting genes, however very few genes showed a significant difference between treatment groups. The small sample size per group (n=3) in addition to the expected *in vivo* heterogeneity may be a reason for this. Increasing sample numbers per group would increase confidence in these results. Furthermore, peripheral mechanisms may also contribute towards the observed *in* vivo efficacy. Literature highlights that NMDARs and NMDAR ligands are important modulators of immune cell responses. Orihara et al. used human primary CD4 T cells obtained from peripheral blood to investigate the role of NMDARs on their response. Stimulation with anti-CD3/CD28 antibodies increases CD4 T cell NMDAR1 protein expression. Stimulation with NMDA decreased Th1 cytokine production, including IFNγ and TNFα, however

Th2 cytokine release remains unaffected. Furthermore, Th1 cells show increased sensitivity to NMDA-induced cell death when compared to Th2 cells[152]. These results indicate a clear role of NMDAR signalling in T cell fate and cytokine expression. Broadening our understanding of how peptide 8 immunisation may affect T cell population fate and subsequent chemokine/cytokine expression may elucidate a peripheral immune mechanism of efficacy. Multiplex immunoassay platforms can be used to detect a plethora of serum chemokine and cytokine markers that are important in EAE and MS[420], including IFNγ, IL-17, IFNγ, TNFα and GM-CSF. Furthermore, characterisation of immune cell populations through fluorescent-activated cell-sorting (FACS) will supplement the proposed multiplex array experiments and allow extensive evaluation of any immune influence. This approach would be particularly useful in characterising immune cell populations involved in EAE and MS pathology, including dendritic cells, T helper cells cells, CD4 T cells, CD8 T cells and B cells.

Western blot analysis aimed to identify changes glial reactivity as well as downstream pathways of NMDAR1 through GFAP and pERK1/2 expression analysis, respectively. Ideally, NMDAR1 expression analysis through western blot would have confirmed if receptor expression was specifically influence in the spinal cord tissue, however primary antibodies were not sufficiently worked up in time. This said, ongoing *in vitro* work aims to confirm antibody target specificity. One of these approaches aims to transfect a functional NMDAR1 into HEK293 cells. Following successful optimisation, non-transfected and transfected cells will be incubated with serum from non-vaccinated, VLP and peptide 8 immunised mice. Whole-cell patch clamp will be performed to record and quantify cell excitability and to elucidate an NMDAR1 specific mechanism of action.

Lastly, ongoing work in our research group and alongside external collaborators aims to utilise rational drug design and structure based virtual screening methods to identify new small molecules that specifically target the peptide 8 region. Successful lead candidates are currently being screened for pre-clinical efficacy and if successful would further validate the therapeutic potential of peptide 8 immunisation.

6 Conclusions

MS is a multifactorial disease and these complex mechanisms change over time. Understanding how these pathways inter-relate and contribute towards disease relapses and progression is vital for identifying therapeutic targets. This complex disease pathology means that multiple treatment options are needed in order for effective disease management. This project aimed to pre-clinically characterise and develop antioxidant carnosine and anti-NMDAR1 vaccination as novel therapies for MS.

Carnosine showed promising *in vitro* data by reducing intracellular ROS accumulation and NMDA-induced excitotoxicity in CNS-relevant cultures. Carnosine also showed a mild remyelinating effect in the OSC model of remyelination. Carnosine's low cytotoxicity coupled with these pleiotropic properties demonstrated in the *in vitro* studies left carnosine a viable option to screen for efficacy in the EAE model of MS. Carnosine treated mice showed a mild improvement in the first relapse of disease in the Biozzi ABH model at a dose of 550 mg/kg. However, following this promising initial study, future studies using the Biozzi ABH model were halted as disease severity became too severe and a number of mice quickly reached experimental endpoints.

Because of this, the C57BL/6 MOG_{35-55} model was used as a viable alternative for further EAE studies. Carnosine did not significantly reduce neurological scores at a dose range of 550 – 2000 mg/kg/day when compared to vehicle control. Although no neurological improvements were observed, further tissue analysis may reveal a beneficial effect within the tissue.

In the second chapter, the efficacy of peptide 8 immunisation was explored using the EAE model. Peptide 8 immunisation significantly reduced neurological deficits in the MOG_{35-55} model when compared to both non-vaccinated and VLP control mice. Further *in vitro* analysis identified that overnight incubation with peptide 8 immunised serum significantly increases primary cortical neuron excitability and NMDAR1 expression. Tissue gene expression analysis further identified gene targets that are be influenced by peptide 8 immunisation. Future work aims to validate these findings through qPCR and western blot analysis.

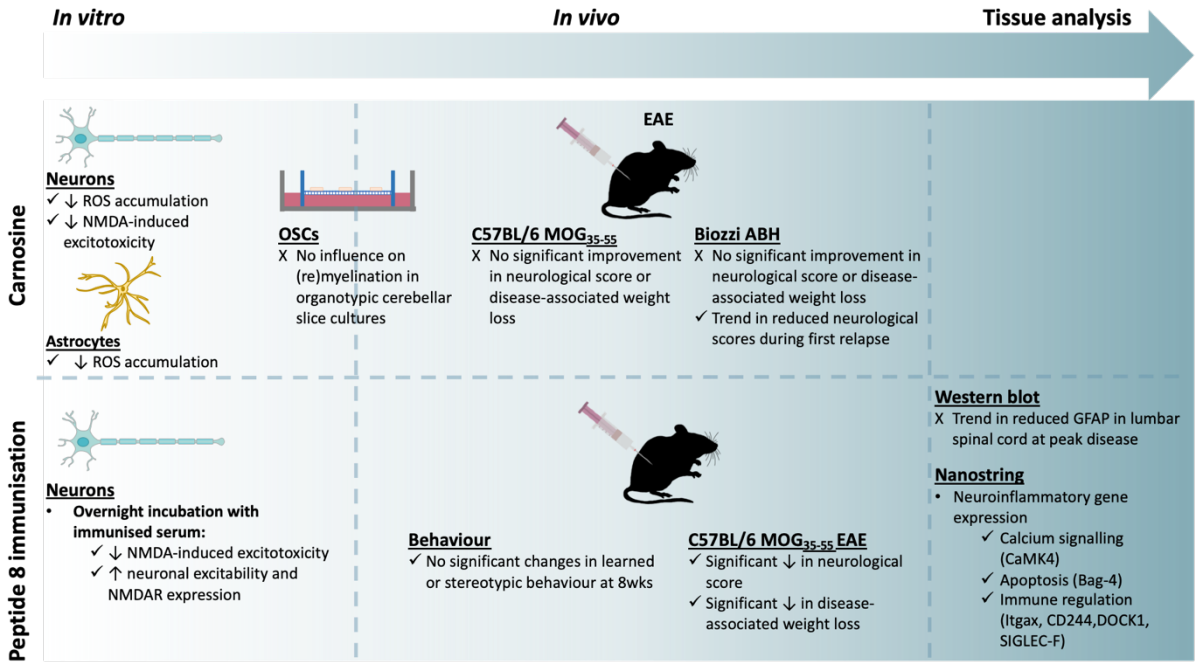

Figure 6.1 Diagrammatic summary of key findings

7 References

1. Minden S, Frankel D, Hadden L, et al. The Sonya Slifka Longitudinal Multiple Sclerosis Study: methods and sample characteristics. *Mult Scler* 2006; 12: 24–38.
2. Gelfand JM. Multiple sclerosis: Diagnosis, differential diagnosis, and clinical presentation. In: *Handbook of Clinical Neurology*. 2014. Epub ahead of print 2014. DOI: 10.1016/B978-0-444-52001-2.00011-X.
3. Kobelt G, Berg J, Lindgren P, et al. Costs and quality of life of multiple sclerosis in the United Kingdom. *Eur J Health Econ* 2006; 7 Suppl 2: S96-104.
4. Grytten Torkildsen N, Lie SA, Aarseth JH, et al. Survival and cause of death in multiple sclerosis: Results from a 50-year follow-up in Western Norway. *Mult Scler* 2008; 14: 1191–1198.
5. Milo R, Kahana E. Multiple sclerosis: Geoepidemiology, genetics and the environment. *Autoimmunity Reviews*; 9. Epub ahead of print 2010. DOI: 10.1016/j.autrev.2009.11.010.
6. Szczepaniak M, Dowden K, Jackson M, et al. Multiple sclerosis: prevalence, incidence and smoking status. *Public Health England*.
7. Alonso A, Jick SS, Olek MJ, et al. Incidence of multiple sclerosis in the United Kingdom: Findings from a population-based cohort. *J Neurol*. Epub ahead of print 2007. DOI: 10.1007/s00415-007-0602-z.
8. Mackenzie IS, Morant S V., Bloomfield GA, et al. Incidence and prevalence of multiple sclerosis in the UK 1990-2010: A descriptive study in the General Practice Research Database. *J Neurol Neurosurg Psychiatry*. Epub ahead of print 2014. DOI: 10.1136/jnnp-2013-305450.
9. Kobelt G, Thompson A, Berg J, et al. New insights into the burden and costs of multiple sclerosis in Europe. *Mult Scler* 2017; 23: 1123–1136.
10. Thomas S, Mynoors G, Simpsone S, et al. *Measuring the burden of hospitalisation in multiple sclerosis: A cross-sectional analysis of the English Hospital Episode Statistics database 2009-2014*. 2015.
11. Miller DH, Chard DT, Ciccarelli O. Clinically isolated syndromes. *The Lancet Neurology*. Epub ahead of print 2012. DOI: 10.1016/S1474-4422(11)70274-5.
12. Polman CH, Reingold SC, Banwell B, et al. Diagnostic criteria for multiple sclerosis: 2010 revisions to the McDonald criteria. *Ann Neurol* 2011; 69: 292–302.
13. Fisniku LK, Brex PA, Altmann DR, et al. Disability and T2 MRI lesions: A 20-year follow-up of patients with relapse onset of multiple sclerosis. *Brain*. Epub ahead of print 2008. DOI: 10.1093/brain/awm329.
14. Lublin FD, Reingold SC. Defining the clinical course of multiple sclerosis: Results of an international survey. *Neurology* 1996; 46: 907–911.
15. Compston A, Coles A. Multiple sclerosis. *Lancet* 2008; 372: 1502–1517.
16. Trojano M, Paolicelli D, Bellacosa A, et al. The transition from relapsing-remitting MS to irreversible disability: Clinical evaluation. *Neurological Sciences*; 24. Epub ahead of print 2003. DOI: 10.1007/s10072-003-0171-6.
17. Hurwitz BJ. The diagnosis of multiple sclerosis and the clinical subtypes. *Ann Indian Acad Neurol* 2009; 12: 226–230.
18. Kawachi I, Lassmann H. Neurodegeneration in multiple sclerosis and neuromyelitis optica. *J Neurol Neurosurg \& Psychiatry* 2017; 88: 137–145.

19. Olsson T, Barcellos LF, Alfredsson L. Interactions between genetic, lifestyle and environmental risk factors for multiple sclerosis. *Nature Reviews Neurology*. Epub ahead of print 2016. DOI: 10.1038/nrneurol.2016.187.
20. Handel AE, Williamson AJ, Disanto G, et al. An updated meta-analysis of risk of multiple sclerosis following infectious mononucleosis. *PLoS One*. Epub ahead of print 2010. DOI: 10.1371/journal.pone.0012496.
21. Hedström AK, Bäärnhielm M, Olsson T, et al. Tobacco smoking, but not Swedish snuff use, increases the risk of multiple sclerosis. *Neurology*. Epub ahead of print 2009. DOI: 10.1212/WNL.0b013e3181b59c40.
22. Munger KL, Bentzen J, Laursen B, et al. Childhood body mass index and multiple sclerosis risk: A long-term cohort study. *Mult Scler J*. Epub ahead of print 2013. DOI: 10.1177/1352458513483889.
23. Munger KL, Köchert K, Simon KC, et al. Molecular mechanism underlying the impact of vitamin D on disease activity of MS. *Ann Clin Transl Neurol*. Epub ahead of print 2014. DOI: 10.1002/acn3.91.
24. Simpson S, Blizzard L, Otahal P, et al. Latitude is significantly associated with the prevalence of multiple sclerosis: A meta-analysis. *J Neurol Neurosurg Psychiatry*. Epub ahead of print 2011. DOI: 10.1136/jnnp.2011.240432.
25. Kirby T, Ochoa-Repáraz J. The Gut Microbiome in Multiple Sclerosis: A Potential Therapeutic Avenue. *Med Sci*. Epub ahead of print 2018. DOI: 10.3390/medsci6030069.
26. Moutsianas L, Jostins L, Beecham AH, et al. Class II HLA interactions modulate genetic risk for multiple sclerosis. *Nat Genet*. Epub ahead of print 2015. DOI: 10.1038/ng.3395.
27. Cusick MF, Libbey JE, Fujinami RS. Molecular mimicry as a mechanism of autoimmune disease. *Clin Rev Allergy Immunol* 2012; 42: 102–111.
28. Correale J, De los Milagros Bassani Molinas M. Oligoclonal bands and antibody responses in Multiple Sclerosis. *Journal of Neurology*. Epub ahead of print 2002. DOI: 10.1007/s004150200026.
29. Arbour N, Holz A, Sipe JC, et al. A new approach for evaluating antigen-specific T cell responses to myelin antigens during the course of multiple sclerosis. *J Neuroimmunol*. Epub ahead of print 2003. DOI: 10.1016/S0165-5728(03)00080-8.
30. DiMasi J. The need for new approaches in CNS drug discovery: Why drugs have failed, and what can be done to improve outcomes. *Tufts Cent Study Drug Dev Website*.
31. Gribkoff VK, Kaczmarek LK. The need for new approaches in CNS drug discovery: Why drugs have failed, and what can be done to improve outcomes. *Neuropharmacology* 2017; 120: 11–19.
32. Dhib-Jalbut S, Marks S. Interferon-beta mechanisms of action in multiple sclerosis. *Neurology* 2010; 74 Suppl 1: S17-24.
33. Neuhaus O, Kieseier BC, Hartung H-P. Mechanisms of mitoxantrone in multiple sclerosis–what is known? *J Neurol Sci* 2004; 223: 25–27.
34. Schrempf W, Ziemssen T. Glatiramer acetate: Mechanisms of action in multiple sclerosis. *Autoimmunity Reviews*. Epub ahead of print 2007. DOI: 10.1016/j.autrev.2007.02.003.
35. Mills EA, Ogrodnik MA, Plave A, et al. Emerging understanding of the mechanism of action for dimethyl fumarate in the treatment of multiple sclerosis. *Frontiers in Neurology*. Epub ahead of print 2018. DOI: 10.3389/fneur.2018.00005.

36. Chun J, Hartung H-P. Mechanism of Action of Oral Fingolimod (FTY720) in Multiple Sclerosis. *Clin Neuropharmacol* 2010; 33: 91–101.
37. Bar-Or A, Pachner A, Menguy-Vacheron F, et al. Teriflunomide and its mechanism of action in multiple sclerosis. *Drugs* 2014; 74: 659–674.
38. Sellebjerg F, Cadavid D, Steiner D, et al. Exploring potential mechanisms of action of natalizumab in secondary progressive multiple sclerosis. *Ther Adv Neurol Disord* 2016; 9: 31–43.
39. Ruck T, Bittner S, Wiendl H, et al. Alemtuzumab in Multiple Sclerosis: Mechanism of Action and Beyond. *Int J Mol Sci* 2015; 16: 16414–16439.
40. Mulero P, Midaglia L, Montalban X. Ocrelizumab: a new milestone in multiple sclerosis therapy. *Ther Adv Neurol Disord* 2018; 11: 1756286418773025–1756286418773025.
41. Leist TP, Weissert R. Cladribine: Mode of Action and Implications for Treatment of Multiple Sclerosis. *Clin Neuropharmacol*; 34.
42. Hestvik ALK. The double-edged sword of autoimmunity: Lessons from multiple sclerosis. *Toxins* 2010; 2: 856–877.
43. Mosmann TR, Cherwinski H, Bond MW, et al. Two types of murine helper T cell clone. I. Definition according to profiles of lymphokine activities and secreted proteins. *J Immunol* 1986; 136: 2348–57.
44. Guenova E, Skabytska Y, Hoetzenecker W, et al. IL-4 abrogates TH17 cell-mediated inflammation by selective silencing of IL-23 in antigen-presenting cells. *Proc Natl Acad Sci U S A*. Epub ahead of print 2015. DOI: 10.1073/pnas.1416922112.
45. Thakker P, Leach MW, Kuang W, et al. IL-23 Is Critical in the Induction but Not in the Effector Phase of Experimental Autoimmune Encephalomyelitis. *J Immunol*. Epub ahead of print 2007. DOI: 10.4049/jimmunol.178.4.2589.
46. Matusevicius D, Kivisäkk P, He B, et al. Interleukin-17 mRNA expression in blood and CSF mononuclear cells is augmented in multiple sclerosis. *Mult Scler*. Epub ahead of print 1999. DOI: 10.1177/135245859900500206.
47. Tzartos JS, Friese MA, Craner MJ, et al. Interleukin-17 production in central nervous system-infiltrating T cells and glial cells is associated with active disease in multiple sclerosis. *Am J Pathol*. Epub ahead of print 2008. DOI: 10.2353/ajpath.2008.070690.
48. Kebir H, Kreymborg K, Ifergan I, et al. Human TH17 lymphocytes promote blood-brain barrier disruption and central nervous system inflammation. *Nat Med*. Epub ahead of print 2007. DOI: 10.1038/nm1651.
49. Huppert J, Closhen D, Croxford A, et al. Cellular mechanisms of IL-17-induced blood-brain barrier disruption. *FASEB J*. Epub ahead of print 2010. DOI: 10.1096/fj.09-141978.
50. Carlson T, Kroenke M, Rao P, et al. The Th17-ELR+ CXC chemokine pathway is essential for the development of central nervous system autoimmune disease. *J Exp Med*. Epub ahead of print 2008. DOI: 10.1084/jem.20072404.
51. Reboldi A, Coisne C, Baumjohann D, et al. C-C chemokine receptor 6-regulated entry of TH-17 cells into the CNS through the choroid plexus is required for the initiation of EAE. *Nat Immunol*. Epub ahead of print 2009. DOI: 10.1038/ni.1716.
52. Zielinski CE. Autoimmunity beyond Th17: GM-CSF producing T cells. *Cell Cycle*. Epub ahead of print 2014. DOI: 10.4161/15384101.2014.946377.
53. González H, Elgueta D, Montoya A, et al. Neuroimmune regulation of microglial activity involved in neuroinflammation and neurodegenerative diseases. *Journal of Neuroimmunology*. Epub ahead of print 2014. DOI:

10.1016/j.jneuroim.2014.07.012.
54. Wiggins-Dohlvik K, Merriman M, Shaji CA, et al. Tumor necrosis factor-α disruption of brain endothelial cell barrier is mediated through matrix metalloproteinase-9. In: *American Journal of Surgery*. 2014. Epub ahead of print 2014. DOI: 10.1016/j.amjsurg.2014.08.014.
55. El-Behi M, Ciric B, Dai H, et al. The encephalitogenicity of TH 17 cells is dependent on IL-1- and IL-23-induced production of the cytokine GM-CSF. *Nat Immunol*. Epub ahead of print 2011. DOI: 10.1038/ni.2031.
56. van Nieuwenhuijze A, Koenders M, Roeleveld D, et al. GM-CSF as a therapeutic target in inflammatory diseases. *Molecular Immunology*. Epub ahead of print 2013. DOI: 10.1016/j.molimm.2013.05.002.
57. Shiomi A, Usui T, Mimori T. GM-CSF as a therapeutic target in autoimmune diseases. *Inflamm Regen*. Epub ahead of print 2016. DOI: 10.1186/s41232-016-0014-5.
58. Constantinescu CS, Asher A, Fryze W, et al. Randomized phase 1b trial of MOR103, a human antibody to GM-CSF, in multiple sclerosis. *Neurol Neuroimmunol NeuroInflammation*. Epub ahead of print 2015. DOI: 10.1212/NXI.0000000000000117.
59. Barry M, Bleackley RC. Cytotoxic T lymphocytes: All roads lead to death. *Nature Reviews Immunology*. Epub ahead of print 2002. DOI: 10.1038/nri819.
60. Hila S, Soane L, Koski CL. Upregulation of transcription factors controlling MHC expression in multiple sclerosis lesions. *Glia*. Epub ahead of print 2001. DOI: 10.1002/glia.1096.
61. Traugott U, Reinherz EL, Raine CS. Multiple sclerosis: Distribution of T cell subsets within active chronic lesions. *Science (80-)*. Epub ahead of print 1983. DOI: 10.1126/science.6217550.
62. Babbe H, Roers A, Waisman A, et al. Clonal expansions of CD8+ T cells dominate the T cell infiltrate in active multiple sclerosis lesions as shown by micromanipulation and single cell polymerase chain reaction. *J Exp Med*. Epub ahead of print 2000. DOI: 10.1084/jem.192.3.393.
63. Bitsch A, Schuchardt J, Bunkowski S, et al. Acute axonal injury in multiple sclerosis. Correlation with demyelination and inflammation. *Brain*. Epub ahead of print 2000. DOI: 10.1093/brain/123.6.1174.
64. Saxena A, Bauer J, Scheikl T, et al. Cutting Edge: Multiple Sclerosis-Like Lesions Induced by Effector CD8 T Cells Recognizing a Sequestered Antigen on Oligodendrocytes. *J Immunol*. Epub ahead of print 2008. DOI: 10.4049/jimmunol.181.3.1617.
65. Medana I, Martinic MA, Wekerle H, et al. Transection of major histocompatibility complex class I-induced neurites by cytotoxic T lymphocytes. *Am J Pathol*. Epub ahead of print 2001. DOI: 10.1016/S0002-9440(10)61755-5.
66. Jurewicz A, Biddison WE, Antel JP. MHC class I-restricted lysis of human oligodendrocytes by myelin basic protein peptide-specific CD8 T lymphocytes. *J Immunol*.
67. Tsuchida T, Parker KC, Turner R V., et al. Autoreactive CD8+ T-cell responses to human myelin protein-derived peptides. *Proc Natl Acad Sci U S A*. Epub ahead of print 1994. DOI: 10.1073/pnas.91.23.10859.
68. Tzartos JS, Friese MA, Craner MJ, et al. Interleukin-17 production in central nervous system-infiltrating T cells and glial cells is associated with active disease in multiple sclerosis. *Am J Pathol* 2008; 172: 146–155.
69. Huber M, Heink S, Pagenstecher A, et al. IL-17A secretion by CD8+ T cells

supports Th17-mediated autoimmune encephalomyelitis. *J Clin Invest*. Epub ahead of print 2013. DOI: 10.1172/JCI63681.
70. Wang HH, Dai YQ, Qiu W, et al. Interleukin-17-secreting T cells in neuromyelitis optica and multiple sclerosis during relapse. *J Clin Neurosci*. Epub ahead of print 2011. DOI: 10.1016/j.jocn.2011.01.031.
71. Linker RA, Haghikia A. Dimethyl fumarate in multiple sclerosis: latest developments, evidence and place in therapy. *Therapeutic Advances in Chronic Disease*. Epub ahead of print 2016. DOI: 10.1177/2040622316653307.
72. Sakaguchi S, Sakaguchi N, Shimizu J, et al. Immunologic tolerance maintained by CD25+ CD4+ regulatory T cells: Their common role in controlling autoimmunity, tumor immunity, and transplantation tolerance. *Immunological Reviews*. Epub ahead of print 2001. DOI: 10.1034/j.1600-065X.2001.1820102.x.
73. Korn T, Mitsdoerffer M, Croxford AL, et al. IL-6 controls Th17 immunity in vivo by inhibiting the conversion of conventional T cells into Foxp3+ regulatory T cells. *Proc Natl Acad Sci U S A*. Epub ahead of print 2008. DOI: 10.1073/pnas.0809850105.
74. Kim CH. FOXP3 and its role in the immune system. *Adv Exp Med Biol*. Epub ahead of print 2009. DOI: 10.1007/978-1-4419-1599-3_2.
75. Lu LF, Rudensky A. Molecular orchestration of differentiation and function of regulatory T cells. *Genes and Development*. Epub ahead of print 2009. DOI: 10.1101/gad.1791009.
76. Viglietta V, Baecher-Allan C, Weiner HL, et al. Loss of Functional Suppression by CD4+CD25+ Regulatory T Cells in Patients with Multiple Sclerosis. *J Exp Med*. Epub ahead of print 2004. DOI: 10.1084/jem.20031579.
77. Schneider A, Long SA, Cerosaletti K, et al. In active relapsing-remitting multiple sclerosis, effector T cell resistance to adaptive Tregs involves IL-6-mediated signaling. *Sci Transl Med*. Epub ahead of print 2013. DOI: 10.1126/scitranslmed.3004970.
78. Sospedra M. B cells in multiple sclerosis. *Current Opinion in Neurology*. Epub ahead of print 2018. DOI: 10.1097/WCO.000000000000563.
79. Lund FE. Cytokine-producing B lymphocytes - key regulators of immunity. *Current Opinion in Immunology*. Epub ahead of print 2008. DOI: 10.1016/j.coi.2008.03.003.
80. Mitsdoerffer M, Lee Y, Jäger A, et al. Proinflammatory T helper type 17 cells are effective B-cell helpers. *Proc Natl Acad Sci U S A*. Epub ahead of print 2010. DOI: 10.1073/pnas.1009234107.
81. Sellebjerg F, Börnsen L, Khademi M, et al. Increased cerebrospinal fluid concentrations of the chemokine CXCL13 in active MS. *Neurology*. Epub ahead of print 2009. DOI: 10.1212/WNL.0b013e3181c5b457.
82. Link H. Comparison of electrophoresis on agar gel and agarose gel in the evaluation of gamma-globulin abnormalities in cerebrospinal fluid and serum in multiple sclerosis. *Clin Chim Acta*. Epub ahead of print 1973. DOI: 10.1016/0009-8981(73)90251-9.
83. Freedman MS, Thompson EJ, Deisenhammer F, et al. Recommended standard of cerebrospinal fluid analysis in the diagnosis of multiple sclerosis: A consensus statement. *Archives of Neurology*. Epub ahead of print 2005. DOI: 10.1001/archneur.62.6.865.
84. Keren DF. Optimizing Detection of Oligoclonal Bands in Cerebrospinal Fluid by Use of Isoelectric Focusing with IgG Immunoblotting. *American Journal of*

Clinical Pathology. Epub ahead of print 2003. DOI: 10.1309/VGAHDTDN3N5QMXUC.
85. Lovato L, Willis SN, Rodig SJ, et al. Related B cell clones populate the meninges and parenchyma of patients with multiple sclerosis. *Brain*. Epub ahead of print 2011. DOI: 10.1093/brain/awq350.
86. Guerrier T, Labalette M, Launay D, et al. Proinflammatory B-cell profile in the early phases of MS predicts an active disease. *Neurol Neuroimmunol NeuroInflammation*. Epub ahead of print 2018. DOI: 10.1212/NXI.0000000000000431.
87. Longbrake EE, Cross AH. Effect of multiple sclerosis disease-modifying therapies on b cells and humoral immunity. *JAMA Neurology*. Epub ahead of print 2016. DOI: 10.1001/jamaneurol.2015.3977.
88. Bielekova B, Becker BL. Monoclonal antibodies in MS: mechanisms of action. *Neurology*. Epub ahead of print 2010. DOI: 10.1212/WNL.0b013e3181c97ed3.
89. Salzer J, Svenningsson R, Alping P, et al. Rituximab in multiple sclerosis A retrospective observational study on safety and efficacy. *Neurology*.
90. Shi FD, Van Kaer L. Reciprocal regulation between natural killer cells and autoreactive T cells. *Nature Reviews Immunology*. Epub ahead of print 2006. DOI: 10.1038/nri1935.
91. Schleinitz N, Vély F, Harlé JR, et al. Natural killer cells in human autoimmune diseases. *Immunology*. Epub ahead of print 2010. DOI: 10.1111/j.1365-2567.2010.03360.x.
92. Cooper MA, Fehniger TA, Caligiuri MA. The biology of human natural killer-cell subsets. *Trends in Immunology*. Epub ahead of print 2001. DOI: 10.1016/S1471-4906(01)02060-9.
93. Fehniger TA, Cooper MA, Nuovo GJ, et al. CD56bright natural killer cells are present in human lymph nodes and are activated by T cell-derived IL-2: A potential new link between adaptive and innate immunity. *Blood*. Epub ahead of print 2003. DOI: 10.1182/blood-2002-09-2876.
94. Cohan SL, Lucassen EB, Romba MC, et al. Daclizumab: Mechanisms of action, therapeutic efficacy, adverse events and its uncovering the potential role of innate immune system recruitment as a treatment strategy for relapsing multiple sclerosis. *Biomedicines*. Epub ahead of print 2019. DOI: 10.3390/biomedicines7010018.
95. Laroni A, Armentani E, Kerlero de Rosbo N, et al. Dysregulation of regulatory CD56bright NK cells/T cells interactions in multiple sclerosis. *J Autoimmun*. Epub ahead of print 2016. DOI: 10.1016/j.jaut.2016.04.003.
96. Sonar SA, Lal G. Differentiation and transmigration of CD4 T cells in neuroinflammation and autoimmunity. *Frontiers in Immunology*. Epub ahead of print 2017. DOI: 10.3389/fimmu.2017.01695.
97. Kivisakk P, Imitola J, Rasmussen S, et al. Localizing central nervous system immune surveillance: Meningeal antigen-presenting cells activate T cells during experimental autoimmune encephalomyelitis. *Ann Neurol* 2009; 65: 457–469.
98. Furtado GC, Marcondes MCG, Latkowski J-A, et al. Swift Entry of Myelin-Specific T Lymphocytes into the Central Nervous System in Spontaneous Autoimmune Encephalomyelitis. *J Immunol* 2008; 181: 4648–4655.
99. Wake H, Fields RD. Physiological function of microglia. *Neuron Glia Biology*. Epub ahead of print 2012. DOI: 10.1017/S1740925X12000166.
100. Luo C, Jian C, Liao Y, et al. The role of microglia in multiple sclerosis. *Neuropsychiatric Disease and Treatment* 2017; 13: 1661–1667.

101. van Horssen J, Schreibelt G, Drexhage J, et al. Severe oxidative damage in multiple sclerosis lesions coincides with enhanced antioxidant enzyme expression. *Free Radic Biol Med*. Epub ahead of print 2008. DOI: 10.1016/j.freeradbiomed.2008.09.023.
102. Hametner S, Wimmer I, Haider L, et al. Iron and neurodegeneration in the multiple sclerosis brain. *Ann Neurol* 2013; 74: 848–861.
103. Masvekar R, Wu T, Kosa P, et al. Cerebrospinal fluid biomarkers link toxic astrogliosis and microglial activation to multiple sclerosis severity. *Mult Scler Relat Disord* 2019; 28: 34–43.
104. Healy LM, Michell-Robinson MA, Antel JP. Regulation of human glia by multiple sclerosis disease modifying therapies. *Seminars in Immunopathology*. Epub ahead of print 2015. DOI: 10.1007/s00281-015-0514-4.
105. Noda H, Takeuchi H, Mizuno T, et al. Fingolimod phosphate promotes the neuroprotective effects of microglia. *J Neuroimmunol*. Epub ahead of print 2013. DOI: 10.1016/j.jneuroim.2012.12.005.
106. Qin C, Fan WH, Liu Q, et al. Fingolimod protects against ischemic white matter damage by modulating microglia toward M2 polarization via STAT3 pathway. *Stroke*. Epub ahead of print 2017. DOI: 10.1161/STROKEAHA.117.018505.
107. Volterra A, Meldolesi J. Astrocytes, from brain glue to communication elements: The revolution continues. *Nature Reviews Neuroscience*. Epub ahead of print 2005. DOI: 10.1038/nrn1722.
108. Bélanger M, Allaman I, Magistretti PJ. Brain energy metabolism: Focus on Astrocyte-neuron metabolic cooperation. *Cell Metabolism*. Epub ahead of print 2011. DOI: 10.1016/j.cmet.2011.08.016.
109. Brown AM, Ransom BR. Astrocyte glycogen and brain energy metabolism. *GLIA*. Epub ahead of print 2007. DOI: 10.1002/glia.20557.
110. Bazargani N, Attwell D. Astrocyte calcium signaling: The third wave. *Nature Neuroscience*. Epub ahead of print 2016. DOI: 10.1038/nn.4201.
111. Attwell D, Buchan AM, Charpak S, et al. Glial and neuronal control of brain blood flow. *Nature*. Epub ahead of print 2010. DOI: 10.1038/nature09613.
112. Potokar M, Jorgačevski J, Zorec R. Astrocyte aquaporin dynamics in health and disease. *International Journal of Molecular Sciences*. Epub ahead of print 2016. DOI: 10.3390/ijms17071121.
113. Tabata H. Diverse subtypes of astrocytes and their development during corticogenesis. *Frontiers in Neuroscience*. Epub ahead of print 2015. DOI: 10.3389/fnins.2015.00114.
114. Kuhlmann T, Ludwin S, Prat A, et al. An updated histological classification system for multiple sclerosis lesions. *Acta Neuropathol*. Epub ahead of print 2017. DOI: 10.1007/s00401-016-1653-y.
115. Sofroniew M V., Vinters H V. Astrocytes: Biology and pathology. *Acta Neuropathologica* 2010; 119: 7–35.
116. Holley JE, Gveric D, Newcombe J, et al. Astrocyte characterization in the multiple sclerosis glial scar. *Neuropathol Appl Neurobiol*. Epub ahead of print 2003. DOI: 10.1046/j.1365-2990.2003.00491.x.
117. Horng S, Therattil A, Moyon S, et al. Astrocytic tight junctions control inflammatory CNS lesion pathogenesis. *J Clin Invest*. Epub ahead of print 2017. DOI: 10.1172/JCI91301.
118. Brambilla R, Morton PD, Ashbaugh JJ, et al. Astrocytes play a key role in EAE pathophysiology by orchestrating in the CNS the inflammatory response of resident and peripheral immune cells and by suppressing remyelination. *Glia*.

Epub ahead of print 2014. DOI: 10.1002/glia.22616.
119. Haindl MT, Köck U, Zeitelhofer-Adzemovic M, et al. The formation of a glial scar does not prohibit remyelination in an animal model of multiple sclerosis. *Glia*. Epub ahead of print 2019. DOI: 10.1002/glia.23556.
120. Liddelow SA, Barres BA. Reactive Astrocytes: Production, Function, and Therapeutic Potential. *Immunity*. Epub ahead of print 2017. DOI: 10.1016/j.immuni.2017.06.006.
121. Miljkovic D, Momcilovic M, Stojanovic I, et al. Astrocytes stimulate interleukin-17 and interferon-γ production in vitro. *J Neurosci Res*. Epub ahead of print 2007. DOI: 10.1002/jnr.21453.
122. Mackay F, Tangye SG. The role of the BAFF/APRIL system in B cell homeostasis and lymphoid cancers. *Current Opinion in Pharmacology*. Epub ahead of print 2004. DOI: 10.1016/j.coph.2004.02.009.
123. Argaw AT, Asp L, Zhang J, et al. Astrocyte-derived VEGF-A drives blood-brain barrier disruption in CNS inflammatory disease. *J Clin Invest*. Epub ahead of print 2012. DOI: 10.1172/JCI60842.
124. Gimenez MAT, Sim JE, Russell JH. TNFR1-dependent VCAM-1 expression by astrocytes exposes the CNS to destructive inflammation. *J Neuroimmunol*. Epub ahead of print 2004. DOI: 10.1016/j.jneuroim.2004.02.012.
125. Dietrich JB. The adhesion molecule ICAM-1 and its regulation in relation with the blood-brain barrier. *Journal of Neuroimmunology*. Epub ahead of print 2002. DOI: 10.1016/S0165-5728(02)00114-5.
126. Zeinstra E, Wilczak N, Chesik D, et al. Simvastatin inhibits interferon-γ-induced MHC class II up-regulation in cultured astrocytes. *J Neuroinflammation*. Epub ahead of print 2006. DOI: 10.1186/1742-2094-3-16.
127. Nikcevich KM, Gordon KB, Tan L, et al. IFN-γ-Activated Primary Murine Astrocytes Express B7 Costimulatory Molecules and Prime Naive Antigen-Specific T Cells. *J Immunol*.
128. Zeinstra E, Wilczak N, De Keyser J. Reactive astrocytes in chronic active lesions of multiple sclerosis express co-stimulatory molecules B7-1 and B7-2. *J Neuroimmunol*. Epub ahead of print 2003. DOI: 10.1016/S0165-5728(02)00462-9.
129. Meinl E, Aloisi F, Ertl B, et al. Multiple sclerosis immunomodulatory effects of human astrocytes on t cells. *Brain*. Epub ahead of print 1994. DOI: 10.1093/brain/117.6.1323.
130. Trapp BD, Peterson J, Ransohoff RM, et al. Axonal transection in the lesions of multiple sclerosis. *N Engl J Med* 1998; 338: 278–285.
131. Miron VE, Kuhlmann T, Antel Jack P. JP. Cells of the oligodendroglial lineage, myelination, and remyelination. *Biochimica et Biophysica Acta - Molecular Basis of Disease* 2011; 1812: 184–193.
132. Franklin RJM, Ffrench-Constant C. Remyelination in the CNS: From biology to therapy. *Nature Reviews Neuroscience*. Epub ahead of print 2008. DOI: 10.1038/nrn2480.
133. Patani R, Balaratnam M, Vora A, et al. Remyelination can be extensive in multiple sclerosis despite a long disease course. *Neuropathol Appl Neurobiol*. Epub ahead of print 2007. DOI: 10.1111/j.1365-2990.2007.00805.x.
134. Gruchot J, Weyers V, Göttle P, et al. The Molecular Basis for Remyelination Failure in Multiple Sclerosis. *Cells*. Epub ahead of print 2019. DOI: 10.3390/cells8080825.
135. Hartley MD, Altowaijri G, Bourdette D. Remyelination and Multiple Sclerosis:

Therapeutic Approaches and Challenges. *Current Neurology and Neuroscience Reports*. Epub ahead of print 2014. DOI: 10.1007/s11910-014-0485-1.
136. Câmara J, Ffrench-Constant C. Lessons from oligodendrocyte biology on promoting repair in multiple sclerosis. *Journal of Neurology*. Epub ahead of print 2007. DOI: 10.1007/s00415-007-1004-y.
137. Nave KA. Myelination and the trophic support of long axons. *Nat Rev Neurosci* 2010; 11: 275–283.
138. Worku Hassen G, Feliberti J, Kesner L, et al. Prevention of axonal injury using calpain inhibitor in chronic progressive experimental autoimmune encephalomyelitis. *Brain Res* 2008; 1236: 206–215.
139. Klugmann M, Schwab MH, Pühlhofer A, et al. Assembly of CNS Myelin in the Absence of Proteolipid Protein. *Neuron* 1997; 18: 59–70.
140. Lu ZH, Chakraborty G, Ledeen RW, et al. N-Acetylaspartate synthase is bimodally expressed in microsomes and mitochondria of brain. *Mol Brain Res* 2004; 122: 71–78.
141. Gonen O, Catalaa I, Babb JS, et al. Total brain N-acetylaspartate: a new measure of disease load in MS. *Neurology* 2000; 54: 15–19.
142. Miljković D, Spasojević I. Multiple sclerosis: molecular mechanisms and therapeutic opportunities. *Antioxid Redox Signal* 2013; 19: 2286–2334.
143. Kensler TW, Wakabayashi N, Biswal S. Cell Survival Responses to Environmental Stresses Via the Keap1-Nrf2-ARE Pathway. *Annu Rev Pharmacol Toxicol*. Epub ahead of print 2007. DOI: 10.1146/annurev.pharmtox.46.120604.141046.
144. Ortiz GG, Pacheco-Moisés FP, Bitzer-Quintero OK, et al. Immunology and oxidative stress in multiple sclerosis: Clinical and basic approach. *Clinical and Developmental Immunology*. Epub ahead of print 2013. DOI: 10.1155/2013/708659.
145. Mahad DH, Trapp BD, Lassmann H. Pathological mechanisms in progressive multiple sclerosis. *The Lancet Neurology*. Epub ahead of print 2015. DOI: 10.1016/S1474-4422(14)70256-X.
146. Murphy MP. How mitochondria produce reactive oxygen species. *Biochemical Journal*. Epub ahead of print 2009. DOI: 10.1042/BJ20081386.
147. Witte ME, Mahad DJ, Lassmann H, et al. Mitochondrial dysfunction contributes to neurodegeneration in multiple sclerosis. *Trends in Molecular Medicine*. Epub ahead of print 2014. DOI: 10.1016/j.molmed.2013.11.007.
148. Yarosz EL, Chang CH. Role of reactive oxygen species in regulating T cell-mediated immunity and disease. *Immune Network*. Epub ahead of print 2018. DOI: 10.4110/in.2018.18.e14.
149. Traynelis SF, Wollmuth LP, McBain CJ, et al. Glutamate receptor ion channels: Structure, regulation, and function. *Pharmacological Reviews*. Epub ahead of print 2010. DOI: 10.1124/pr.109.002451.
150. Wenzel A, Fritschy JM, Mohler H, et al. NMDA receptor heterogeneity during postnatal development of the rat brain: Differential expression of the NR2A, NR2B, and NR2C subunit proteins. *J Neurochem*. Epub ahead of print 1997. DOI: 10.1046/j.1471-4159.1997.68020469.x.
151. Inagaki N, Kuromi H, Gonoi T, et al. Expression and role of ionotropic glutamate receptors in pancreatic islet cells. *FASEB J*. Epub ahead of print 1995. DOI: 10.1096/fasebj.9.8.7768362.
152. Orihara K, Odemuyiwa SO, Stefura WP, et al. Neurotransmitter signalling via NMDA receptors leads to decreased T helper type 1-like and enhanced T helper

type 2-like immune balance in humans. *Immunology*. Epub ahead of print 2018. DOI: 10.1111/imm.12846.
153. Laketić-Ljubojević I, Suva LJ, Maathuis FJM, et al. Functional characterization of N-methyl-D-aspartic acid-gated channels in bone cells. *Bone*. Epub ahead of print 1999. DOI: 10.1016/S8756-3282(99)00224-0.
154. Hansen KB, Yi F, Perszyk RE, et al. Structure, function, and allosteric modulation of NMDA receptors. *Journal of General Physiology*. Epub ahead of print 2018. DOI: 10.1085/jgp.201812032.
155. Monyer H, Sprengel R, Schoepfer R, et al. Heteromeric NMDA receptors: Molecular and functional distinction of subtypes. *Science (80-)*. Epub ahead of print 1992. DOI: 10.1126/science.256.5060.1217.
156. Llansola M, Sanchez-Perez A, Cauli O, et al. Modulation of NMDA receptors in the cerebellum. 1. Properties of the NMDA receptor that modulate its function. *Cerebellum*. Epub ahead of print 2005. DOI: 10.1080/14734220510007996.
157. Zukin RS, Bennett MVL. Alternatively spliced isoforms of the NMDARI receptor subunit. *Trends in Neurosciences*. Epub ahead of print 1995. DOI: 10.1016/0166-2236(95)93920-S.
158. Regan MC, Romero-Hernandez A, Furukawa H. A structural biology perspective on NMDA receptor pharmacology and function. *Current Opinion in Structural Biology*. Epub ahead of print 2015. DOI: 10.1016/j.sbi.2015.07.012.
159. Madry C, Mesic I, Bartholomäus I, et al. Principal role of NR3 subunits in NR1/NR3 excitatory glycine receptor function. *Biochem Biophys Res Commun*. Epub ahead of print 2007. DOI: 10.1016/j.bbrc.2006.12.153.
160. Salter MW, Dong Y, Kalia L V., et al. Regulation of NMDA receptors by kinases and phosphatases. In: *Biology of the NMDA Receptor*. 2008. Epub ahead of print 2008. DOI: 10.1201/9781420044157.ch7.
161. Lüscher C, Malenka RC. NMDA receptor-dependent long-term potentiation and long-term depression (LTP/LTD). *Cold Spring Harb Perspect Biol*. Epub ahead of print 2012. DOI: 10.1101/cshperspect.a005710.
162. Cotman CW, Monaghan DT. Excitatory Amino Acid Neurotransmission: NMDA Receptors and Hebb-Type Synaptic Plasticity. *Annu Rev Neurosci*. Epub ahead of print 1988. DOI: 10.1146/annurev.ne.11.030188.000425.
163. Collingridge GL, Singer W. Excitatory amino acid receptors and synaptic plasticity. *Trends in Pharmacological Sciences*. Epub ahead of print 1990. DOI: 10.1016/0165-6147(90)90011-V.
164. Choi DW. Ionic dependence of glutamate neurotoxicity. *J Neurosci*. Epub ahead of print 1987. DOI: 10.1523/jneurosci.07-02-00369.1987.
165. Tymianski M, Charlton MP, Carlen PL, et al. Source specificity of early calcium neurotoxicity in cultured embryonic spinal neurons. *J Neurosci*. Epub ahead of print 1993. DOI: 10.1523/jneurosci.13-05-02085.1993.
166. Higuchi M, Tomioka M, Takano J, et al. Distinct mechanistic roles of calpain and caspase activation in neurodegeneration as revealed in mice overexpressing their specific inhibitors. *J Biol Chem*. Epub ahead of print 2005. DOI: 10.1074/jbc.M500939200.
167. Vosler PS, Brennan CS, Chen J. Calpain-mediated signaling mechanisms in neuronal injury and neurodegeneration. *Molecular Neurobiology*. Epub ahead of print 2008. DOI: 10.1007/s12035-008-8036-x.
168. D'Orsi B, Bonner H, Tuffy LP, et al. Calpains are downstream effectors of bax-dependent excitotoxic apoptosis. *J Neurosci*. Epub ahead of print 2012. DOI: 10.1523/JNEUROSCI.2345-11.2012.

169. Sinor JD, Du S, Venneti S, et al. NMDA and glutamate evoke excitotoxicity at distinct cellular locations in rat cortical neurons In vitro. *J Neurosci*. Epub ahead of print 2000. DOI: 10.1523/jneurosci.20-23-08831.2000.
170. Papazian I, Kyrargyri V, Evangelidou M, et al. Mesenchymal stem cell protection of neurons against glutamate excitotoxicity involves reduction of NMDA-triggered calcium responses and surface GluR1, and is partly mediated by TNF. *Int J Mol Sci*. Epub ahead of print 2018. DOI: 10.3390/ijms19030651.
171. Yang X, Si P, Qin H, et al. The Neuroprotective Effects of SIRT1 on NMDA-Induced Excitotoxicity. *Oxid Med Cell Longev*. Epub ahead of print 2017. DOI: 10.1155/2017/2823454.
172. Zhou X, Hollern D, Liao J, et al. NMDA receptor-mediated excitotoxicity depends on the coactivation of synaptic and extrasynaptic receptors. *Cell Death Dis*. Epub ahead of print 2013. DOI: 10.1038/cddis.2013.82.
173. Arundine M, Tymianski M. Molecular mechanisms of calcium-dependent neurodegeneration in excitotoxicity. *Cell Calcium*. Epub ahead of print 2003. DOI: 10.1016/S0143-4160(03)00141-6.
174. Lau A, Tymianski M. Glutamate receptors, neurotoxicity and neurodegeneration. *Pflugers Archiv European Journal of Physiology*. Epub ahead of print 2010. DOI: 10.1007/s00424-010-0809-1.
175. Tokita Y, Bessho Y, Masu M, et al. Characterization of excitatory amino acid neurotoxicity in N-methyl-D-aspartate receptor-deficient mouse cortical neuronal cells. *Eur J Neurosci*. Epub ahead of print 1996. DOI: 10.1111/j.1460-9568.1996.tb01168.x.
176. Wahlestedt C, Golanov E, Yamamoto S, et al. Antisense oligodeoxynucleotides to NMDA-R1 receptor channel protect cortical neurons from excitotoxicity and reduce focal ischaemic infarctions. *Nature*. Epub ahead of print 1993. DOI: 10.1038/363260a0.
177. Wang R, Reddy PH. Role of Glutamate and NMDA Receptors in Alzheimer's Disease. *Journal of Alzheimer's Disease*. Epub ahead of print 2017. DOI: 10.3233/JAD-160763.
178. Lai TW, Shyu WC, Wang YT. Stroke intervention pathways: NMDA receptors and beyond. *Trends in Molecular Medicine*. Epub ahead of print 2011. DOI: 10.1016/j.molmed.2010.12.008.
179. Fan MMY, Raymond LA. N-Methyl-d-aspartate (NMDA) receptor function and excitotoxicity in Huntington's disease. *Progress in Neurobiology*. Epub ahead of print 2007. DOI: 10.1016/j.pneurobio.2006.11.003.
180. Ahmed I, Bose SK, Pavese N, et al. Glutamate NMDA receptor dysregulation in Parkinson's disease with dyskinesias. *Brain*. Epub ahead of print 2011. DOI: 10.1093/brain/awr028.
181. Javitt DC. Glutamate as a therapeutic target in psychiatric disorders. *Molecular Psychiatry*. Epub ahead of print 2004. DOI: 10.1038/sj.mp.4001551.
182. Pitt D, Werner P, Raine CS. Glutamate excitotoxicity in a model of multiple sclerosis. *Nat Med*. Epub ahead of print 2000. DOI: 10.1038/71555.
183. Cianfoni A, Niku S, Imbesi SG. Metabolite findings in tumefactive demyelinating lesions utilizing short echo time proton magnetic resonance spectroscopy. *Am J Neuroradiol*. Epub ahead of print 2007. DOI: 10.1016/s0098-1672(08)70230-3.
184. Sarchielli P, Greco L, Floridi A, et al. Excitatory Amino Acids and Multiple Sclerosis. *Arch Neurol*. Epub ahead of print 2003. DOI: 10.1001/archneur.60.8.1082.

185. Newcombe J, Uddin A, Dove R, et al. Glutamate receptor expression in multiple sclerosis lesions. *Brain Pathol*. Epub ahead of print 2008. DOI: 10.1111/j.1750-3639.2007.00101.x.
186. Bleich S, Römer K, Wiltfang J, et al. Glutamate and the glutamate receptor system: A target for drug action. In: *International Journal of Geriatric Psychiatry*. 2003. Epub ahead of print 2003. DOI: 10.1002/gps.933.
187. van der Star BJ, Vogel DY, Kipp M, et al. In vitro and in vivo models of multiple sclerosis. *CNS Neurol Disord Drug Targets* 2012; 11: 570–588.
188. Vesterinen HM, Sena ES, Ffrench-Constant C, et al. Improving the translational hit of experimental treatments in multiple sclerosis. *Mult Scler* 2010; 16: 1044–55.
189. Steinman L. Assessment of animal models for MS and demyelinating disease in the design of rational therapy. *Neuron* 1999; 24: 511–514.
190. Constantinescu CS, Farooqi N, O'Brien K, et al. Experimental autoimmune encephalomyelitis (EAE) as a model for multiple sclerosis (MS). *Br J Pharmacol* 2011; 164: 1079–1106.
191. Jones M V., Nguyen TT, DeBoy CA, et al. Behavioral and pathological outcomes in MOG 35-55 experimental autoimmune encephalomyelitis. *J Neuroimmunol* 2008; 199: 83–93.
192. Bittner S, Afzali AM, Wiendl H, et al. Myelin oligodendrocyte glycoprotein (MOG35-55) induced experimental autoimmune encephalomyelitis (EAE) in C57BL/6 mice. *J Vis Exp* 2014; e51275.
193. Baker D, Pryce G, Croxford JL, et al. Cannabinoids control spasticity and tremor in a multiple sclerosis model. *Nature* 2000; 404: 84–87.
194. Al-Izki S, Pryce G, Giovannoni G, et al. Evaluating potential therapies for bladder dysfunction in a mouse model of multiple sclerosis with high-resolution ultrasonography. *Mult Scler* 2009; 15: 795–801.
195. Al-Izki S, Pryce G, Jackson SJ, et al. Immunosuppression with FTY720 is insufficient to prevent secondary progressive neurodegeneration in experimental autoimmune encephalomyelitis. *Mult Scler* 2011; 17: 939–948.
196. Jackson SJ, Lee J, Nikodemova M, et al. Quantification of myelin and axon pathology during relapsing progressive experimental autoimmune encephalomyelitis in the Biozzi ABH mouse. *J Neuropathol Exp Neurol* 2009; 68: 616–25.
197. Lassmann H, Bradl M. Multiple sclerosis: experimental models and reality. *Acta Neuropathologica*, 2016, pp. 1–22.
198. Mccarthy DP, Richards MH, Miller SD. Mouse Models of Multiple Sclerosis: Experimental Autoimmune Encephalomyelitis and Theiler's Virus-Induced Demyelinating Disease. 2012; 900: 1–19.
199. Brown AM, McFarlin DE. Relapsing experimental allergic encephalomyelitis in the SJL/J mouse. *Lab Invest* 1981; 45: 278–284.
200. Hofstetter HH, Toyka K V, Tary-Lehmann M, et al. Kinetics and organ distribution of IL-17-producing CD4 cells in proteolipid protein 139-151 peptide-induced experimental autoimmune encephalomyelitis of SJL mice. *J Immunol* 2007; 178: 1372–1378.
201. McRae BL, Kennedy MK, Tan LJ, et al. Induction of active and adoptive relapsing experimental autoimmune encephalomyelitis (EAE) using an encephalitogenic epitope of proteolipid protein. *J Neuroimmunol* 1992; 38: 229–240.
202. Marracci GH, Jones RE, McKeon GP, et al. Alpha lipoic acid inhibits T cell

migration into the spinal cord and suppresses and treats experimental autoimmune encephalomyelitis. *J Neuroimmunol* 2002; 131: 104–114.
203. Swanborg RH. Experimental autoimmune encephalomyelitis in the rat: lessons in T-cell immunology and autoreactivity. *Immunol Rev* 2001; 184: 129–135.
204. Krishnamoorthy G, Wekerle H. EAE: An immunologist's magic eye. *Eur J Immunol* 2009; 39: 2031–2035.
205. Croxford AL, Kurschus FC, Waisman A. Mouse models for multiple sclerosis: historical facts and future implications. *Biochim Biophys Acta* 2011; 1812: 177–183.
206. Shin T, Ahn M, Matsumoto Y. Mechanism of experimental autoimmune encephalomyelitis in Lewis rats: recent insights from macrophages. *Anat Cell Biol* 2012; 45: 141.
207. Shin T, Kojima T, Tanuma N, et al. The subarachnoid space as a site for precursor T cell proliferation and effector T cell selection in experimental autoimmune encephalomyelitis. *J Neuroimmunol* 1995; 56: 171–8.
208. Stosic-Grujicic S, Ramic Z, Bumbasirevic V, et al. Induction of experimental autoimmune encephalomyelitis in Dark Agouti rats without adjuvant. *Clin Exp Immunol* 2004; 136: 49–55.
209. Kap YS, Smith P, Jagessar SA, et al. Fast progression of recombinant human myelin/oligodendrocyte glycoprotein (MOG)-induced experimental autoimmune encephalomyelitis in marmosets is associated with the activation of MOG34-56-specific cytotoxic T cells. *J Immunol* 2008; 180: 1326–1337.
210. Kap YS, Laman JD, 't Hart BA. Experimental autoimmune encephalomyelitis in the common marmoset, a bridge between rodent EAE and multiple sclerosis for immunotherapy development. *J Neuroimmune Pharmacol* 2010; 5: 220–230.
211. Becher B, Durell BG, Noelle RJ. Experimental autoimmune encephalitis and inflammation in the absence of interleukin-12. *J Clin Invest* 2002; 110: 493–497.
212. Panitch HS, Hirsch RL, Haley AS, et al. Exacerbations of Multiple Sclerosis in Patients Treated With Gamma Interferon. *Lancet* 1987; 329: 893–895.
213. Kroenke M a, Carlson TJ, Andjelkovic A V, et al. IL-12- and IL-23-modulated T cells induce distinct types of EAE based on histology, CNS chemokine profile, and response to cytokine inhibition. *J Exp Med* 2008; 205: 1535–1541.
214. Cua DJ, Sherlock J, Chen Y, et al. Interleukin-23 rather than interleukin-12 is the critical cytokine for autoimmune inflammation of the brain. *Nature*. Epub ahead of print 2003. DOI: 10.1038/nature01355.
215. Haak S, Croxford AL, Kreymborg K, et al. IL-17A and IL-17F do not contribute vitally to autoimmune neuro-inflammation in mice. *J Clin Invest*. Epub ahead of print 2009. DOI: 10.1172/JCI35997.
216. Yednock TA, Cannon C, Fritz LC, et al. Prevention of experimental autoimmune encephalomyelitis by antibodies against [alpha]4[beta]l integrin. *Nature* 1992; 356: 63–66.
217. Kawakami N, Lassmann S, Li Z, et al. The activation status of neuroantigen-specific T cells in the target organ determines the clinical outcome of autoimmune encephalomyelitis. *J Exp Med* 2004; 199: 185–97.
218. Lees JR, Golumbek PT, Sim J, et al. Regional CNS responses to IFN-gamma determine lesion localization patterns during EAE pathogenesis. *J Exp Med* 2008; 205: 2633–42.
219. Johnson TA, Jirik FR, Fournier S. Exploring the roles of CD8+ T lymphocytes in the pathogenesis of autoimmune demyelination. *Semin Immunopathol* 2010; 32: 197–209.

220. J. van der Star B, Y.S. Vogel D, Kipp M, et al. In Vitro and In Vivo Models of Multiple Sclerosis. *CNS Neurol Disord - Drug Targets*. Epub ahead of print 2012. DOI: 10.2174/187152712801661284.
221. Humpel C. Neuroscience forefront review organotypic brain slice cultures: A review. *Neuroscience* 2015; 305: 86–98.
222. Zhang H, Jarjour AA, Boyd A, et al. Central nervous system remyelination in culture - A tool for multiple sclerosis research. *Exp Neurol* 2011; 230: 138–148.
223. Jackson MC, Lenney JF. The distribution of carnosine and related dipeptides in rat and human tissues. *Inflamm Res* 1996; 45: 132–135.
224. Bellia F, Vecchio G, Rizzarelli E. Carnosinases, their substrates and diseases. *Molecules*. Epub ahead of print 2014. DOI: 10.3390/molecules19022299.
225. Vistoli G, Orioli M, Pedretti A, et al. Design, synthesis, and evaluation of carnosine derivatives as selective and efficient sequestering agents of cytotoxic reactive carbonyl species. *ChemMedChem*. Epub ahead of print 2009. DOI: 10.1002/cmdc.200800433.
226. Guiotto A, Calderan A, Ruzza P, et al. Carnosine and Carnosine-Related Antioxidants: A Review. *Curr Med Chem* 2005; 12: 2293–2315.
227. Parkhouse WS, McKenzie DC, Hochachka PW, et al. Buffering capacity of deproteinized human vastus lateralis muscle. *J Appl Physiol*. Epub ahead of print 1985. DOI: 10.1152/jappl.1985.58.1.14.
228. Hobson RM, Saunders B, Ball G, et al. Effects of β-alanine supplementation on exercise performance: A meta-analysis. *Amino Acids*. Epub ahead of print 2012. DOI: 10.1007/s00726-011-1200-z.
229. Stvolinskii SL, Dobrota D, Mezeshova V, et al. Carnosine and anserine in working muscles--study using proton NMR spectroscopy. *Biokhimiia*.
230. De Marchis S, Modena C, Peretto P, et al. Carnosine-Related Dipeptides in Neurons and Glia. *Biochemistry (Moscow)*.
231. De Marchis S, Melcangi RC, Modena C, et al. Identification of the glial cell types containing carnosine-related peptides in the rat brain. *Neurosci Lett*. Epub ahead of print 1997. DOI: 10.1016/S0304-3940(97)00800-8.
232. Caruso G, Caraci F, Jolivet RB. Pivotal role of carnosine in the modulation of brain cells activity: Multimodal mechanism of action and therapeutic potential in neurodegenerative disorders. *Progress in Neurobiology*. Epub ahead of print 2019. DOI: 10.1016/j.pneurobio.2018.12.004.
233. Hasanein P, Felegari Z. Chelating effects of carnosine in ameliorating nickel-induced nephrotoxicity in rats. *Can J Physiol Pharmacol*. Epub ahead of print 2017. DOI: 10.1139/cjpp-2016-0647.
234. Schön M, Mousa A, Berk M, et al. The potential of carnosine in brain-related disorders: A comprehensive review of current evidence. *Nutrients*. Epub ahead of print 2019. DOI: 10.3390/nu11061196.
235. Budzeń S, Aszewska JR. The biological role of carnosine and its possible applications in medicine. *Advances in Clinical and Experimental Medicine*.
236. Aloisi A, Barca A, Romano A, et al. Anti-Aggregating Effect of the Naturally Occurring Dipeptide Carnosine on Aβ1-42 Fibril Formation. *PLoS One*. Epub ahead of print 2013. DOI: 10.1371/journal.pone.0068159.
237. Caruso G, Fresta CG, Martinez-Becerra F, et al. Carnosine modulates nitric oxide in stimulated murine RAW 264.7 macrophages. *Mol Cell Biochem*. Epub ahead of print 2017. DOI: 10.1007/s11010-017-2991-3.
238. Tiedje KE, Stevens K, Barnes S, et al. β-Alanine as a small molecule neurotransmitter. *Neurochemistry International*. Epub ahead of print 2010. DOI:

10.1016/j.neuint.2010.06.001.
239. Mal'tseva V V., Sergienko V V., Stvolinskiĭ SL. The effect of carnosine on hematopoietic stem cell activity in irradiated animals. *Biokhimiya*.
240. Jain S, Kim ES, Kim D, et al. Comparative cerebroprotective potential of d- and l-carnosine following ischemic stroke in mice. *Int J Mol Sci*. Epub ahead of print 2020. DOI: 10.3390/ijms21093053.
241. Zhao J, Shi L, Zhang LR. Neuroprotective effect of carnosine against salsolinol-induced Parkinson's disease. *Exp Ther Med*. Epub ahead of print 2017. DOI: 10.3892/etm.2017.4571.
242. Hipkiss AR. Could carnosine or related structures suppress Alzheimer's disease? *J Alzheimer's Dis*. Epub ahead of print 2007. DOI: 10.3233/JAD-2007-11210.
243. Bae ON, Serfozo K, Baek SH, et al. Safety and efficacy evaluation of carnosine, an endogenous neuroprotective agent for ischemic stroke. *Stroke* 2013; 44: 205–212.
244. Gardner ML, Illingworth KM, Kelleher J, et al. Intestinal absorption of the intact peptide carnosine in man, and comparison with intestinal permeability to lactulose. *J Physiol*. Epub ahead of print 1991. DOI: 10.1113/jphysiol.1991.sp018673.
245. Rajanikant GK, Zemke D, Senut MC, et al. Carnosine is neuroprotective against permanent focal cerebral ischemia in mice. *Stroke*. Epub ahead of print 2007. DOI: 10.1161/STROKEAHA.107.488502.
246. Baye E, Ukropec J, de Courten MPJ, et al. Carnosine supplementation improves serum resistin concentrations in overweight or obese otherwise healthy adults: A pilot randomized trial. *Nutrients*. Epub ahead of print 2018. DOI: 10.3390/nu10091258.
247. Yang Y, Wang Y, Kong Y, et al. Carnosine prevents type 2 diabetes-induced osteoarthritis through the ROS/NF-κB pathway. *Front Pharmacol*. Epub ahead of print 2018. DOI: 10.3389/fphar.2018.00598.
248. Baye E, Ukropcova B, Ukropec J, et al. Physiological and therapeutic effects of carnosine on cardiometabolic risk and disease. *Amino Acids*. Epub ahead of print 2016. DOI: 10.1007/s00726-016-2208-1.
249. Wassif WS, Sherwood RA, Amir A, et al. Serum carnosinase activities in central nervous system disorders. *Clin Chim Acta*. Epub ahead of print 1994. DOI: 10.1016/0009-8981(94)90027-2.
250. Keytsman C, Blancquaert L, Wens I, et al. Muscle carnosine in experimental autoimmune encephalomyelitis and multiple sclerosis. *Mult Scler Relat Disord*. Epub ahead of print 2018. DOI: 10.1016/j.msard.2018.02.013.
251. Rusnock AA. Historical context and the roots of Jenner's discovery. *Human Vaccines and Immunotherapeutics*. Epub ahead of print 2016. DOI: 10.1080/21645515.2016.1158369.
252. Weiner HL, Selkoe DJ. Inflammation and therapeutic vaccination in CNS diseases. *Nature*. Epub ahead of print 2002. DOI: 10.1038/nature01325.
253. Schenk D, Barbour R, Dunn W, et al. Immunization with amyloid-β attenuates Alzheimer disease-like pathology in the PDAPP mouse. *Nature*. Epub ahead of print 1999. DOI: 10.1038/22124.
254. Bard F, Cannon C, Barbour R, et al. Peripherally administered antibodies against amyloid β-peptide enter the central nervous system and reduce pathology in a mouse model of Alzheimer disease. *Nat Med*. Epub ahead of print 2000. DOI: 10.1038/78682.

255. Bielekova B, Goodwin B, Richert N, et al. Encephalitogenic potential of the myelin basic protein peptide (amino acids 83-99) in multiple sclerosis: Results of a phase II clinical trial with an altered peptide ligand. *Nat Med*. Epub ahead of print 2000. DOI: 10.1038/80516.
256. Campbell BCV, De Silva DA, Macleod MR, et al. Ischaemic stroke. *Nat Rev Dis Prim*; 5. Epub ahead of print 2019. DOI: 10.1038/s41572-019-0118-8.
257. Kushnir N, Streatfield SJ, Yusibov V. Virus-like particles as a highly efficient vaccine platform: Diversity of targets and production systems and advances in clinical development. *Vaccine*. Epub ahead of print 2012. DOI: 10.1016/j.vaccine.2012.10.083.
258. Akache B, Weeratna RD, Deora A, et al. Anti-IgE Qb-VLP Conjugate Vaccine Self-Adjuvants through Activation of TLR7. *Vaccines* 2016; 4: 3.
259. Mohsen MO, Zha L, Cabral-Miranda G, et al. Major findings and recent advances in virus–like particle (VLP)-based vaccines. *Semin Immunol* 2017; 34: 123–132.
260. Metz SW, Thomas A, White L, et al. Dengue virus-like particles mimic the antigenic properties of the infectious dengue virus envelope. *Virol J*. Epub ahead of print 2018. DOI: 10.1186/s12985-018-0970-2.
261. Dombrowski Y, O'Hagan T, Dittmer M, et al. Regulatory T cells promote myelin regeneration in the central nervous system. *Nat Neurosci* 2017; 20: 674–680.
262. MANDERS EMM, VERBEEK FJ, ATEN JA. Measurement of co-localization of objects in dual-colour confocal images. *J Microsc*. Epub ahead of print 1993. DOI: 10.1111/j.1365-2818.1993.tb03313.x.
263. Deacon RMJ. Burrowing in rodents: A sensitive method for detecting behavioral dysfunction. *Nat Protoc*. Epub ahead of print 2006. DOI: 10.1038/nprot.2006.19.
264. Toni LS, Garcia AM, Jeffrey DA, et al. Optimization of phenol-chloroform RNA extraction. *MethodsX*. Epub ahead of print 2018. DOI: 10.1016/j.mex.2018.05.011.
265. Faul F, Erdfelder E, Lang AG, et al. G*Power 3: A flexible statistical power analysis program for the social, behavioral, and biomedical sciences. In: *Behavior Research Methods*. 2007. Epub ahead of print 2007. DOI: 10.3758/BF03193146.
266. Li Q, Han X, Wang J. Organotypic Hippocampal Slices as Models for Stroke and Traumatic Brain Injury. *Molecular Neurobiology* 2016; 53: 4226–4237.
267. Gähwiler B. Organotypic slice cultures: a technique has come of age. *Trends Neurosci* 1997; 20: 471–477.
268. Takuma H, Sakurai M, Kanazawa I. In vitro formation of corticospinal synapses in an organotypic slice co-culture. *Neuroscience* 2002; 109: 359–370.
269. Muramatsu R, Hamaguchi M, Muramatsu R, et al. Lysophosphatidylcholine-induced demyelination model of mouse. *Protoc Exch*. Epub ahead of print 2017. DOI: 10.1038/protex.2017.121.
270. Plemel JR, Michaels NJ, Weishaupt N, et al. Mechanisms of lysophosphatidylcholine-induced demyelination: A primary lipid disrupting myelinopathy. *Glia*. Epub ahead of print 2018. DOI: 10.1002/glia.23245.
271. Dunn KW, Kamocka MM, McDonald JH. A practical guide to evaluating colocalization in biological microscopy. *American Journal of Physiology - Cell Physiology*. Epub ahead of print 2011. DOI: 10.1152/ajpcell.00462.2010.
272. Doussau F, Dupont JL, Neel D, et al. Organotypic cultures of cerebellar slices as a model to investigate demyelinating disorders. *Expert Opinion on Drug Discovery*. Epub ahead of print 2017. DOI: 10.1080/17460441.2017.1356285.

273. Al-Izki S, Pryce G, O'Neill JK, et al. Practical guide to the induction of relapsing progressive experimental autoimmune encephalomyelitis in the Biozzi ABH mouse. *Mult Scler Relat Disord*. Epub ahead of print 2012. DOI: 10.1016/j.msard.2011.09.001.
274. Lobner D. Comparison of the LDH and MTT assays for quantifying cell death: Validity for neuronal apoptosis? *J Neurosci Methods*. Epub ahead of print 2000. DOI: 10.1016/S0165-0270(99)00193-4.
275. Belle AM, Enright HA, Sales AP, et al. Evaluation of in vitro neuronal platforms as surrogates for in vivo whole brain systems. *Sci Rep*. Epub ahead of print 2018. DOI: 10.1038/s41598-018-28950-5.
276. Lesuisse C, Martin LJ. Long-term culture of mouse cortical neurons as a model for neuronal development, aging, and death. *J Neurobiol*. Epub ahead of print 2002. DOI: 10.1002/neu.10037.
277. Liu Y, Tak PW, Aarts M, et al. NMDA receptor subunits have differential roles in mediating excitotoxic neuronal death both in vitro and in vivo. *J Neurosci*. Epub ahead of print 2007. DOI: 10.1523/JNEUROSCI.0116-07.2007.
278. Shen Y, He P, Fan Y ying, et al. Carnosine protects against permanent cerebral ischemia in histidine decarboxylase knockout mice by reducing glutamate excitotoxicity. *Free Radic Biol Med*. Epub ahead of print 2010. DOI: 10.1016/j.freeradbiomed.2009.12.021.
279. Gallant S, Kukley M, Stvolinsky S, et al. Effect of carnosine on rats under experimental brain ischemia. *Tohoku J Exp Med*. Epub ahead of print 2000. DOI: 10.1620/tjem.191.85.
280. Brewer GJ, Torricelli JR, Evege EK, et al. Optimized survival of hippocampal neurons in B27-supplemented neurobasal™, a new serum-free medium combination. *J Neurosci Res*. Epub ahead of print 1993. DOI: 10.1002/jnr.490350513.
281. Roth S, Zhang SJ, Chiu J, et al. Development of a serum-free supplement for primary neuron culture reveals the interplay of selenium and vitamin E in neuronal survival. *J Trace Elem Med Biol*. Epub ahead of print 2010. DOI: 10.1016/j.jtemb.2010.01.007.
282. Lopachev A V., Lopacheva OM, Abaimov DA, et al. Neuroprotective effect of carnosine on primary culture of rat cerebellar cells under oxidative stress. *Biochem*. Epub ahead of print 2016. DOI: 10.1134/S0006297916050084.
283. Bettger WJ, McKeehan WL. Mechanisms of cellular nutrition. *Physiological Reviews*. Epub ahead of print 1986. DOI: 10.1152/physrev.1986.66.1.1.
284. Lee SB, Kim JJ, Kim TW, et al. Serum deprivation-induced reactive oxygen species production is mediated by Romo1. *Apoptosis*. Epub ahead of print 2010. DOI: 10.1007/s10495-009-0411-1.
285. Aldini G, Facino RM, Beretta G, et al. Carnosine and related dipeptides as quenchers of reactive carbonyl species: From structural studies to therapeutic perspectives. *BioFactors*. Epub ahead of print 2005. DOI: 10.1002/biof.5520240109.
286. Gariballa S. Review. Carnosine: physiological properties and therapeutic potential. *Age Ageing*. Epub ahead of print 2000. DOI: 10.1093/ageing/29.3.207.
287. Cararo JH, Streck EL, Schuck PF, et al. Carnosine and related peptides: Therapeutic Potential in Age-Related Disorders. *Aging and Disease*. Epub ahead of print 2015. DOI: 10.14336/AD.2015.0616.
288. Boldyrev AA, Stvolinsky SL, Fedorova TN, et al. Carnosine as a natural antioxidant and geroprotector: From molecular mechanisms to clinical trials.

Rejuvenation Research. Epub ahead of print 2010. DOI: 10.1089/rej.2009.0923.
289. Nishiyama A. Organotypic slice cultures to study oligodendrocyte dynamics and myelination. *J Vis Exp*. Epub ahead of print 2014. DOI: 10.3791/51835.
290. Kipp M, van der Star B, Vogel DYS, et al. Experimental in vivo and in vitro models of multiple sclerosis: EAE and beyond. *Mult Scler Relat Disord* 2012; 1: 15–28.
291. Cho S, Wood A, Bowlby M. Brain Slices as Models for Neurodegenerative Disease and Screening Platforms to Identify Novel Therapeutics. *Curr Neuropharmacol*. Epub ahead of print 2007. DOI: 10.2174/157015907780077105.
292. Humpel C. Organotypic brain slice cultures: A review. *Neuroscience* 2015; 305: 86–98.
293. Tanaka T, Ueno M, Yamashita T. Engulfment of axon debris by microglia requires p38 MAPK activity. *J Biol Chem*. Epub ahead of print 2009. DOI: 10.1074/jbc.M109.005603.
294. Heppner FL, Greter M, Marino D, et al. Experimental autoimmune encephalomyelitis repressed by microglial paralysis. *Nat Med* 2005; 11: 146–152.
295. Vogel DYS, Vereyken EJF, Glim JE, et al. Macrophages in inflammatory multiple sclerosis lesions have an intermediate activation status. *J Neuroinflammation*. Epub ahead of print 2013. DOI: 10.1186/1742-2094-10-35.
296. Wang J, Wang J, Wang J, et al. Targeting microglia and macrophages: A potential treatment strategy for multiple sclerosis. *Front Pharmacol*. Epub ahead of print 2019. DOI: 10.3389/fphar.2019.00286.
297. Moser K V., Schmidt-Kastner R, Hinterhuber H, et al. Brain capillaries and cholinergic neurons persist in organotypic brain slices in the absence of blood flow. *Eur J Neurosci* 2003; 18: 85–94.
298. Pritchard AJ, Mir AK, Dev KK. Fingolimod attenuates splenocyte-induced demyelination in cerebellar slice cultures. *PLoS One*; 9. Epub ahead of print 2014. DOI: 10.1371/journal.pone.0099444.
299. Miron VE, Ludwin SK, Darlington PJ, et al. Fingolimod (FTY720) Enhances Remyelination Following Demyelination of Organotypic Cerebellar Slices. *Am J Pathol* 2010; 176: 2682–2694.
300. Medina-Rodríguez EM, Bribián A, Boyd A, et al. Promoting in vivo remyelination with small molecules: a neuroreparative pharmacological treatment for Multiple Sclerosis. *Sci Rep* 2017; 7: 43545.
301. Harrer MD, von Büdingen HC, Stoppini L, et al. Live imaging of remyelination after antibody-mediated demyelination in an ex-vivo model for immune mediated CNS damage. *Exp Neurol* 2009; 216: 431–438.
302. Bin JM, Leong SY, Bull SJ, et al. Oligodendrocyte precursor cell transplantation into organotypic cerebellar shiverer slices: A model to study myelination and myelin maintenance. *PLoS One*; 7. Epub ahead of print 2012. DOI: 10.1371/journal.pone.0041237.
303. O'Sullivan C, Schubart A, Mir AK, et al. The dual S1PR1/S1PR5 drug BAF312 (Siponimod) attenuates demyelination in organotypic slice cultures. *J Neuroinflammation* 2016; 13: 31.
304. Smith ME, Kocsis JD, Waxman SG. Myelin protein metabolism in demyelination and remyelination in the sciatic nerve. *Brain Res* 1983; 270: 37–44.
305. Allt G, Ghabriel MN, Sikri K. Lysophosphatidyl choline-induced demyelination - A freeze-fracture study. *Acta Neuropathol* 1988; 75: 456–464.

306. Al-Izki S, Pryce G, O'Neill JK, et al. Practical guide to the induction of relapsing progressive experimental autoimmune encephalomyelitis in the Biozzi ABH mouse. *Mult Scler Relat Disord* 2012; 1: 29–38.
307. Stromnes IM, Goverman JM. Active induction of experimental allergic encephalomyelitis. *Nat Protoc* 2006; 1: 1810–1819.
308. Abadier M, Haghayegh Jahromi N, Cardoso Alves L, et al. Cell surface levels of endothelial ICAM-1 influence the transcellular or paracellular T-cell diapedesis across the blood-brain barrier. *Eur J Immunol* 2015; 45: 1043–1058.
309. Döring A, Wild M, Vestweber D, et al. E- and P-selectin are not required for the development of experimental autoimmune encephalomyelitis in C57BL/6 and SJL mice. *J Immunol* 2007; 179: 8470–9.
310. Mendel I, de Rosbo NK, Ben-Nun A. A myelin oligodendrocyte glycoprotein peptide induces typical chronic experimental autoimmune encephalomyelitis in H-2b mice: Fine specificity and T cell receptor Vβ expression of encephalitogenic T cells. *Eur J Immunol* 1995; 25: 1951–1959.
311. Tietz SM, Zwahlen M, Jahromi NH, et al. Refined clinical scoring in comparative EAE studies does not enhance the chance to observe statistically significant differences. *Eur J Immunol* 2016; 46: 2481–2483.
312. Hampton DW, Anderson J, Pryce G, et al. An experimental model of secondary progressive multiple sclerosis that shows regional variation in gliosis, remyelination, axonal and neuronal loss. *J Neuroimmunol* 2008; 201–202: 200–211.
313. Baker D, O'Neill JK, Gschmeissner SE, et al. Induction of chronic relapsing experimental allergic encephalomyelitis in Biozzi mice. *J Neuroimmunol* 1990; 28: 261–270.
314. Allen SJ, Baker D, O'Neill JK, et al. Isolation and characterization of cells infiltrating the spinal cord during the course of chronic relapsing experimental allergic encephalomyelitis in the biozzi ab/h mouse. *Cell Immunol*. Epub ahead of print 1993. DOI: 10.1006/cimm.1993.1031.
315. Bidaran S, Ahmadi AR, Yaghmaei P, et al. Astaxanthin effectiveness in preventing multiple sclerosis in animal model. *Bratislava Med J*. Epub ahead of print 2018. DOI: 10.4149/BLL_2018_031.
316. Choi BY, Jang BG, Kim JH, et al. Copper/zinc chelation by clioquinol reduces spinal cord white matter damage and behavioral deficits in a murine MOG-induced multiple sclerosis model. *Neurobiol Dis* 2013; 54: 382–391.
317. Hawkins RA, O'Kane RL, Simpson IA, et al. Structure of the blood-brain barrier and its role in the transport of amino acids. In: *Journal of Nutrition*. 2006. Epub ahead of print 2006. DOI: 10.1093/jn/136.1.218s.
318. Kim ES, Kim D, Nyberg S, et al. LRP-1 functionalized polymersomes enhance the efficacy of carnosine in experimental stroke. *Sci Rep*. Epub ahead of print 2020. DOI: 10.1038/s41598-020-57685-5.
319. Min J, Senut MC, Rajanikant K, et al. Differential neuroprotective effects of carnosine, anserine, and N-acetyl carnosine against permanent focal ischemia. *J Neurosci Res*. Epub ahead of print 2008. DOI: 10.1002/jnr.21744.
320. Deacon RMJ. Digging and marble burying in mice: Simple methods for in vivo identification of biological impacts. *Nat Protoc*. Epub ahead of print 2006. DOI: 10.1038/nprot.2006.20.
321. Deacon RMJ. Assessing nest building in mice. *Nat Protoc*. Epub ahead of print 2006. DOI: 10.1038/nprot.2006.170.
322. Gould TD, Dao DT, Kovacsics CE. The Open Field Test. In: Gould TD (ed) *Mood*

and Anxiety Related Phenotypes in Mice: Characterization Using Behavioral Tests. Totowa, NJ: Humana Press, 2009, pp. 1–20.
323. Cruz C, Cruz F. The ERK 1 and 2 Pathway in the Nervous System: From Basic Aspects to Possible Clinical Applications in Pain and Visceral Dysfunction. *Curr Neuropharmacol*. Epub ahead of print 2007. DOI: 10.2174/157015907782793630.
324. Mohsen MO, Gomes AC, Cabral-Miranda G, et al. Delivering adjuvants and antigens in separate nanoparticles eliminates the need of physical linkage for effective vaccination. *J Control Release*. Epub ahead of print 2017. DOI: 10.1016/j.jconrel.2017.02.031.
325. Tighe PJ, Ryder RR, Todd I, et al. ELISA in the multiplex era: Potentials and pitfalls. *Proteomics - Clinical Applications*. Epub ahead of print 2015. DOI: 10.1002/prca.201400130.
326. Büttel IC, Chamberlain P, Chowers Y, et al. Taking immunogenicity assessment of therapeutic proteins to the next level. *Biologicals*. Epub ahead of print 2011. DOI: 10.1016/j.biologicals.2011.01.006.
327. Flaxman A, Ewer KJ. Methods for measuring T-cell memory to vaccination: From mouse to man. *Vaccines*. Epub ahead of print 2018. DOI: 10.3390/vaccines6030043.
328. Calarota SA, Baldanti F. Enumeration and characterization of human memory t cells by enzyme-linked immunospot assays. *Clinical and Developmental Immunology*. Epub ahead of print 2013. DOI: 10.1155/2013/637649.
329. Dalmau J, Lancaster E, Martinez-Hernandez E, et al. Clinical experience and laboratory investigations in patients with anti-NMDAR encephalitis. *The Lancet Neurology*. Epub ahead of print 2011. DOI: 10.1016/S1474-4422(10)70253-2.
330. Dalmau J, Gleichman AJ, Hughes EG, et al. Anti-NMDA-receptor encephalitis: case series and analysis of the effects of antibodies. *Lancet Neurol*. Epub ahead of print 2008. DOI: 10.1016/S1474-4422(08)70224-2.
331. Hammer C, Stepniak B, Schneider A, et al. Neuropsychiatric disease relevance of circulating anti-NMDA receptor autoantibodies depends on blood-brain barrier integrity. *Mol Psychiatry*. Epub ahead of print 2014. DOI: 10.1038/mp.2013.110.
332. Minagar A, Alexander JS. Blood-brain barrier disruption in multiple sclerosis. *Multiple Sclerosis*. Epub ahead of print 2003. DOI: 10.1191/1352458503ms965oa.
333. Linthicum DS, Munoz JJ, Blaskett A. Acute experimental autoimmune encephalomyelitis in mice. I. Adjuvant action of Bordetella pertussis is due to vasoactive amine sensitization and increased vascular permeability of the central nervous system. *Cell Immunol*. Epub ahead of print 1982. DOI: 10.1016/0008-8749(82)90457-9.
334. Olechowski CJ, Tenorio G, Sauve Y, et al. Changes in nociceptive sensitivity and object recognition in experimental autoimmune encephalomyelitis (EAE). *Exp Neurol* 2013; 241: 113–121.
335. Ziehn MO, Avedisian AA, Tiwari-Woodruff S, et al. Hippocampal CA1 atrophy and synaptic loss during experimental autoimmune encephalomyelitis, EAE. *Lab Invest* 2010; 90: 774–86.
336. D'Intino G, Paradisi M, Fernandez M, et al. Cognitive deficit associated with cholinergic and nerve growth factor down-regulation in experimental allergic encephalomyelitis in rats. *Proc Natl Acad Sci U S A* 2005; 102: 3070–5.
337. Olechowski CJ, Truong JJ, Kerr BJ. Neuropathic pain behaviours in a chronic-relapsing model of experimental autoimmune encephalomyelitis (EAE). *Pain*

2009; 141: 156–164.
338. Acharjee S, Nayani N, Tsutsui M, et al. Altered cognitive-emotional behavior in early experimental autoimmune encephalitis - Cytokine and hormonal correlates. *Brain Behav Immun* 2013; 33: 164–172.
339. Pollak Y, Ovadia H, Goshen I, et al. Behavioral aspects of experimental autoimmune encephalomyelitis. *J Neuroimmunol* 2000; 104: 31–6.
340. Lewerenz J, Maher P. Chronic glutamate toxicity in neurodegenerative diseases-What is the evidence? *Frontiers in Neuroscience*. Epub ahead of print 2015. DOI: 10.3389/fnins.2015.00469.
341. Hynd MR, Scott HL, Dodd PR. Glutamate-mediated excitotoxicity and neurodegeneration in Alzheimer's disease. *Neurochemistry International*. Epub ahead of print 2004. DOI: 10.1016/j.neuint.2004.03.007.
342. Foran E, Trotti D. Glutamate transporters and the excitotoxic path to motor neuron degeneration in amyotrophic lateral sclerosis. *Antioxidants and Redox Signaling*. Epub ahead of print 2009. DOI: 10.1089/ars.2009.2444.
343. Gonsette RE. Neurodegeneration in multiple sclerosis: The role of oxidative stress and excitotoxicity. *J Neurol Sci*. Epub ahead of print 2008. DOI: 10.1016/j.jns.2008.06.029.
344. Marte A, Cavallero A, Morando S, et al. Alterations of glutamate release in the spinal cord of mice with experimental autoimmune encephalomyelitis. *J Neurochem*. Epub ahead of print 2010. DOI: 10.1111/j.1471-4159.2010.06923.x.
345. Rossi S, De Chiara V, Furlan R, et al. Abnormal activity of the Na/Ca exchanger enhances glutamate transmission in experimental autoimmune encephalomyelitis. *Brain Behav Immun*. Epub ahead of print 2010. DOI: 10.1016/j.bbi.2010.07.241.
346. Farjam M, Zarandi FB addini B, Farjadian S, et al. Inhibition of NR2B-containing N-methyl-D-aspartate receptors (NMDARs) in experimental autoimmune encephalomyelitis, a model of multiple sclerosis. *Iran J Pharm Res*. Epub ahead of print 2014. DOI: 10.22037/ijpr.2014.1505.
347. Grasselli G, Rossi S, Musella A, et al. Abnormal NMDA receptor function exacerbates experimental autoimmune encephalomyelitis. *Br J Pharmacol*. Epub ahead of print 2013. DOI: 10.1111/j.1476-5381.2012.02178.x.
348. Martinez B, Peplow P V. Protective effects of pharmacological therapies in animal models of multiple sclerosis: A review of studies 2014-2019. *Neural Regeneration Research*. Epub ahead of print 2020. DOI: 10.4103/1673-5374.272572.
349. Manahan-Vaughan D, Von Haebler D, Winter C, et al. A single application of MK801 causes symptoms of acute psychosis, deficits in spatial memory, and impairment of synaptic plasticity in rats. *Hippocampus*. Epub ahead of print 2008. DOI: 10.1002/hipo.20367.
350. Monastero R, Camarda C, Pipia C, et al. Visual hallucinations and agitation in Alzheimer's disease due to memantine: Report of three cases [3]. *Journal of Neurology, Neurosurgery and Psychiatry*. Epub ahead of print 2007. DOI: 10.1136/jnnp.2006.096420.
351. Xue JG, Masuoka T, Gong X Di, et al. NMDA receptor activation enhances inhibitory GABAergic transmission onto hippocampal pyramidal neurons via presynaptic and postsynaptic mechanisms. *J Neurophysiol*. Epub ahead of print 2011. DOI: 10.1152/jn.00287.2010.
352. Newcomer JW, Farber NB, Olney JW. NMDA receptor function, memory, and

brain aging. *Dialogues Clin Neurosci*.
353. Thomas P, Smart TG. HEK293 cell line: A vehicle for the expression of recombinant proteins. *J Pharmacol Toxicol Methods*. Epub ahead of print 2005. DOI: 10.1016/j.vascn.2004.08.014.
354. Domingues A, Oliveira TC, Laço MLN, et al. Expression of NR1/NR2B N-methyl-D-aspartate receptors enhances heroin toxicity in HEK293 cells. In: *Annals of the New York Academy of Sciences*. 2006. Epub ahead of print 2006. DOI: 10.1196/annals.1369.046.
355. Eng LF, Ghirnikar RS. GFAP and Astrogliosis. In: *Brain Pathology*. 1994. Epub ahead of print 1994. DOI: 10.1111/j.1750-3639.1994.tb00838.x.
356. Brenner M. Role of GFAP in CNS injuries. *Neuroscience Letters*. Epub ahead of print 2014. DOI: 10.1016/j.neulet.2014.01.055.
357. Wang D, Ayers MM, Catmull D V., et al. Astrocyte-associated axonal damage in pre-onset stages of experimental autoimmune encephalomyelitis. *Glia*. Epub ahead of print 2005. DOI: 10.1002/glia.20199.
358. Smith ME, Somera FP, Eng LF. Immunocytochemical staining for glial fibrillary acidic protein and the metabolism of cytoskeletal proteins in experimental allergic encephalomyelitis. *Brain Res*. Epub ahead of print 1983. DOI: 10.1016/0006-8993(83)90822-3.
359. Hampton DW, Serio A, Pryce G, et al. Neurodegeneration progresses despite complete elimination of clinical relapses in a mouse model of multiple sclerosis. *Acta Neuropathol Commun*. Epub ahead of print 2014. DOI: 10.1186/2051-5960-1-84.
360. Costa O, Divoux D, Ischenko A, et al. Optimization of an animal model of experimental autoimmune encephalomyelitis achieved with a multiple MOG35-55 peptide in C57BL6/J strain of mice. *J Autoimmun*. Epub ahead of print 2003. DOI: 10.1016/S0896-8411(02)00108-7.
361. Toader LE, Rosu GC, Catalin B, et al. Clinical and Histopathological Assessment on an Animal Model with Experimental Autoimmune Encephalomyelitis. *Curr Heal Sci J*. Epub ahead of print 2018. DOI: 10.12865/CHSJ.44.03.12.
362. Cowan KJ, Storey KB. Mitogen-activated protein kinases: New signaling pathways functioning in cellular responses to environmental stress. *Journal of Experimental Biology*. Epub ahead of print 2003. DOI: 10.1242/jeb.00220.
363. Moodie SA, Wolfman A. The 3Rs of life: Ras, Raf and growth regulation. *Trends Genet*. Epub ahead of print 1994. DOI: 10.1016/0168-9525(94)90147-3.
364. David Sweatt J. The neuronal MAP kinase cascade: A biochemical signal integration system subserving synaptic plasticity and memory. *Journal of Neurochemistry*. Epub ahead of print 2001. DOI: 10.1046/j.1471-4159.2001.00054.x.
365. Bading H, Greenberg ME. Stimulation of protein tyrosine phosphorylation by NMDA receptor activation. *Science (80-)*. Epub ahead of print 1991. DOI: 10.1126/science.1715095.
366. Krapivinsky G, Krapivinsky L, Manasian Y, et al. The NMDA receptor is coupled to the ERK pathway by a direct interaction between NR2B and RasGRF1. *Neuron*. Epub ahead of print 2003. DOI: 10.1016/S0896-6273(03)00645-7.
367. Wang SL, Ribar TJ, Means AR. Expression of Ca2+/calmodulin-dependent protein kinase IV (CaMKIV) messenger RNA during murine embryogenesis. *Cell Growth Differ*.
368. Chin D, Means AR. Calmodulin: A prototypical calcium sensor. *Trends in Cell*

Biology. Epub ahead of print 2000. DOI: 10.1016/S0962-8924(00)01800-6.
369. Racioppi L, Means AR. Calcium/calmodulin-dependent kinase IV in immune and inflammatory responses: novel routes for an ancient traveller. *Trends in Immunology*. Epub ahead of print 2008. DOI: 10.1016/j.it.2008.08.005.
370. Koga T, Kawakami A. The role of CaMK4 in immune responses. *Modern Rheumatology*. Epub ahead of print 2018. DOI: 10.1080/14397595.2017.1413964.
371. Koga T, Hedrich CM, Mizui M, et al. CaMK4-dependent activation of AKT/mTOR and CREM-α underlies autoimmunity-associated Th17 imbalance. *J Clin Invest*. Epub ahead of print 2014. DOI: 10.1172/JCI73411.
372. Redmond L, Kashani AH, Ghosh A. Calcium regulation of dendritic growth via CaM kinase IV and CREB-mediated transcription. *Neuron*. Epub ahead of print 2002. DOI: 10.1016/S0896-6273(02)00737-7.
373. Kabbage M, Dickman MB. The BAG proteins: A ubiquitous family of chaperone regulators. *Cellular and Molecular Life Sciences*. Epub ahead of print 2008. DOI: 10.1007/s00018-008-7535-2.
374. Annunziata CM, Kleinberg L, Davidson B, et al. BAG-4/SODD and associated antiapoptotic proteins are linked to aggressiveness of epithelial ovarian cancer. *Clin Cancer Res*. Epub ahead of print 2007. DOI: 10.1158/1078-0432.CCR-07-0327.
375. Davidson B, Valborg Reinertsen K, Trinh D, et al. BAG-1/SODD, HSP70, and HSP90 are potential prognostic markers of poor survival in node-negative breast carcinoma. *Hum Pathol*. Epub ahead of print 2016. DOI: 10.1016/j.humpath.2016.02.023.
376. Ozawa F, Friess H, Zimmermann A, et al. Enhanced expression of silencer of death domains (SODD/BAG-4) in pancreatic cancer. *Biochem Biophys Res Commun*. Epub ahead of print 2000. DOI: 10.1006/bbrc.2000.2610.
377. Reuland SN, Smith SM, Bemis LT, et al. MicroRNA-26a is strongly downregulated in melanoma and induces cell death through repression of silencer of death domains (SODD). *J Invest Dermatol*. Epub ahead of print 2013. DOI: 10.1038/jid.2012.400.
378. Jiang Y, Woronicz JD, Liu W, et al. Prevention of constitutive TNF receptor 1 signaling by silencer of death domains. *Science (80-)*. Epub ahead of print 1999. DOI: 10.1126/science.283.5401.543.
379. Tschopp J, Martinon F, Hofmann K. Apoptosis: Silencing the death receptors. *Current Biology*. Epub ahead of print 1999. DOI: 10.1016/S0960-9822(99)80233-4.
380. Kassiotis G, Kollias G. Uncoupling the proinflammatory from the immunosuppressive properties of tumor necrosis factor (TNF) at the p55 TNF receptor level: Implications for pathogenesis and therapy of autoimmune demyelination. *J Exp Med*. Epub ahead of print 2001. DOI: 10.1084/jem.193.4.427.
381. Steeland S, Van Ryckeghem S, Van Imschoot G, et al. TNFR1 inhibition with a Nanobody protects against EAE development in mice. *Sci Rep*. Epub ahead of print 2017. DOI: 10.1038/s41598-017-13984-y.
382. Probert L. TNF and its receptors in the CNS: The essential, the desirable and the deleterious effects. *Neuroscience*. Epub ahead of print 2015. DOI: 10.1016/j.neuroscience.2015.06.038.
383. Hynes RO. Integrins: Bidirectional, allosteric signaling machines. *Cell*. Epub ahead of print 2002. DOI: 10.1016/S0092-8674(02)00971-6.

384. Erik H. J Danen. *Integrins: An Overview of Structural and Functional Aspects*. 2003. Epub ahead of print 2003. DOI: 10.1128/MCB.01172-14.
385. Wu J, Wu H, An J, et al. Critical role of integrin CD11c in splenic dendritic cell capture of missing-self CD47 cells to induce adaptive immunity. *Proc Natl Acad Sci U S A*. Epub ahead of print 2018. DOI: 10.1073/pnas.1805542115.
386. Wang L, Li Z, Ciric B, et al. Selective depletion of CD11c+CD11b+ dendritic cells partially abrogates tolerogenic effects of intravenous MOG in murine EAE. *Eur J Immunol*. Epub ahead of print 2016. DOI: 10.1002/eji.201546274.
387. Li H, Zhang G-X, Chen Y, et al. CD11c + CD11b + Dendritic Cells Play an Important Role in Intravenous Tolerance and the Suppression of Experimental Autoimmune Encephalomyelitis . *J Immunol*. Epub ahead of print 2008. DOI: 10.4049/jimmunol.181.4.2483.
388. Wlodarczyk A, Løbner M, Cédile O, et al. Comparison of microglia and infiltrating CD11c+ cells as antigen presenting cells for T cell proliferation and cytokine response. *J Neuroinflammation*. Epub ahead of print 2014. DOI: 10.1186/1742-2094-11-57.
389. Wlodarczyk A, Cédile O, Jensen KN, et al. Pathologic and protective roles for microglial subsets and bone marrow- and blood-derived myeloid cells in central nervous system inflammation. *Front Immunol*. Epub ahead of print 2015. DOI: 10.3389/fimmu.2015.00463.
390. Kim SK, Schluns KS, Lefrançois L. Induction and visualization of mucosal memory CD8 T cells following systemic virus infection. *J Immunol*.
391. Lin Y, Roberts TJ, Sriram V, et al. Myeloid marker expression on antiviral CD8+ T cells following an acute virus infection. *Eur J Immunol*. Epub ahead of print 2003. DOI: 10.1002/eji.200324087.
392. Ward C, Whitford H, Snell G, et al. Bronchoalveolar lavage macrophage and lymphocyte phenotypes in lung transplant recipients. *J Hear Lung Transplant*. Epub ahead of print 2001. DOI: 10.1016/S1053-2498(01)00319-9.
393. Beyer M, Wang H, Peters N, et al. The beta2 integrin CD11c distinguishes a subset of cytotoxic pulmonary T cells with potent antiviral effects in vitro and in vivo. *Respir Res*. Epub ahead of print 2005. DOI: 10.1186/1465-9921-6-70.
394. Seo SK, Choi JH, Kim YH, et al. 4-1BB-mediated immunotherapy of rheumatoid arthritis. *Nat Med*. Epub ahead of print 2004. DOI: 10.1038/nm1107.
395. Vinay DS, Kim CH, Choi BK, et al. Origins and functional basis of regulatory CD11c+CD8+ T cells. *Eur J Immunol*. Epub ahead of print 2009. DOI: 10.1002/eji.200839057.
396. Vinay DS, Kwon BS. CD11c+CD8+ T cells: Two-faced adaptive immune regulators. *Cell Immunol* 2010; 264: 18–22.
397. Nakajima H, Cella M, Langen H, et al. Activating interactions in human NK cell recognition: The role of 2B4-CD48. *Eur J Immunol*. Epub ahead of print 1999. DOI: 10.1002/(SICI)1521-4141(199905)29:05<1676::AID-IMMU1676>3.0.CO;2-Y.
398. Valiante NM, Trinchieri G. Identification of a novel signal transduction surface molecule on human cytotoxic lymphocytes. *J Exp Med*. Epub ahead of print 1993. DOI: 10.1084/jem.178.4.1397.
399. Georgoudaki AM, Khodabandeh S, Puiac S, et al. CD244 is expressed on dendritic cells and regulates their functions. *Immunol Cell Biol*. Epub ahead of print 2015. DOI: 10.1038/icb.2014.124.
400. Boles KS, Nakajima H, Colonna M, et al. Molecular characterization of a novel human natural killer cell receptor homologous to mouse 2B4. *Tissue Antigens*.

Epub ahead of print 1999. DOI: 10.1034/j.1399-0039.1999.540103.x.
401. Eissmann P, Beauchamp L, Wooters J, et al. Molecular basis for positive and negative signaling by the natural killer cell receptor 2B4 (CD244). *Blood*. Epub ahead of print 2005. DOI: 10.1182/blood-2004-09-3796.
402. Chlewicki LK, Velikovsky CA, Balakrishnan V, et al. Molecular Basis of the Dual Functions of 2B4 (CD244). *J Immunol*. Epub ahead of print 2008. DOI: 10.4049/jimmunol.180.12.8159.
403. McNerney ME, Lee KM, Kumar V. 2B4 (CD244) is a non-MHC binding receptor with multiple functions on natural killer cells and CD8+ T cells. *Molecular Immunology*. Epub ahead of print 2005. DOI: 10.1016/j.molimm.2004.07.032.
404. Blackburn SD, Shin H, Haining WN, et al. Coregulation of CD8+ T cell exhaustion by multiple inhibitory receptors during chronic viral infection. *Nat Immunol*. Epub ahead of print 2009. DOI: 10.1038/ni.1679.
405. McArdel SL, Brown DR, Sobel RA, et al. Anti-CD48 Monoclonal Antibody Attenuates Experimental Autoimmune Encephalomyelitis by Limiting the Number of Pathogenic CD4 + T Cells . *J Immunol*. Epub ahead of print 2016. DOI: 10.4049/jimmunol.1600706.
406. Katoh H, Negishi M. RhoG activates Rac1 by direct interaction with the Dock180-binding protein Elmo. *Nature*. Epub ahead of print 2003. DOI: 10.1038/nature01817.
407. Barrett A, Pellet-Many C, Zachary IC, et al. P130Cas: A key signalling node in health and disease. *Cellular Signalling*. Epub ahead of print 2013. DOI: 10.1016/j.cellsig.2012.12.019.
408. Lopez-Ramirez MA, Wu D, Pryce G, et al. MicroRNA-155 negatively affects blood-brain barrier function during neuroinflammation. *FASEB J*. Epub ahead of print 2014. DOI: 10.1096/fj.13-248880.
409. Pillai S, Netravali IA, Cariappa A, et al. Siglecs and immune regulation. *Annual Review of Immunology*. Epub ahead of print 2012. DOI: 10.1146/annurev-immunol-020711-075018.
410. MacAuley MS, Crocker PR, Paulson JC. Siglec-mediated regulation of immune cell function in disease. *Nature Reviews Immunology*. Epub ahead of print 2014. DOI: 10.1038/nri3737.
411. Tateno H, Crocker PR, Paulson JC. Mouse Siglec-F and human Siglec-8 are functionally convergent paralogs that are selectively expressed on eosinophils and recognize 6′-sulfo-sialyl Lewis X as a preferred glycan ligand. *Glycobiology*. Epub ahead of print 2005. DOI: 10.1093/glycob/cwi097.
412. Zhang M, Angata T, Jae YC, et al. Defining the in vivo function of Siglec-F, a CD33-related Siglec expressed on mouse eosinophils. *Blood*. Epub ahead of print 2007. DOI: 10.1182/blood-2006-08-039255.
413. Adamko D, Odemuyiwa SO, Moqbel R. The eosinophil as a therapeutic target in asthma: Beginning of the end, or end of the beginning? *Current Opinion in Pharmacology*. Epub ahead of print 2003. DOI: 10.1016/S1471-4892(03)00040-7.
414. Zhang H, Verkman AS. Eosinophil pathogenicity mechanisms and therapeutics in neuromyelitis optica. *J Clin Invest*. Epub ahead of print 2013. DOI: 10.1172/JCI67554.
415. Fujihara K. Neuromyelitis optica spectrum disorders: Still evolving and broadening. *Current Opinion in Neurology*. Epub ahead of print 2019. DOI: 10.1097/WCO.0000000000000694.
416. Wingerchuk DM, Banwell B, Bennett JL, et al. International consensus

diagnostic criteria for neuromyelitis optica spectrum disorders. *Neurology*. Epub ahead of print 2015. DOI: 10.1212/WNL.0000000000001729.
417. Kim GH, Kim JE, Rhie SJ, et al. The Role of Oxidative Stress in Neurodegenerative Diseases. *Experimental Neurobiology*. Epub ahead of print 2015. DOI: 10.5607/en.2015.24.4.325.
418. Gandhi S, Abramov AY. Mechanism of oxidative stress in neurodegeneration. *Oxidative Medicine and Cellular Longevity*. Epub ahead of print 2012. DOI: 10.1155/2012/428010.
419. Qian C, Liu X, Xu Q, et al. Recent progress on the versatility of virus-like particles. *Vaccines*. Epub ahead of print 2020. DOI: 10.3390/vaccines8010139.
420. Manglani M, Rua R, Hendricksen A, et al. Method to quantify cytokines and chemokines in mouse brain tissue using Bio-Plex multiplex immunoassays. *Methods*. Epub ahead of print 2019. DOI: 10.1016/j.ymeth.2019.02.007.

8 Appendix

Table 8.1 Nanostring Mouse Neuroinflammation panel

Gene	Probe_ID
Abcc3-mRNA	NM_029600.3:2730
Abcc8-mRNA	NM_011510.3:1740
Abl1-mRNA	NM_009594.4:1378
Adamts16-mRNA	NM_172053.2:1918
Agt-mRNA	NM_007428.3:881
Al464131-mRNA	NM_001085515.2:1232
Ak1-mRNA	NM_001198790.1:1625
Akt1-mRNA	NM_001165894.1:898
Akt2-mRNA	NM_001110208.1:2504
Aldh1l1-mRNA	NM_027406.1:1340
Ambra1-mRNA	NM_001080754.1:944
Amigo2-mRNA	NM_178114.4:2425
Anapc15-mRNA	NM_027532.3:350
Anxa1-mRNA	NM_010730.2:400
Apc-mRNA	NM_007462.3:645
Apex1-mRNA	NM_009687.2:289
Apoe-mRNA	NM_001305844.1:903
Arc-mRNA	NM_018790.2:2715
Arhgap24-mRNA	NM_029270.2:1164
Arid1a-mRNA	NM_001080819.1:5193
Asb2-mRNA	NM_023049.1:996
Ash2l-mRNA	NM_001080793.1:2125
Asph-mRNA	NM_001177849.1:400
Atf3-mRNA	NM_007498.3:387
Atg14-mRNA	NM_172599.4:204
Atg3-mRNA	NM_026402.3:862
Atg5-mRNA	NM_001314013.1:262
Atg7-mRNA	NM_028835.1:855
Atg9a-mRNA	NM_001003917.3:340
Atm-mRNA	NM_007499.2:5543
Atp6v0e-mRNA	NM_025272.2:585
Atp6v1a-mRNA	NM_007508.5:434
Atr-mRNA	NM_019864.1:4392
Axl-mRNA	NM_009465.3:3820
B3gnt5-mRNA	NM_001159407.1:1738
Bad-mRNA	NM_007522.3:1146
Bag3-mRNA	NM_013863.4:1000
Bag4-mRNA	NM_026121.3:3735
Bak1-mRNA	NM_007523.2:470
Bard1-mRNA	NM_007525.3:306
Bax-mRNA	NM_007527.3:735
Bbc3-mRNA	NM_133234.1:1461
Bcas1-mRNA	NM_029815.2:932
Bcl10-mRNA	NM_009740.1:1168
Bcl2-mRNA	NM_009741.3:1844
Bcl2a1a-mRNA	NM_009742.3:175
Bcl2l1-mRNA	NM_009743.4:200
Bcl2l11-mRNA	NM_001284410.1:236
Bcl2l2-mRNA	NM_007537.1:1592
Bdnf-mRNA	NM_007540.4:3260
Becn1-mRNA	NM_019584.3:1145
Bid-mRNA	NM_007544.3:1307
Bin1-mRNA	NM_001083334.1:1400
Birc2-mRNA	NM_007465.2:1230
Birc3-mRNA	NM_007464.3:425
Birc5-mRNA	NM_009689.2:237
Blm-mRNA	NM_001042527.2:264
Blnk-mRNA	NM_008528.4:1546
Bmi1-mRNA	NM_007552.4:3354
Bnip3-mRNA	NM_009760.4:1108
Bnip3l-mRNA	NM_009761.3:1738
Bok-mRNA	NM_016778.2:635
Bola2-mRNA	NM_175103.3:94
Braf-mRNA	NM_139294.5:1102

Brca1-mRNA	NM_009764.3:2027
Brd2-mRNA	NM_010238.3:2800
Brd3-mRNA	NM_001113573.1:2690
Brd4-mRNA	NM_001286630.1:1492
Btk-mRNA	NM_013482.2:2255
C1qa-mRNA	NM_007572.2:566
C1qb-mRNA	NM_009777.2:865
C1qc-mRNA	NM_007574.2:708
C3-mRNA	XM_011246258.1:2702
C3ar1-mRNA	NM_009779.2:555
C4a-mRNA	NM_011413.2:56
C5ar1-mRNA	NM_007577.3:595
Cables1-mRNA	NM_001146287.1:3120
Calr-mRNA	NM_007591.3:551
Camk4-mRNA	NM_009793.3:3280
Casp1-mRNA	NM_009807.2:259
Casp2-mRNA	NM_007610.1:420
Casp3-mRNA	NM_009810.2:630
Casp4-mRNA	NM_007609.2:408
Casp6-mRNA	NM_009811.3:360
Casp7-mRNA	NM_007611.2:1468
Casp8-mRNA	NM_009812.2:1463
Casp9-mRNA	NM_015733.4:1675
Ccl2-mRNA	NM_011333.3:415
Ccl3-mRNA	NM_011337.1:60
Ccl4-mRNA	NM_013652.1:140
Ccl5-mRNA	NM_013653.1:165
Ccl7-mRNA	NM_013654.3:141
Ccng2-mRNA	NM_007635.4:1536
Ccni-mRNA	NM_017367.3:1180
Ccr2-mRNA	NM_009915.2:2965
Ccr5-mRNA	NM_009917.5:1340
Cd109-mRNA	NM_153098.3:2720
Cd14-mRNA	NM_009841.3:235
Cd244-mRNA	NM_018729.2:262
Cd24a-mRNA	NM_009846.2:584
Cd300lf-mRNA	NM_001169153.1:665
Cd33-mRNA	NM_001111058.1:598
Cd36-mRNA	NM_007643.3:1520
Cd3d-mRNA	NM_013487.2:289
Cd3e-mRNA	NM_007648.4:380
Cd3g-mRNA	NM_009850.2:430
Cd40-mRNA	NM_011611.2:1425
Cd47-mRNA	NM_010581.3:165
Cd6-mRNA	NM_001037801.2:1315
Cd68-mRNA	NM_009853.1:636
Cd69-mRNA	NM_001033122.3:1370
Cd72-mRNA	NM_001110320.1:987
Cd74-mRNA	NM_001042605.1:391
Cd83-mRNA	NM_009856.2:1624
Cd84-mRNA	NM_013489.2:915
Cd86-mRNA	NM_019388.3:251
Cd8a-mRNA	NM_001081110.2:355
Cd8b1-mRNA	NM_009858.2:1075
Cdc25a-mRNA	NM_007658.3:855
Cdc7-mRNA	NM_001271566.1:2804
Cdk20-mRNA	NM_053180.2:352
Cdkn1a-mRNA	NM_007669.4:1670
Cdkn1c-mRNA	NM_009876.3:1240
Cflar-mRNA	NM_207653.3:990
Ch25h-mRNA	NM_009890.1:487
Chek2-mRNA	NM_016681.3:790
Chn2-mRNA	NM_001163640.1:1510
Chst8-mRNA	NM_175140.4:1196
Chuk-mRNA	NM_001162410.1:222
Cidea-mRNA	NM_007702.2:514
Cideb-mRNA	NM_009894.3:179
Cks1b-mRNA	NM_016904.1:185
Clec7a-mRNA	NM_020008.2:1008
Clic4-mRNA	NM_013885.2:3280
Cldn5-mRNA	NM_013805.4:975

Cln3-mRNA	NM_001146311.1:378
Clstn1-mRNA	NM_023051.4:2352
Cnn2-mRNA	NM_007725.2:350
Cnp-mRNA	NM_009923.2:166
Cntnap2-mRNA	NM_001004357.2:3985
Coa5-mRNA	NM_198006.4:1808
Col6a3-mRNA	XM_897036.2:4583
Cotl1-mRNA	NM_028071.3:325
Cox5b-mRNA	NM_009942.2:332
Cp-mRNA	NM_001042611.1:1750
Creb1-mRNA	NM_001037726.1:2734
Crebbp-mRNA	NM_001025432.1:3770
Crem-mRNA	NM_001110853.1:1840
Crip1-mRNA	NM_007763.3:47
Cryba4-mRNA	NM_021351.1:440
Csf1-mRNA	NM_001113530.1:833
Csf1r-mRNA	NM_001037859.1:3655
Csf2rb-mRNA	NM_007780.4:4185
Csf3r-mRNA	NM_001252651.1:1294
Csk-mRNA	NM_007783.2:268
Cst7-mRNA	NM_009977.3:690
Ctsf-mRNA	NM_019861.1:625
Ctss-mRNA	NM_021281.2:740
Ctsw-mRNA	NM_009985.4:190
Cx3cl1-mRNA	NM_009142.3:125
Cx3cr1-mRNA	NM_009987.3:2696
Cxcl10-mRNA	NM_021274.1:115
Cxcl9-mRNA	NM_008599.2:40
Cycs-mRNA	NM_007808.4:2510
Cyp27a1-mRNA	NM_024264.3:1725
Cyp7b1-mRNA	NM_007825.4:1030
Cytip-mRNA	NM_139200.4:1080
Dab2-mRNA	NM_023118.2:415
Dapk1-mRNA	NM_134062.1:4935
Ddb2-mRNA	NM_028119.5:94
Ddx58-mRNA	NM_172689.3:1751
Dicer1-mRNA	NM_148948.2:5270
Dlg1-mRNA	NM_001252433.1:1064
Dlg4-mRNA	NM_001109752.1:1866
Dna2-mRNA	NM_177372.3:1734
Dnmt1-mRNA	NM_010066.3:2380
Dnmt3a-mRNA	NM_007872.4:7160
Dock1-mRNA	NM_001033420.2:405
Dock2-mRNA	NM_033374.3:2410
Dot1l-mRNA	NM_199322.1:5490
Dst-mRNA	NM_010081.2:226
Dusp7-mRNA	NM_153459.4:2094
E2f1-mRNA	NM_007891.4:926
Eed-mRNA	NM_021876.3:1000
Eef2k-mRNA	NM_007908.3:1166
Egfr-mRNA	NM_207655.2:1335
Egr1-mRNA	NM_007913.5:515
Ehmt2-mRNA	NM_145830.1:3475
Eif1-mRNA	NM_011508.1:664
Emcn-mRNA	**NM_001163522.1:230**
Emp1-mRNA	NM_010128.4:1080
Enpp6-mRNA	NM_177304.3:922
Entpd2-mRNA	NM_009849.2:1016
Ep300-mRNA	NM_177821.6:4305
Epg5-mRNA	NM_001195633.1:2436
Erbb3-mRNA	NM_010153.1:1290
Ercc2-mRNA	NM_007949.4:1800
Esam-mRNA	NM_027102.3:495
Ets2-mRNA	NM_011809.2:3284
Ezh1-mRNA	NM_007970.1:3950
Ezh2-mRNA	NM_007971.2:425
F3-mRNA	NM_010171.3:1170
Fa2h-mRNA	NM_178086.3:644
Fabp5-mRNA	NM_010634.3:430
Fadd-mRNA	NM_010175.5:2641
Fancc-mRNA	NM_007985.2:1115

Fancg-mRNA	NM_053081.2:250
Fas-mRNA	NM_007987.2:95
Fasl-mRNA	NM_010177.3:645
Fbln5-mRNA	NM_011812.4:2138
Fcer1g-mRNA	NM_010185.4:264
Fcgr1-mRNA	NM_010186.5:185
Fcgr2b-mRNA	NM_001077189.1:1225
Fcgr3-mRNA	NM_010188.5:1175
Fcrls-mRNA	NM_030707.3:925
Fen1-mRNA	NM_001271614.1:1880
Fgd2-mRNA	NM_001159538.1:882
Fgf13-mRNA	NM_010200.2:700
Fgl2-mRNA	NM_008013.2:3470
Fkbp5-mRNA	NM_010220.3:2125
Flt1-mRNA	NM_010228.3:1550
Fos-mRNA	NM_010234.2:1330
Foxp3-mRNA	NM_054039.2:194
Fpr1-mRNA	NM_013521.2:750
Fscn1-mRNA	NM_007984.2:1645
Fyn-mRNA	NM_008054.2:1030
Gadd45a-mRNA	NM_007836.1:654
Gadd45g-mRNA	NM_011817.2:208
Gal3st1-mRNA	NM_001177691.1:1197
Gba-mRNA	NM_001077411.1:820
Gbp2-mRNA	NM_010260.1:1996
Gclc-mRNA	NM_010295.2:1102
Gdpd2-mRNA	NM_023608.3:1438
Gja1-mRNA	NM_010288.3:1450
Gjb1-mRNA	NM_008124.2:113
Gna15-mRNA	NM_010304.3:323
Gpr183-mRNA	NM_183031.2:238
Gpr34-mRNA	NM_011823.4:256
Gpr62-mRNA	NM_001159652.1:1576
Gpr84-mRNA	NM_030720.1:315
Grap-mRNA	NM_027817.3:121
Gria1-mRNA	NM_001252403.1:2476
Gria2-mRNA	NM_001039195.1:300
Gria4-mRNA	NM_001113180.1:1274
Grin2a-mRNA	NM_008170.2:1788
Grin2b-mRNA	NM_008171.3:6340
Grm2-mRNA	NM_001160353.1:2770
Grm3-mRNA	NM_181850.2:2525
Grn-mRNA	NM_008175.3:2010
Gsn-mRNA	NM_146120.3:624
Gstm1-mRNA	NM_010358.5:50
Gzma-mRNA	NM_010370.2:188
Gzmb-mRNA	NM_013542.2:1020
H2-T23-mRNA	NM_010398.3:365
H2afx-mRNA	NM_010436.2:980
Hat1-mRNA	NM_026115.4:1270
Hcar2-mRNA	NM_030701.1:770
Hdac1-mRNA	NM_008228.2:470
Hdac2-mRNA	NM_008229.2:1010
Hdac4-mRNA	NM_207225.1:2800
Hdac6-mRNA	NM_010413.3:564
Hdc-mRNA	NM_008230.4:745
Hells-mRNA	NM_008234.3:1082
Hif1a-mRNA	NM_010431.2:1294
Hilpda-mRNA	NM_023516.5:236
Hira-mRNA	NM_010435.2:3210
Hmgb1-mRNA	NM_010439.3:1574
Hmox1-mRNA	NM_010442.2:610
Homer1-mRNA	NM_147176.2:1165
Hpgds-mRNA	NM_019455.4:425
Hprt-mRNA	NM_013556.2:30
Hps4-mRNA	NM_138646.3:1265
Hrk-mRNA	NM_007545.2:3458
Hsd11b1-mRNA	NM_008288.2:110
Hspb1-mRNA	NM_013560.2:630
Hus1-mRNA	NM_008316.2:2505
Icam2-mRNA	NM_010494.1:375

Ifi30-mRNA	NM_023065.3:806
Ifih1-mRNA	NM_027835.2:1997
Ifitm2-mRNA	NM_030694.1:87
Ifitm3-mRNA	NM_025378.2:370
Ifnar1-mRNA	NM_010508.1:1195
Ifnar2-mRNA	NM_001110498.1:725
Igf1r-mRNA	NM_010513.2:3390
Igf2r-mRNA	NM_010515.1:2585
Igsf10-mRNA	NM_001162884.1:3100
Igsf6-mRNA	NM_030691.1:115
Ikbkb-mRNA	NM_010546.2:498
Ikbke-mRNA	NM_019777.3:618
Ikbkg-mRNA	NM_178590.2:525
Il10rb-mRNA	NM_008349.5:465
Il15ra-mRNA	NM_008358.2:800
Il1a-mRNA	NM_010554.4:512
Il1b-mRNA	NM_008361.3:1120
Il1r1-mRNA	NM_001123382.1:820
Il1r2-mRNA	NM_010555.4:458
Il1rap-mRNA	NM_134103.2:945
Il1rl2-mRNA	NM_133193.3:860
Il1rn-mRNA	NM_031167.5:224
Il21r-mRNA	NM_021887.1:619
Il2rg-mRNA	NM_013563.3:566
Il3ra-mRNA	NM_008369.1:567
Il6ra-mRNA	NM_010559.2:2825
Inpp5d-mRNA	NM_001110192.1:2186
Iqsec1-mRNA	NM_001134383.1:1792
Irak1-mRNA	NM_008363.2:951
Irak2-mRNA	NM_001113553.1:485
Irak3-mRNA	NM_028679.3:2608
Irak4-mRNA	NM_029926.5:250
Irf1-mRNA	NM_008390.1:365
Irf2-mRNA	NM_008391.2:440
Irf3-mRNA	NM_016849.4:526
Irf4-mRNA	NM_013674.1:1878
Irf7-mRNA	NM_016850.2:705
Irf8-mRNA	NM_008320.3:2274
Itga6-mRNA	NM_008397.3:910
Itga7-mRNA	NM_008398.2:2435
Itgam-mRNA	NM_001082960.1:3025
Itgav-mRNA	NM_008402.2:3145
Itgax-mRNA	NM_021334.2:327
Itgb5-mRNA	NM_001145884.1:1270
Jag1-mRNA	NM_013822.2:2155
Jam2-mRNA	NM_023844.4:1090
Jarid2-mRNA	NM_021878.2:2160
Jun-mRNA	NM_010591.2:2212
Kat2a-mRNA	NM_020004.5:1700
Kat2b-mRNA	NM_020005.3:3030
Kcnd1-mRNA	NM_008423.1:1400
Kcnj10-mRNA	NM_001039484.1:400
Kcnk13-mRNA	NM_146037.1:1430
Kdm1a-mRNA	NM_133872.1:1263
Kdm1b-mRNA	NM_172262.3:2034
Kdm2a-mRNA	NM_001001984.2:4160
Kdm2b-mRNA	NM_001003953.1:3984
Kdm3a-mRNA	NM_001038695.2:4110
Kdm4a-mRNA	NM_172382.2:1675
Kdm4b-mRNA	NM_172132.1:3704
Kdm4c-mRNA	NM_144787.1:2859
Kdm4d-mRNA	NM_173433.2:2255
Kdm5a-mRNA	XR_377436.1:2314
Kdm5b-mRNA	NM_152895.2:3620
Kdm5c-mRNA	NM_013668.3:750
Kdm6a-mRNA	NM_009483.1:2560
Kif2c-mRNA	NM_134471.3:915
Kit-mRNA	NM_001122733.1:4275
Klrd1-mRNA	NM_010654.2:434
Klrk1-mRNA	NM_001083322.1:144
Kmt2a-mRNA	NM_001081049.1:2080

Kmt2c-mRNA	NM_001081383.1:7075
Lacc1-mRNA	NM_172488.2:1025
Lag3-mRNA	NM_008479.1:1700
Lair1-mRNA	NM_001113474.1:1865
Lamp1-mRNA	NM_010684.2:2080
Lamp2-mRNA	NM_001017959.1:908
Lcn2-mRNA	NM_008491.1:190
Ldha-mRNA	NM_010699.2:1354
Ldlrad3-mRNA	NM_178886.2:1570
Lfng-mRNA	NM_008494.3:1965
Lgmn-mRNA	NM_011175.3:370
Lig1-mRNA	NM_001083188.1:1456
Lilrb4a-mRNA	NM_013532.3:348
Lingo1-mRNA	NM_181074.4:1087
Lmna-mRNA	NM_001002011.2:1611
Lmnb1-mRNA	NM_010721.2:805
Lrrc25-mRNA	NM_153074.3:246
Lrrc3-mRNA	NM_145152.4:1830
Lsr-mRNA	NM_001164184.1:445
Lst1-mRNA	NM_010734.2:104
Lta-mRNA	NM_010735.2:776
Ltb-mRNA	NM_008518.2:163
Ltbr-mRNA	NM_010736.3:1962
Ly6a-mRNA	NM_010738.2:206
Ly9-mRNA	NM_008534.2:1190
Lyn-mRNA	NM_010747.1:1725
Mafb-mRNA	NM_010658.2:2658
Maff-mRNA	NM_010755.3:743
Mag-mRNA	NM_010758.2:1670
Mal-mRNA	NM_001171187.1:685
Man2b1-mRNA	NM_010764.2:1658
Map1lc3a-mRNA	NM_025735.1:685
Map2k1-mRNA	NM_008927.3:1695
Map2k4-mRNA	NM_009157.4:1335
Map3k1-mRNA	NM_011945.2:1640
Map3k14-mRNA	NM_016896.3:3930
Mapk10-mRNA	NM_001081567.1:1496
Mapk12-mRNA	NM_013871.3:1586
Mapk14-mRNA	NM_011951.2:1420
Mapt-mRNA	NM_001038609.2:1202
Mavs-mRNA	NM_144888.2:1162
Mb21d1-mRNA	NM_173386.4:1068
Mbd2-mRNA	NM_010773.2:655
Mbd3-mRNA	NM_013595.2:420
Mcm2-mRNA	NM_008564.2:2585
Mcm5-mRNA	NM_008566.2:2244
Mcm6-mRNA	NM_008567.1:1118
Mdc1-mRNA	NM_001010833.2:5900
Mdm2-mRNA	NM_010786.4:1664
Mef2c-mRNA	NM_001170537.1:4341
Mertk-mRNA	NM_008587.1:1320
Mfge8-mRNA	NM_008594.2:1357
Mgmt-mRNA	NM_008598.2:350
Mmp12-mRNA	NM_008605.3:592
Mmp14-mRNA	NM_008608.3:554
Mobp-mRNA	NM_001039364.2:152
Mog-mRNA	NM_010814.2:750
Mpeg1-mRNA	NM_010821.1:4135
Mpg-mRNA	NM_010822.3:276
Mr1-mRNA	NM_008209.4:1360
Mre11a-mRNA	NM_018736.2:2376
Ms4a4a-mRNA	XM_003086124.1:252
Msh2-mRNA	NM_008628.2:1870
Msn-mRNA	NM_010833.2:515
Msr1-mRNA	NM_001113326.1:555
Mvp-mRNA	NM_080638.2:1845
Myc-mRNA	NM_010849.4:630
Myct1-mRNA	NM_026793.2:180
Myd88-mRNA	NM_010851.2:1595
Myrf-mRNA	NM_001033481.1:4465
Nbn-mRNA	NM_013752.3:1000

Ncaph-mRNA	NM_144818.3:1540
Ncf1-mRNA	NM_001286037.1:970
Ncor1-mRNA	NM_011308.2:211
Ncor2-mRNA	NM_011424.2:1156
Nefl-mRNA	NM_010910.1:1303
Nfe2l2-mRNA	NR_132727.1:144
Nfkb1-mRNA	NM_008689.2:2125
Nfkb2-mRNA	NM_019408.2:1150
Nfkbia-mRNA	NM_010907.2:646
Nfkbie-mRNA	NM_008690.3:630
Ninj2-mRNA	NM_016718.2:244
Nkg7-mRNA	NM_024253.4:530
Nlgn1-mRNA	NM_138666.3:1028
Nlgn2-mRNA	NM_198862.2:1204
Nlrp3-mRNA	NM_145827.3:508
Nod1-mRNA	NM_172729.2:1446
Nostrin-mRNA	NM_181547.3:1452
Npl-mRNA	NM_028749.1:600
Npnt-mRNA	NM_001029836.1:2650
Nptx1-mRNA	NM_008730.2:4748
Nqo1-mRNA	NM_008706.5:430
Nrgn-mRNA	NM_022029.2:192
Nrm-mRNA	NM_134122.2:466
Nrp2-mRNA	NM_001077403.1:610
Nthl1-mRNA	NM_008743.2:34
Nwd1-mRNA	NM_176940.5:3564
Oas1g-mRNA	NM_011852.2:457
Ogg1-mRNA	NM_010957.4:168
Olfml3-mRNA	NM_133859.2:1035
Opalin-mRNA	NM_153520.1:201
Optn-mRNA	NM_181848.4:1018
Osmr-mRNA	NM_011019.3:395
P2rx7-mRNA	NM_001038839.2:378
P2ry12-mRNA	NM_027571.3:439
Pacsin1-mRNA	NM_011861.3:2936
Padi2-mRNA	NM_008812.2:1016
Pak1-mRNA	NM_011035.2:1615
Parp1-mRNA	NM_007415.2:3020
Parp2-mRNA	NM_009632.2:1325
Pcna-mRNA	NM_011045.2:590
Pdpn-mRNA	NM_010329.2:1625
Pecam1-mRNA	NM_008816.2:1100
Pex14-mRNA	NM_019781.2:597
Pik3ca-mRNA	NM_008839.1:1255
Pik3cb-mRNA	NM_029094.3:1970
Pik3cd-mRNA	XM_003945690.1:4648
Pik3cg-mRNA	NM_020272.2:2890
Pik3r1-mRNA	NM_001024955.1:5664
Pik3r2-mRNA	NM_008841.2:230
Pik3r5-mRNA	NM_177320.2:3342
Pilra-mRNA	NM_153510.3:1050
Pilrb1-mRNA	NM_133209.2:704
Pink1-mRNA	NM_026880.2:688
Pla2g4a-mRNA	NM_008869.2:1525
Pla2g5-mRNA	NM_001122954.1:1540
Plcg2-mRNA	NM_172285.1:978
Pld1-mRNA	NM_001164056.1:520
Pld2-mRNA	NM_008876.2:1134
Plekhb1-mRNA	NM_001163184.1:1616
Plekhm1-mRNA	NM_183034.1:3060
Pllp-mRNA	NM_026385.3:345
Plp1-mRNA	NM_011123.2:795
Plxdc2-mRNA	NM_026162.5:1580
Plxnb3-mRNA	NM_019587.2:2862
Pmp22-mRNA	NM_008885.2:395
Pms2-mRNA	NM_008886.2:265
Pnoc-mRNA	NM_001205075.1:332
Pole-mRNA	NM_011132.2:823
Ppfia4-mRNA	NM_001144855.1:454
Ppp3ca-mRNA	NM_008913.4:1675
Ppp3cb-mRNA	NM_008914.2:2950

Ppp3r1-mRNA	NM_024459.2:1390
Ppp3r2-mRNA	NM_001004025.4:1500
Prdx1-mRNA	NM_011034.4:1131
Prkaca-mRNA	NM_008854.3:699
Prkacb-mRNA	NM_011100.3:3754
Prkar1a-mRNA	NM_021880.2:2235
Prkar2a-mRNA	NM_008924.2:2135
Prkar2b-mRNA	NM_011158.3:918
Prkce-mRNA	NM_011104.2:1510
Prkcq-mRNA	NM_008859.2:1210
Prkdc-mRNA	NM_011159.2:3108
Pros1-mRNA	NM_011173.2:2720
Psen2-mRNA	NM_001128605.1:560
Psmb8-mRNA	NM_010724.2:362
Pten-mRNA	NM_008960.2:5160
Ptger4-mRNA	NM_008965.1:315
Ptgs2-mRNA	NM_011198.3:675
Ptms-mRNA	NM_026988.2:755
Ptpn6-mRNA	NM_013545.2:1691
Ptprc-mRNA	NM_011210.3:2320
Pttg1-mRNA	NM_001131054.1:288
Ptx3-mRNA	NM_008987.3:692
Pycard-mRNA	NM_023258.4:1654
Rab6b-mRNA	NM_173781.4:715
Rab7-mRNA	NM_009005.2:490
Rac1-mRNA	NM_009007.2:1045
Rac2-mRNA	NM_009008.3:2258
Rad1-mRNA	NM_011232.2:406
Rad17-mRNA	NM_001044371.1:386
Rad50-mRNA	NM_009012.2:4165
Rad51-mRNA	NM_011234.4:286
Rad51c-mRNA	NM_053269.3:402
Rad9a-mRNA	NM_011237.2:490
Rala-mRNA	NM_019491.5:605
Ralb-mRNA	NM_022327.5:1120
Rapgef3-mRNA	NM_001177810.1:564
Rb1cc1-mRNA	NM_009826.4:497
Rbfox3-mRNA	NM_001024931.2:2700
Rela-mRNA	NM_009045.4:645
Relb-mRNA	NM_009046.2:2013
Reln-mRNA	NM_011261.2:2545
Rgl1-mRNA	NM_016846.3:3320
Rhoa-mRNA	NM_016802.4:1885
Ripk1-mRNA	NM_009068.3:1246
Ripk2-mRNA	NM_138952.3:830
Rnf8-mRNA	NM_021419.2:1671
Rpa1-mRNA	NM_026653.2:930
Rpl28-mRNA	NM_009081.2:106
Rpl29-mRNA	NM_009082.2:110
Rpl36al-mRNA	NM_025589.4:74
Rpl9-mRNA	NM_011292.2:142
Rps10-mRNA	NM_025963.3:318
Rps2-mRNA	NM_008503.5:304
Rps21-mRNA	NM_025587.2:153
Rps3-mRNA	NM_012052.2:886
Rps9-mRNA	NM_029767.2:173
Rrm2-mRNA	NM_009104.1:265
Rsad2-mRNA	NM_021384.2:3185
Rtn4rl1-mRNA	NM_177708.4:2075
S100a10-mRNA	NM_009112.2:154
S100b-mRNA	NM_009115.3:1090
S1pr3-mRNA	NM_010101.3:2939
S1pr5-mRNA	NM_053190.2:840
Sall1-mRNA	NM_021390.3:4875
Sell-mRNA	XM_006496716.1:1035
Serpina3n-mRNA	NM_009252.2:119
Serpine1-mRNA	NM_008871.2:1822
Serpinf1-mRNA	NM_011340.3:745
Serping1-mRNA	NM_009776.3:1480
Sesn1-mRNA	NM_001013370.2:497
Sesn2-mRNA	NM_144907.1:1416

Setd1a-mRNA	NM_178029.3:1612
Setd1b-mRNA	NM_001040398.1:2880
Setd2-mRNA	NM_001081340.2:1345
Setd7-mRNA	NM_080793.5:3905
Setdb1-mRNA	NM_018877.2:1625
Shank3-mRNA	NM_021423.3:1855
Siglec1-mRNA	NM_011426.3:4550
Siglecf-mRNA	NM_145581.1:355
Sin3a-mRNA	NM_001110350.1:3585
Sirt1-mRNA	NM_019812.2:843
Slamf8-mRNA	NM_029084.3:1366
Slamf9-mRNA	NM_029612.4:748
Slc10a6-mRNA	NM_029415.2:622
Slc17a6-mRNA	NM_080853.3:2825
Slc17a7-mRNA	NM_182993.2:530
Slc1a3-mRNA	NM_148938.3:3865
Slc2a1-mRNA	NM_011400.3:2190
Slc2a5-mRNA	NM_019741.3:2305
Slc44a1-mRNA	NM_001159633.1:944
Slc6a1-mRNA	NM_178703.4:1865
Slco2b1-mRNA	NM_175316.3:2720
Slfn8-mRNA	NM_181545.4:2806
Smarca4-mRNA	NM_011417.2:3540
Smarca5-mRNA	NM_053124.2:2934
Smarcd1-mRNA	NM_031842.1:2220
Smc1a-mRNA	NM_019710.2:1675
Snca-mRNA	NM_009221.2:285
Socs3-mRNA	NM_007707.2:585
Sod2-mRNA	NM_013671.3:1495
Sox10-mRNA	XM_128139.6:2646
Sox4-mRNA	NM_009238.2:2635
Sox9-mRNA	NM_011448.4:3540
Spint1-mRNA	NM_016907.3:1366
Spp1-mRNA	NM_009263.3:420
Sqstm1-mRNA	NM_011018.2:1430
Srgn-mRNA	NM_011157.2:168
Srxn1-mRNA	NM_029688.4:2010
St3gal6-mRNA	NM_018784.2:1252
St8sia6-mRNA	NM_145838.1:1578
Stat1-mRNA	NM_009283.3:1590
Steap4-mRNA	NM_054098.3:765
Stmn1-mRNA	NM_019641.3:595
Stx18-mRNA	NM_026959.2:770
Sumo1-mRNA	NM_009460.1:720
Suv39h1-mRNA	NM_011514.2:396
Suv39h2-mRNA	NM_022724.4:1427
Suz12-mRNA	NM_199196.1:820
Syk-mRNA	NM_001198977.1:2064
Syn2-mRNA	NM_013681.1:1330
Syp-mRNA	NM_009305.2:732
Tarbp2-mRNA	NM_001253795.1:813
Tbc1d4-mRNA	NM_001081278.2:2610
Tcirg1-mRNA	NM_001136091.1:1345
Tet1-mRNA	NM_027384.1:2192
Tfg-mRNA	NM_001252443.1:578
Tgfa-mRNA	NM_031199.2:3360
Tgfb1-mRNA	NM_011577.1:1470
Tgfbr1-mRNA	NM_009370.2:4425
Tgm1-mRNA	NM_001161714.1:1530
Tgm2-mRNA	NM_009373.3:1260
Tie1-mRNA	NM_011587.2:2715
Timeless-mRNA	NM_011589.1:3720
Timp1-mRNA	NM_011593.2:436
Tle3-mRNA	NM_009389.2:3584
Tlr2-mRNA	NM_011905.2:255
Tlr4-mRNA	NM_021297.2:2510
Tlr7-mRNA	NM_133211.3:3210
Tm4sf1-mRNA	NM_008536.3:652
Tmc7-mRNA	NM_172476.4:1285
Tmcc3-mRNA	NM_172051.2:3825
Tmem100-mRNA	NM_026433.2:1350

Tmem119-mRNA	NM_146162.2:1550
Tmem144-mRNA	NM_027495.4:1525
Tmem173-mRNA	NM_028261.1:1792
Tmem204-mRNA	NM_001001183.1:1006
Tmem206-mRNA	NM_025864.3:845
Tmem37-mRNA	NM_019432.2:445
Tmem64-mRNA	NM_181401.3:1125
Tmem88b-mRNA	NM_001033394.3:1122
Tnf-mRNA	NM_013693.2:514
Tnfrsf10b-mRNA	NM_020275.3:1625
Tnfrsf11b-mRNA	NM_008764.3:35
Tnfrsf12a-mRNA	NM_001161746.1:517
Tnfrsf13c-mRNA	NM_028075.2:1170
Tnfrsf1a-mRNA	NM_011609.2:615
Tnfrsf1b-mRNA	NM_011610.3:3270
Tnfrsf4-mRNA	NM_011659.2:320
Tnfsf10-mRNA	NM_009425.2:2055
Tnfsf12-mRNA	NM_011614.3:1215
Tnfsf13b-mRNA	NM_033622.1:225
Top2a-mRNA	NM_011623.2:1953
Topbp1-mRNA	NM_176979.5:3564
Tpd52-mRNA	NM_001025262.1:2054
Tradd-mRNA	NM_001033161.2:562
Traf1-mRNA	NM_009421.3:566
Traf2-mRNA	NM_009422.2:1334
Traf3-mRNA	NM_011632.3:884
Traf6-mRNA	NM_009424.2:980
Trat1-mRNA	NM_198297.3:535
Trem2-mRNA	NM_031254.2:646
Trim47-mRNA	NM_001205081.1:2019
Trp53-mRNA	NM_011640.1:1835
Trp53bp2-mRNA	NM_173378.2:2328
Trpm4-mRNA	NM_175130.4:1145
Tspan18-mRNA	NM_183180.2:1008
Tubb3-mRNA	NM_023279.2:179
Tubb4a-mRNA	NM_009451.3:1819
Txnrd1-mRNA	NM_015762.2:2245
Tyrobp-mRNA	NM_011662.2:130
Ugt8a-mRNA	NM_011674.4:138
Ulk1-mRNA	NM_009469.3:4050
Ung-mRNA	NM_001040691.1:336
Uty-mRNA	NM_009484.2:3530
Vamp7-mRNA	NM_011515.4:390
Vav1-mRNA	NM_011691.4:1640
Vegfa-mRNA	NM_001025250.3:3015
Vim-mRNA	NM_011701.4:34
Vps4a-mRNA	NM_126165.1:994
Vps4b-mRNA	NM_009190.2:640
Was-mRNA	NM_009515.2:1617
Wdr5-mRNA	NM_080848.2:1704
Xcl1-mRNA	NM_008510.1:103
Xiap-mRNA	NM_009688.2:1654
Xrcc6-mRNA	NM_010247.2:1640
Zbp1-mRNA	NM_021394.2:473
Zfp367-mRNA	NM_175494.4:1235